MODULATION OF ENDOCYTIC AND EXOCYTIC TRAFFIC IN POLARIZED EPITHELIAL CELLS

by

Christina Mae Szalinski

B.S. Biology, State University of New York at Geneseo, 2008

Submitted to the Graduate Faculty of

The School of Medicine in partial fulfillment

of the requirements for the degree of

Doctor of Philosophy

University of Pittsburgh

2013

UNIVERSITY OF PITTSBURGH

SCHOOL OF MEDICINE

This dissertation was presented

by

Christina Mae Szalinski

It was defended on

May 20, 2013

and approved by

Linton M. Traub, PhD

Manojkumar A. Puthenveedu, PhD

Nuria M. Pastor-Soler, MD, PhD

Peter F. Drain, PhD

Thesis Advisor: Ora A. Weisz, PhD

MODULATION OF ENDOCYTIC AND EXOCYTIC TRAFFIC IN POLARIZED EPITHELIAL CELLS

Christina Mae Szalinski, PhD

University of Pittsburgh, 2013

Efficient and selective delivery and retrieval of cargo to polarized plasma membrane domains are essential for the maintenance of epithelial cell function. My studies focused on events involved in protein endocytosis from and delivery to the apical surface.

Endocytosis is a multi-step process that is crucial for cells to take up nutrients and modulate receptor density. Temporal synthesis and degradation of the lipid phosphatidylinositol-4,5-bisphosphate [PtdIns(4,5)P$_2$] is critical for endocytosis to proceed. PtdIns(4,5)P$_2$ is generated by three differentially localized phosphatidylinositol 4-phosphate 5-kinase (PIP5KI) isoforms (α, β, and γ). My studies examined the requirement for PtdIns(4,5)P$_2$ in apical and basolateral endocytosis in polarized kidney epithelial cells by testing the effects of overexpressing individual PIP5KI isoforms. I found that PtdIns(4,5)P$_2$ synthesis by PIP5KIβ is rate limiting for apical but not basolateral endocytosis, and that this is likely due to changes in coated pit maturation at the apical plasma membrane. The selective modulation of apical endocytosis by PtdIns(4,5)P$_2$ has potential consequences on the maintenance of kidney cell function.

Maintaining apical and basolateral membrane domain composition requires selective vesicle fusion and is mediated by Soluble *N*-ethylmaleimide-sensitive factor Attachment protein Receptor (SNARE) proteins. A number of pathways exist for the delivery of newly synthesized proteins to these surface domains and the post-Golgi vesicle SNAREs, or VAMPs, that mediate fusion in these pathways have not been identified. I sought to determine the role of VAMP7 in

these pathways. VAMP7 expressed in polarized Madin Darby canine kidney cells colocalized primarily with LAMP2-positive compartments, and changes in VAMP7 levels modulated lysosome size, consistent with the known function of VAMP7 in lysosomal delivery. Surprisingly, VAMP7 knockdown had no effect on apical delivery of numerous cargoes tested but did decrease the length and frequency of primary cilia and disrupted cyst morphology. The effects of VAMP7 depletion on ciliogenesis and cystogenesis are not directly linked to the disruption of lysosomal function, as cilia lengths and cyst morphology were unaffected in a MDCK lysosomal storage disorder model. Together, my data suggest that VAMP7 plays an essential role in ciliogenesis and cystogenesis. This is the first study implicating an R-SNARE in ciliogenesis and cystogenesis.

TABLE OF CONTENTS

LIST OF TABLES

LIST OF FIGURES

PREFACE

I could not have done this thesis without the generous support of many people. I am grateful to my mentor and advisor, Dr. Ora Weisz, for an amazing experience in graduate school. When I set out to find a lab, my goal was to find a mentor that would facilitate my growth as a scientist. Five years later, I am still proud of my decision to join the Weisz lab. Ora has done more for me than I could have imagined, from daily advice and guidance to helping me become a better scientist, writer, and colleague. I will always be inspired by her mentorship, and I hope that I can guide others as she has guided me.

I would like to thank my labmates, who have been exceptionally helpful, supportive and a pleasure to work with; they made every day in the lab more fun. Dr. Christopher Guerriero patiently trained me and started me on a path to becoming a better scientist. Dr. Polly Mattila was always available for insightful advice about experiments and life. Jennifer Bruns was eager to share her wealth of experience in lab and life, and without her mandatory lab organization, I'm confident that it would have taken me much longer to graduate. Simone Costa graciously provided technical support in desperate times. Dr. Robert Youker provided helpful and challenging conversations. I'd also like to thank all the Weisz lab members who helped me throughout my graduate education especially Dr. Shanshan Cui, Dr. Di Mo, Brianne Docter, Dr. Anatália Labilloy and Venktasesan Raghavan.

I am grateful to my thesis committee members; Dr. Linton Traub, Dr. Peter Drain, Dr. Manojkumar Puthenveedu and Dr. Nuria Pastor-Soler. They provided guidance and great advice along my path to graduation. Their ideas contributed to the success of my projects.

The Renal-Electrolyte Division has been a tremendous place to work; everyone generously provided advice, reagents, and support. Altogether I could not have imagined a better group of people to work with, and I hope all my future workplaces are as collaborative.

My parents, without whom I would not have had such incredible opportunities in life and so much support and inspiration, deserve tremendous appreciation. My mother, Sandra Szalinski, who worked in Scaife Hall 45 years ago, paved the way for me as a woman in science and has always been my role model. My father, Paul Szalinski, cultivated my passion for food and gardening, and started my training as a scientist at a young age by challenging me and encouraging me to think independently. I am so proud of my brother, Ian Szalinski, for chasing his entrepreneurial goals with incredible ambition.

My life outside the lab would certainly not have been as much fun without my friends, especially Nina Chi Sabins. I am so glad to have met her during our hectic time in graduate school. She has been a tremendous ally, source of moral support and best friend.

My husband, Mark Gorski, has helped make the past five years among the best years of my life. I am so thankful for his enduring love and his incredible support of my ambitions. He left his happy life in Buffalo to be with me in Pittsburgh, and he has been my champion every step of the way. I could not imagine having a better partner.

Everyone in this journey has believed in me, often more so than myself, and I am grateful for everyone's support along the way. I feel incredibly fortunate to have such wonderful colleagues, friends and family.

ABBREVIATIONS

α-gal A   α-galactosidase A

ARE   apical recycling endosome

ARH   autosomal recessive hypercholesterolemia

CCP   clathrin coated pit

CRE   common recycling endosome

Dab2   disabled 2

DOX   doxycycline

DPPIV   dipeptidyl peptidase IV

EM   electron microscopy

ENTH   epsin N-terminal homology

FRT   Fischer rat thyroid

GPCR   G-protein coupled receptor

GST   glutathione S-transferase

KO   knockout

KD   knockdown

LAMP   lysosome associated membrane protein

mCCD   murine cortical collecting duct

MDCK   Madin-Darby canine kidney

MEM	modified Eagle's medium
MOI	multiplicity of infection
PIP5K	phosphatidylinositol 5-kinase
pIgR	polymeric immunoglobulin receptor
PLAP	placental alkaline phosphatase
PTB	phosphotyrosine binding
PtdIns(4,5)P$_2$	phosphatidylinositol 4,5-bisphosphate
SNARE	soluble N-ethylmaleimide-sensitive factor attachment protein receptors
TGN	trans-Golgi network
TIRF	total internal reflection fluorescence
TLC	thin layer chromatography
VAMP	vesicle associated membrane protein

1.0   INTRODUCTION

1.1   OVERVIEW OF POLARIZED EPITHELIAL CELLS

Epithelial cells serve as a barrier between the body and the outside world. Specialized epithelial cells polarize to form distinct apical and basolateral domains and line organs such as kidney, intestine, lung, and thyroid. The apical domain faces the lumen whereas the basolateral domain faces the interstitium, close to blood vessels. Junctional complexes surround each cell like a belt and separate apical and basolateral domains. These complexes serve to connect cells, maintain the integrity of the tissue, and maintain polarity. Junctions have both a "gate" and "fence" function. The gate functions allows for some small molecules, such as ions and water, to pass through. The fence function prevents the diffusion of membrane proteins from the apical to basolateral domains.

To maintain polarity, newly synthesized transmembrane and luminal proteins must be selectively delivered to the apical or basolateral domains. In eukaryotic cells, trafficking between organelles occurs via membrane bound vesicles (1). Proteins destined for the surface of polarized cells are sorted into endosomal vesicles at the trans-Golgi network (TGN). The vesicles then traffic to the apical or basolateral domains, or to secondary compartments that act as sorting stations. At their intended destination the vesicles fuse with the target membrane, typically using a process known as exocytosis or secretion. A specialized family of proteins known as SNAREs

1

(Soluble N-ethylmaleimide-sensitive factor Attachment protein Receptors) drive the final step in fusion. Vesicles and organelles each have unique SNAREs that stick out like antennae. When a vesicle comes close to its intended destination, the SNAREs bind one another like twist-ties, and their binding provides energy that drives membrane fusion. My research has focused on the vesicle SNARE, VAMP7, which has been implicated in apical delivery and fusion with lysosomes.

Proteins at the apical or basolateral cell surface are retrieved through a process known as endocytosis. Endocytosis allows for the cell to take up nutrients and for modulation of the number of proteins at the cell surface in response to various stimuli. SNAREs that fused with their target membrane must also be retrieved and returned to their original compartment via endocytosis. A multitude of proteins are involved in orchestrating clathrin-mediated endocytic events, including coat proteins, clathrin adaptors, fission components, cellular scaffolds and molecular motors. However, my work is centered on a the lipid phosphatidylinositol-4,5-bisphosphate [PtdIns(4,5)P$_2$] and its critical role in endocytosis.

The processes of endocytosis and exocytosis are crucial for the function and survival of polarized epithelial cells. My thesis focuses on epithelial cells of the kidney tubule, some of which have the unique task of processing approximately 200 liters of plasma every day. This tremendous amount of filtering requires the cells to tightly regulate the processes of delivery and retrieval of proteins to and from the apical cell surface. My goal was to further understand the mechanisms by which the processes of exocytosis and endocytosis are modulated in kidney epithelial cells. This introduction provides a context for my work towards understanding fundamental processes of polarized kidney cells.

1.2   MODULATION OF ENDOCYTOSIS

Internalization of proteins at the cell surface allows for uptake of nutrients that keep cells alive as well as for modulation of the number of proteins at the cell surface. For example, under conditions of high blood pressure, sodium channels such as ENaC (epithelial sodium channel) are retrieved from the plasma membrane to decrease salt uptake from the kidney, and thereby lower blood volume. In order for the kidney to function properly, this endocytic process must be tightly regulated. Dysregulation of this process can lead to diseases such as hypertension, which can be due, in part, to the improper modulation of the number of sodium channels at the cell surface (2-3). Internalization of ENaC from the apical surface of cells that line the cortical collecting duct occurs via a clathrin-dependent pathway, and can be modulated by numerous hormones including aldosterone and vasopressin (4-6). My research in Chapter 2 focuses on a mechanism for modulation of clathrin-dependent endocytosis via changes in the lipid PtdIns(4,5)P$_2$. I investigated how increasing PtdIns(4,5)P$_2$ affects endocytosis in polarized epithelial cells, which have unique endocytic properties at the apical versus basolateral domains (7-11).

1.2.1 Clathrin-dependent endocytosis

Clathrin-mediated endocytosis is a multi-step process of cargo internalization from the plasma membrane that is essential for the regulation of cell receptor density and uptake of nutrients essential for cell function (12). For example, cholesterol ingested in the diet is packaged into lipoprotein particles that are internalized via ubiquitously expressed cellular LDL-receptors to enable distribution of the lipid to peripheral tissues (13). Similarly, the transferrin receptor mediates internalization of iron-loaded transferrin from the cell surface to maintain iron homeostasis. The incorporation of these and other diverse cargoes into forming clathrin-coated pits (CCPs) is facilitated by endocytic adaptors proteins, including AP-2, epsin, autosomal recessive hypercholesterolemia (ARH), and disabled 2 (Dab2) (14). In addition to recruiting cargo, these proteins also recruit additional factors necessary for membrane invagination (14-15). In turn, the lipid PtdIns(4,5)P$_2$ plays a key role in recruitment of clathrin adaptors and other regulatory proteins critical for endocytosis to the plasma membrane (16). PtdIns(4,5)P$_2$ is synthesized and hydrolyzed by a number of kinases and phosphatases (Figure 1.1). Coordinated synthesis and hydrolysis of PtdIns(4,5)P$_2$ at the plasma membrane is critical for regulating clathrin-mediated endocytosis.
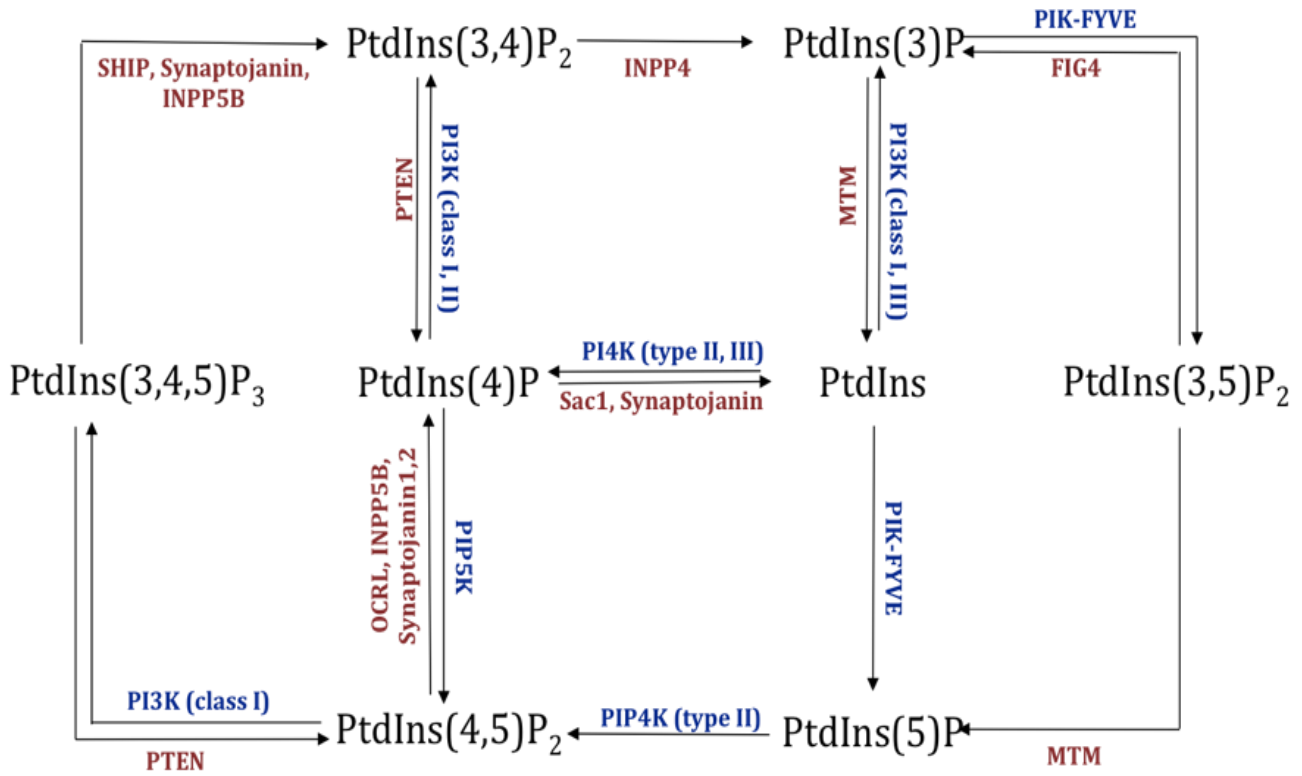
Figure 1.1 Known substrates of phosphoinositide kinases and phosphatases.

Phosphorylation and dephosphorylation of three positions on the phosphoinositide ring of phosphatidylinositol (PtdIns) by various kinases (blue) and phosphatases (brown) can result in seven phosphoinositide phosphates. Adapted from Jean and Kiger 2012.

1.2.2 Role of PtdIns(4,5)P$_2$ and PIP5K in modulating endocytosis

PtdIns(4,5)P$_2$ is localized to both the apical and basolateral plasma membrane domains of polarized epithelial cells (17-19). The synthesis and degradation of PtdIns(4,5)P$_2$ by kinases and phosphatases is necessary for execution of four critical steps in clathrin-mediated endocytosis (16, 20-24). First, PtdIns(4,5)P$_2$ recruits clathrin adaptors that bind to PtdIns(4,5)P$_2$ via distinct structural domains (25-28). After clathrin adaptors recruit clathrin and a coated pit is formed, dynamin is recruited to the membrane by binding to PtdIns(4,5)P$_2$, where it then promotes scission of the vesicle (21). The vesicle is then internalized by actin motor myosin VI, which also binds to PtdIns(4,5)P$_2$ on the membrane (29). Finally, after internalization, the hydrolysis of PtdIns(4,5)P$_2$ by the 5' phosphatase synaptojanin is important for vesicle uncoating (30).

During clathrin mediated endocytosis, clathrin adaptors facilitate sorting of cargo into forming pits (31). CCPs enriched in individual cargoes have been described by several groups (14-15, 32-33). Because clathrin adaptors have different PtdIns(4,5)P$_2$ binding domains one might speculate that this is due in part to PtdIns(4,5)P$_2$ dependent modulation of clathrin adaptor recruitment to the membrane. Indeed, changes in surface PtdIns(4,5)P$_2$ (both increases and decreases) have been shown to differentially modulate surface density/endocytosis of membrane proteins. For example, hydrolysis of PtdIns(4,5)P$_2$ due to G-protein coupled receptor (GPCR) signaling events leads to a decrease in internalization of insulin but not β2 glycoprotein I (34). Conversely, our lab has shown that overexpression of PIP5KIβ can decrease the surface density of ENaC, but increases surface density of another channel, ROMK (8). As endocytosis of ENaC

and ROMK are epsin- and ARH- dependent, respectively, this suggests that the clathrin adaptors that engage these proteins may have unique PtdIns(4,5)P$_2$ requirements.

The majority of cellular PtdIns(4,5)P$_2$ is synthesized by phosphorylation of phosphatidylinositol 4-phosphate at the D-5 position of the inositol ring by phosphatidylinositol 4-phosphate 5-kinases type I (PIP5KI). Three isoforms of this enzyme exist (PIP5KIα, β, and γ) that are widely expressed in mammalian tissues (35-38). All three isoforms of PIP5KI have been shown to be involved in clathrin-mediated endocytosis in nonpolarized cells. Overexpression of PIP5KIβ has been shown to increase transferrin endocytosis in HeLa cells (39). Conversely, PIP5KIα is apparently required for the endocytosis of EGFR (40). PIP5KIγ has been implicated as the primary enzyme that synthesizes PtdIns(4,5)P$_2$ at the synapse (41). All three isoforms can bind the AP-2 adaptor protein complex, though AP-2 has been shown to be specifically recruited by PIP5KIβ and γ (39, 42-44). However, each of these isoforms is differentially localized in polarized epithelial cells (45), and it is not known how the pools of PtdIns(4,5)P$_2$ they generate affect endocytosis from the apical or basolateral cell surface domains in polarized cells.

1.2.3   PtdIns(4,5)P$_2$ and polarized endocytosis

Despite the critical role for PtdIns(4,5)P$_2$ in endocytosis, it is unclear how changes in cell surface PtdIns(4,5)P$_2$ levels affect endocytosis. Acute hydrolysis of PtdIns(4,5)P$_2$ using targeted delivery of PtdIns(4,5)P$_2$ phosphatase domains to the membrane causes rapid and profound blockade in endocytosis (46-48), however, the effects of less drastic manipulations on PtdIns(4,5)P$_2$ levels has not been rigorously tested. Changes in PtdIns(4,5)P$_2$ might modulate the efficiency of endocytosis at specialized plasma membrane domains. For example, endocytosis of the same cargoes from the apical surface of polarized cells proceeds considerably more slowly compared

7

with internalization from the basolateral domain of the same cells or in nonpolarized cells (7-11). These differences may be due to steric constraints of the apical membrane, as CCP formation is limited to the base of microvilli, or to differences in cytoskeletal dynamics. Actin filaments are concentrated in the subapical terminal web and in microvilli, and might inhibit CCP invagination, fission, and/or vesicular traffic. Actin appears to be critical for apical endocytosis, as disruption of actin polymerization by cytochalasin D or jasplakinolide inhibits apical but not basolateral or non-polarized endocytosis (9, 49-51). Actin, as well as the actin nucleators Neural-Wiskott Aldrich Syndrome Protein and Arp2/3, is recruited to sites of clathrin endocytosis (52-53). The activities of these actin nucleators is enhanced by $PtdIns(4,5)P_2$ (54-56) implicating $PtdIns(4,5)P_2$ in actin dynamics involved in endocytosis.

1.3   MECHANISMS OF VESICLE TARGETING AND FUSION

Newly synthesized proteins must be properly trafficked to their intended organelle in order to function properly. For example, megalin must be sorted to the apical surface in order to reabsorb small molecular weight proteins filtered through the glomerulus. After newly synthesized transmembrane and luminal cargo are synthesized in the endoplasmic reticulum and processed in the Golgi, they are packaged into vesicles with specific destinations. Motor proteins shuttle these vesicles along cytoskeletal tracks to their intended target. When in close proximity to the target membrane, the vesicle docks and undergoes SNARE-mediated fusion with its final compartment. This well-orchestrated process of protein synthesis, processing, sorting and delivery is known as secretion or exocytosis. As with endocytosis, a large number of proteins are involved in this secretory process, from proteins that help sort and cluster cargo at the Golgi, to coat proteins,

motor proteins, cytoskeletal proteins, and fusion proteins. The goal of my research in Chapter 3 was to identify the role of a post-Golgi SNARE, VAMP7, in protein trafficking to the apical surface.

1.3.1 Fusion machinery

The directional transfer of membrane and soluble proteins from one cellular compartment to another is essential for cell survival. A critical step in these membrane trafficking events is the selective fusion of vesicles with target organelles. SNAREs are key components of the machinery required to maintain selectivity, and are directly responsible for fusion. These small proteins localize to organelle and vesicle membranes and interact when the two membranes are in close proximity. The energy released from this interaction is thought to drive fusion (57). After fusion, NSF and α-SNAP serve to uncouple the helical bundle so that the vesicular SNARE can be sorted back to its compartment (57).

Cognate SNAREs were originally categorized into vesicle-SNAREs (v-SNARE) or target-SNAREs (t-SNARE). However, in 1998 Fasshauer and colleagues proposed a renaming of v-SNAREs to R-SNAREs (synatobrevins/VAMPs) and t-SNAREs to Qa-SNAREs (syntaxins) and Qbc-SNAREs (SNAPs) based on conserved argenine (R) and glutamine (Q) residues at the center of the synaptic complex (58). One R-SNARE on the vesicle membrane and three Q-SNAREs on the target membrane interact to form a helical bundle. In general, four distinct SNAREs participate in the helical bundle, although there are some Q-SNAREs, such as SNAP-47, that contribute two helices to the coil (59). Most SNAREs are transmembrane proteins, but a few, such as SNAP-25 are palmitoylated (57). A subset of R-SNAREs fall into a family known

as VAMPs (Vesicle Associated Membrane Proteins), based on their initial discovery in synaptic vesicle membranes.

Deciphering the role of VAMPs is complicated because SNAREs can assemble in many combinations to provide a large array of selective complexes (Figure 1.2). That said, there are redundancies in SNARE function, such that the same SNARE complex may function at multiple steps in membrane traffic (Figure 1.2). SNAP23 is involved in fusion of post-Golgi vesicles with the plasma membrane (60-61), as well as in transcytosis (62). Additionally, multiple SNARE complexes may mediate the same fusion pathway. For example, both VAMP7 and VAMP8 can form complexes with syntaxin-7 and both are involved in late-endosome to lysosome fusion (63). Such redundancies have made it difficult to sort out the SNAREs involved in a given trafficking pathway.
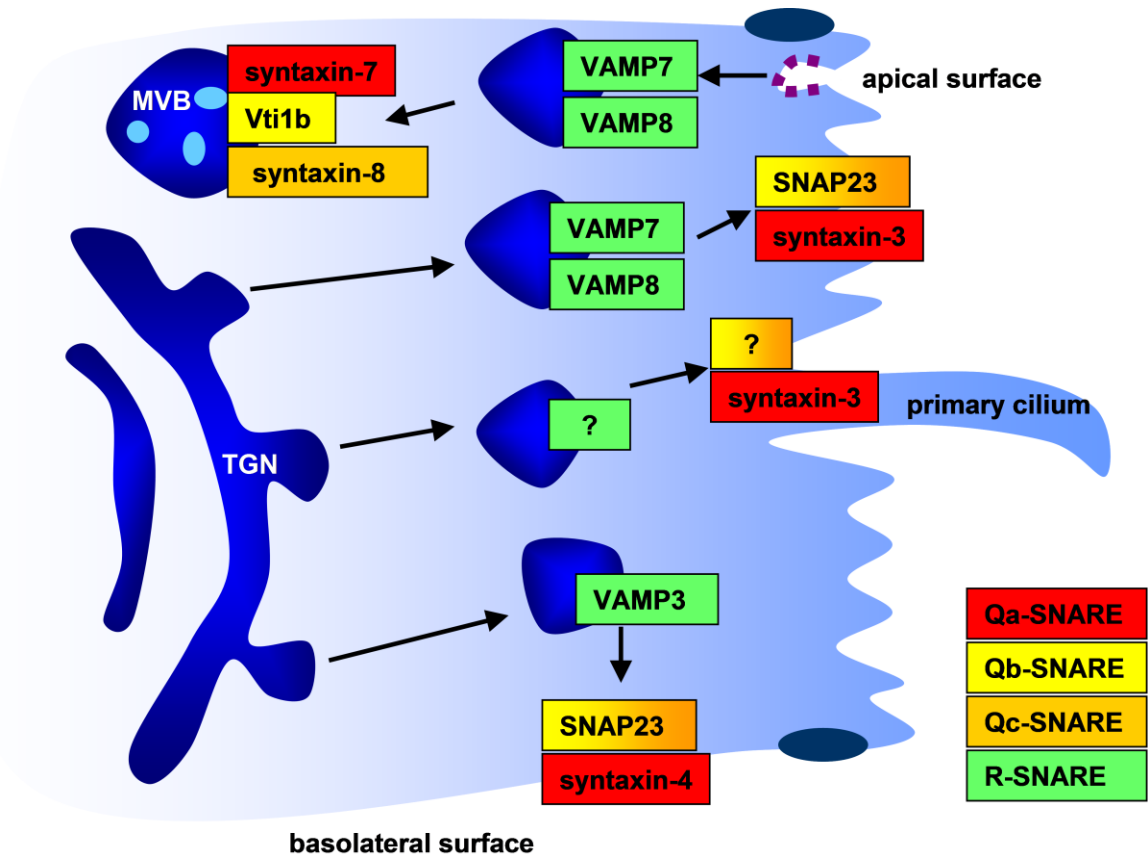
Figure 1.2 Diversity and redundancy of SNAREs in trafficking.

SNAREs can assemble in many combinations to provide a large array of selective complexes that act in different trafficking pathways. However, there are also redundancies in SNARE function, such that the same SNARE complex may function at multiple steps in membrane traffic. Shown are SNAREs that have been identified in delivery to the apical and basolateral surface, the primary cilium, and to lysosomes/multi-vesicular bodies (MVBs).

1.3.1.1 VAMP7 in exocytosis

In 1995, apical exocytosis was shown to be unaffected by treatment with clostridial neurotoxins, unlike many other exocytic events; which suggested that there were unidentified SNARE proteins that were insensitive to neurotoxins (64-66). The toxin-insensitive VAMP (TI-VAMP) was identified as a VAMP protein involved in apical exocytosis (67). TI-VAMP was later renamed VAMP7. VAMP7 is enriched in the apical plasma membrane of polarized intestinal cells, and has been implicated in the apical trafficking of cargo in intestinal cells, thyroid cells and MDCK cells (60, 67-69).

VAMP7 is predominately found in heart, brain, lung, liver, skeletal muscle and kidney tissue (70-72). The gene encoding VAMP7, *SYBL1*, was identified before its role in apical exocytosis was discovered (73). *SYBL1* (Xq28) was the first identified gene in the pseudoautosomal PAR region that undergoes X inactivation (73). Polymorphisms in the *SYBL1* gene have been reported with bipolar disorder (74-76). In particular, a G-C transversion in the regulatory region of *SYBL1*, was found by two studies (74-75). *SYBL1* also was identified in a screen of polymorphisms in bipolar disorder patients, although the position of the mutation was not mapped (76). The VAMP7 knockout mouse has only minor changes in brain weight and ventricular volume, but exhibited increased anxiety responses (77). Despite the evidence that VAMP7 is involved in apical trafficking, its role in apical delivery is controversial because the VAMP7 knockout mice have no overt kidney phenotype (74, 77).

VAMP7 is unique among VAMPs in that it contains an N-terminal longin domain. The longin domain was named as such because although proteins with this domain share the SNARE domain of the synaptobrevins (brevin referring to the Latin term for short: *brevis*), they have an additional domain that makes them longer; hence 'longin' (78). Longin domains are 120-140

amino acids long with a globular fold of a five strand beta sheet sandwiched between three alpha helices (79). There are two additional longin domain-containing R-SNAREs: Ykt6, and Sec22. Intriguingly, the R-SNAREs that contain longin domains are the only R-SNAREs that are conserved in all eukaryotes (79) suggesting a critical role for this domain in trafficking.

In addition to its role in apical trafficking, there is considerable evidence for a role of VAMP7 in additional trafficking steps, especially in fusion of lysosomes. VAMP7 has previously been shown to colocalize with lysosomal proteins lysosomal glycoprotein 120, Niemann-Pick C1, lysosome associated membrane protein (LAMP) 1, and CD63 suggesting a role in endosomes/lysosomes in various cell types (70-71, 80-85). Moreover, blocking VAMP7 with antibodies or by overexpression of the longin domain inhibited EGF degradation (71) and reduced the delivery of dextran and gold conjugated BSA to lysosomes, respectively (63, 86). VAMP7 may also have a role in endocytosis, as MDCK cells overexpressing the VAMP7 longin domain had reduced endocytosis of dextran (86). Additionally, in HeLa cells, VAMP7 knockdown had an indirect effect of increasing EGFR endocytosis by modulating the surface expression of CD82, a tetraspanin that regulates the compartmentalization of EGFR (69).

VAMP7 has been shown to have a number of binding partners in different cell types. VAMP7 can form a SNARE complex with the ubiquitously expressed SNAP23 or the neuron-specific SNAP25, both Qbc-SNAREs (67, 87-89). There is evidence that VAMP7 associates with Qa-SNAREs syntaxin-1 (in neuronal and HeLa cells), syntaxin-3 (in epithelial cells and by yeast two-hybrid) or syntaxin 4 (in mast cells), syntaxin-7 (in brain and liver) and possibly syntaxin-13 (*in vitro*) (63, 82, 84-85, 87, 89-92). It is likely that VAMP7 uses distinct partners for each of its cellular functions.

1.3.2 Tethering machinery

After cargo is sorted into small vesicles and traffics to its destinations, protein complexes, such as the exocyst, tether them prior to fusion. The exocyst is a highly conserved octomeric protein complex (comprised of Sec3, Sec5, Sec6, Sec8, Sec10, Sec15, Exo70 and Exo80). The exocyst was first identified in *Saccharomyces cerevisiae*, where mutation of the subunits was shown to inhibit secretion (93). Exocyst proteins are rod shaped structures composed of two or more alpha helices. Although it is not completely understood how the complex assembles, it seems that subunits associate side-by-side (94). A study in yeast showed that most of the exocyst complex associates with vesicles, whereas Sec3 and Exo70 localize to the membrane (95). Sec3 and Exo70 are recruited to the membrane by $PtdIns(4,5)P_2$ in yeast and mammalian cells (96-98).

In polarized epithelial cells, the exocyst complex is localized to cell-cell contacts, the primary cilium, recycling endosomes, and early endosomes (99-103). The complex has been shown to be involved in trafficking to the basolateral surface (99, 102), apical and basolateral recycling, transcytosis (100), as well as ciliogenesis (101, 104-105). However, the exocyst appears to be dispensable for trafficking of some newly synthesized apical transmembrane proteins (99, 102). The exocyst is thought to be important for SNARE-mediated fusion as the exocyst was shown to associate with SNAREs in mammalian cells (106) and yeast (107). Additionally, formation of SNARE complexes is blocked in yeast exocyst mutants (108).

1.3.3 Trafficking to the polarized cell surface

Proteins were once thought to traffic directly from the TGN to the cell surface. However, in 1988, Schmid and colleagues observed distinct subpopulations of endosomes containing proteins

14

not found on the membrane, suggesting the presence of intermediate compartments for biosynthetic traffic (109). Since then, it has become clear that many unique trafficking pathways exist for newly synthesized proteins to reach the apical and basolateral domains of polarized cells (Figure 1.3)(110). Proteins depend on sorting determinants, such as lipid-rafts, glycans, or peptide motifs to traffic through these distinct pathways (110).

Many apical proteins traffic through the Apical Recycling Endosome (ARE) prior to reaching the apical surface, and there appear to be multiple, differentially regulated exit pathways from this compartment (111-112). For example, endolyn, a transmembrane protein that is sorted by an N-glycan dependent mechanism, traffics through the ARE *en route* to the apical surface. From the ARE, endolyn is delivered to the apical surface via a pathway that requires the motor protein myosinVb (113). Other apical proteins may bypass the ARE and instead transit through apical early endosomes (113). For example, the lipid-raft-associated protein influenza HA is excluded from the ARE (113).

There is also a transcytotic pathway for apical proteins, in which apical proteins are first delivered to the basolateral surface and are then internalized and delivered to the apical surface. For example, the polymeric immunogloubin receptor (pIgR) is delivered basolaterally then is internalized and trafficked through the common recycling endosome (CRE) and ARE before delivery to the apical surface (114). Some basolateral proteins also traffic through intermediate compartments such as the Basolateral Early Endosome or Common Recycling Endosome (115). Basolateral proteins are sorted using the same cytosolic motifs that serve as internalization motifs, such as YXXØ, NPXY or dileucine motifs (115).

Specific Rab GTPases act in these trafficking pathways. For example, Rab11a is known to localize to the ARE where it modulates export with motor protein, myosin Vb (116-117).

15

Rab8 and Rab10 are involved with trafficking to the basolateral surface through the CRE (118). Rab8 has also been implicated in trafficking to the apical surface where it interacts with myosin Vb (117, 119).

Distinct SNARE proteins may be involved in the trafficking through these diverse pathways. Indeed, a number of SNAREs have been implicated in polarized trafficking. Although their localizations were initially controversial (120-121), it is now well established that the Q-SNAREs syntaxin-3 and syntaxin-4 localize to the apical and basolateral surfaces, respectively, in the kidney and in MDCK cells (122-123). The R-SNARE VAMP3 (aka cellubrevin) has been suggested to pair with syntaxin-4 in basolateral delivery (124). However, the R-SNAREs required for apical trafficking pathways have not been identified. Some studies have suggested that VAMP7 and VAMP8 are involved in apical trafficking (67-68) but no defects in cell polarity have been observed in mouse knockout models (74, 77).

Recent studies in thyroid and intestinal cells have implicated VAMP7 in a subset of apical delivery events. In polarized Fischer rat thyroid cells, where apically destined proteins are vectorially delivered to the cell surface, knockdown of VAMP7 disrupted apical delivery of both the lipid-raft associated protein placental alkaline phosphatase (PLAP) and the lipid-raft independent protein dipeptidylpeptidase IV (DPPIV) (68). Different results were obtained in the intestinal epithelial cell line Caco-2, which use both transcytotic and vectorial routes to deliver newly synthesized proteins to the apical surface (125-126). In these cells, delivery of DPPIV, which traffics primarily through the transcytotic pathway, was unaffected by VAMP7 knockdown, whereas vectorial delivery of the lipid-raft dependent protein PLAP was disrupted (68). Given these recent discoveries, I hypothesized that VAMP7 may be involved in the delivery of a subset of cargo known to take a distinct pathway to the apical surface.
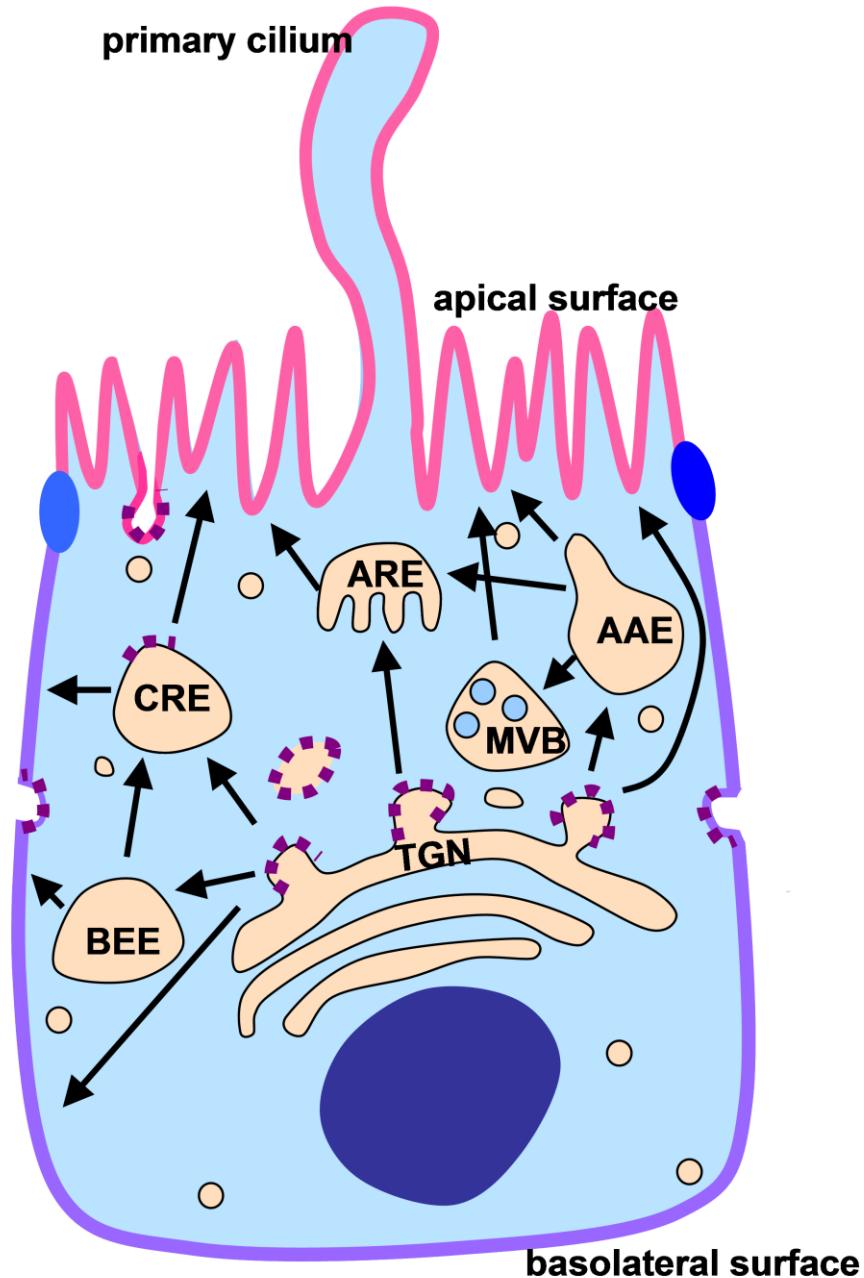
Figure 1.3 Trafficking pathways in polarized epithelial cells.

In polarized epithelial cells there are a number of transport pathways to the apical and basolateral domains used by different pathways. Some proteins traffic directly to the surface, while others transport through intermediate compartments prior to reaching the surface. Endolyn, an N-glycoslyated transmembrane protein, traffics through the ARE *en route* to the apical surface. In contrast, the lipid-raft-associated protein influenza HA is excluded from the ARE (116). Soluble proteins also enter the ARE but exit via myosinVb-dependent or -independent pathways (114). Trafficking through these pathways is dependent on sorting determinants, such as peptide motifs, lipid-rafts or glycans (113). Figure adapted from Weisz and Rodriguez-Boulan 2009.

1.3.4 Delivery of proteins to the primary cilium and modulation of ciliogenesis

The primary cilium is a specialized subdomain of the apical surface. I became interested in VAMP7's role in cilia construction (ciliogenesis) because some machinery involved in apical trafficking is shared in ciliogenesis. For example, membrane trafficking regulators Rab8a, Rab11, Rab17, and Rab23 have been implicated in ciliogenesis (127-130). Certain tethering and fusion proteins have also been implicated in ciliogenesis. The exocyst subunits localize to cilia and knockdown of Sec10 inhibits ciliogenesis, suggesting a critical role for exocyst tethering in this process (101, 103-105). Intriguingly, two VAMP7 partners; syntaxin3 and SNAP25, have been implicated in ciliogenesis (61, 131-132). This suggests that VAMP7 is also involved in ciliogenesis.

A non-motile primary cilium emanates from a basal body on almost every cell in the body. The primary cilium features an arrangement of nine outer microtube doublets (9 + 0) [in contrast to arrangement in motile cilia of two central microtubule doublets and nine outer microtubule doublets (9 + 2)]. For many years the primary cilium was thought to be vestigial, but it is now known to be required for critical signaling pathways during development (133) and for mechanosensation in the kidney (134). Defects in ciliogenesis lead to a group of diseases known as ciliopathies, such as polycystic kidney disease (135).

The cilium is formed in non-cycling quiescent cells (136). The mother centriole acquires distal appendages and docks to a ciliary vesicle to become the basal body (137-138). This complex then fuses with the plasma membrane, where the microtubule-based axoneme extends to form the cilium (137). The distal appendages and base of the axoneme generate a barrier between the ciliary compartment and the rest of the cell (139), known as the transition zone. As

18

no protein synthesis occurs in the cilium, proteins must be selectively delivered across the transition zone to the cilium. Once inside the cilium, they can traffic using the intraflagellar transport (IFT) system. IFT proteins, including IFT subunits and motor proteins, are required for normal ciliogenesis (138).

There is selective import of proteins into the cilium, similar to nuclear entry. Indeed, proteins implicated in nuclear entry such as nucleoporins and Ran-GTP have also been implicated in ciliary entry (140-141). Additionally, ciliary localization signals have been reported to be necessary and sufficient for ciliary targeting of soluble proteins (140).

As there is no vesicular trafficking within the cilium, how transmembrane proteins traffic to the cilium is not well understood, but there are several proposed mechanisms. Proteins could be delivered to the apical surface then enter the cilium by lateral diffusion across the transition zone. The Sonic hedgehog receptor, Smoothened, was shown to diffuse laterally from the apical surface into the cilia when it is activated (142). Alternatively (or additionally), proteins could be delivered directly to the base of the cilium. From the ciliary base, membrane proteins are transported into the cilium by IFT proteins (143). An IFT subunit, IFT20, localizes to the base of the cilium and is important for ciliary delivery of polycystin-2 (144). Each of these possible pathways would require trafficking, tethering and fusion machinery, such as those mentioned above. To my knowledge, an R-SNARE involved in cilia formation has never been identified.

2.0   THE ROLE OF PHOSPHATIDYLINOSITOL METABOLISM IN POLARIZED ENDOCYTOSIS

2.1   INTRODUCTION

Localized synthesis of PtdIns(4,5)P$_2$ at clathrin coated pits is crucial for the recruitment of clathrin adaptors and other components of the internalization machinery, as well as in regulating actin dynamics during endocytosis. PtdIns(4,5)P$_2$ is synthesized from PIP5KI isoforms (α, β, or γ). PIP5KIβ localizes almost exclusively to the apical surface in polarized mouse cortical collecting duct cells, whereas the other isoforms have a basolateral membrane distribution. I therefore investigated the role of PIP5KI isoforms in endocytosis at the apical and basolateral domains.

2.2   RESULTS

2.2.1   PIP5KI isoform localization, expression, and activity in kidney cells

All three isoforms of PIP5KI are known to be expressed in mammalian kidney (35-38). To confirm that they are also expressed endogenously in immortalized murine cortical collecting duct (mCCD) cell lines, I amplified mRNA isolated from these cells using primers specific for each isoform. As shown in Figure 2.1A, message for all three isoforms could be readily detected in these cells by RT-PCR.

To examine the distribution and role of PIP5KI isoforms in mCCD cells, I generated DOX-repressible replication-deficient adenoviruses expressing each PIP5KI isoform tagged C-terminally with the HA epitope. mCCD cells were co-infected with varying MOIs of adenovirus together with adenovirus constitutively expressing the tetracycline transactivator, which is required for expression of PIP5KIs driven by the tet operon. Cells were incubated with 20 ng/ml DOX overnight to allow cell repolarization following infection in the absence of viral expression, and then DOX was washed out overnight to enable PIP5KI expression. Cells were solubilized and blotted with anti-HA antibody to compare protein expression. The blot was imaged on a VersaDoc (Bio-Rad) imaging system and the bands were quantitated using Quantity One (Bio-Rad) software. As shown in Figure 2.1B, PIP5KIβ expression was linear with viral MOI over the tested range of 25-250. Moreover, all PIP5KI isoforms showed similar expression levels when infected with the same MOI based on the densitometric analysis of the HA-tagged protein intensities (Figure 2.1C).

21
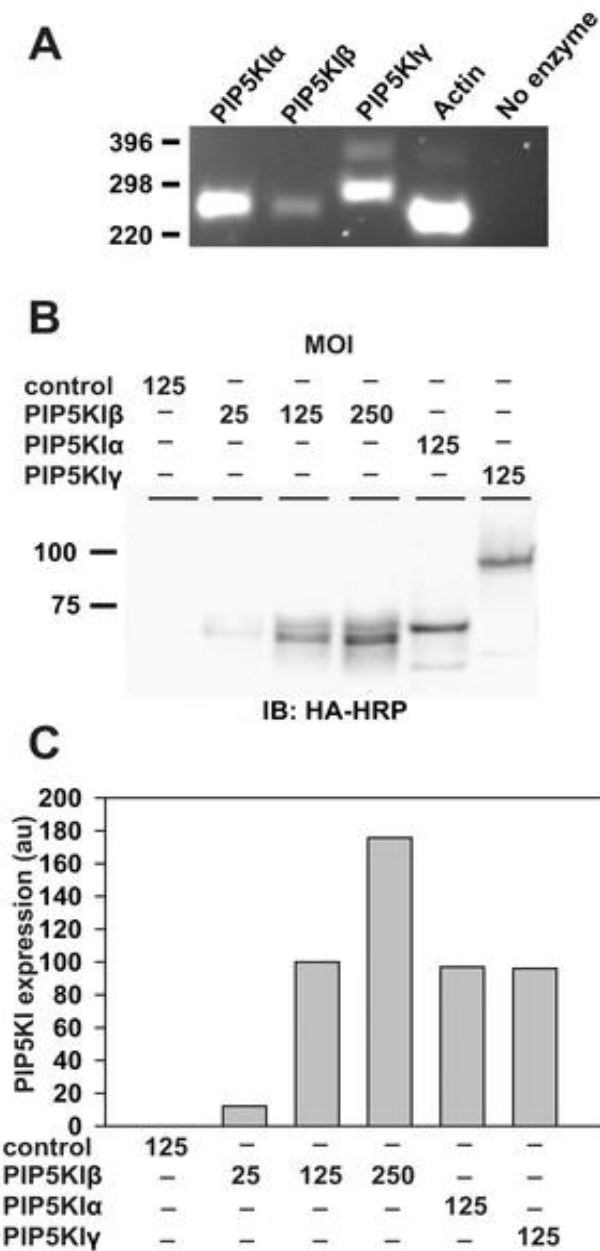
Figure 2.1 Endogenous and adenovirus-mediated expression of PIP5KI isoforms in renal epithelial cells.

(A) Reverse-transcriptase PCR of mRNA isolated from mCCD cells was performed to detect expression of endogenous PIP5KI isoforms. Actin was amplified as a positive control, and actin primers were included in the sample with no enzyme. Predicted sizes are 246 (PIP5KIα), 247 (PIP5KIβ), 276 (PIP5KIγ), and 231 bases (actin). (B) Polarized mCCD cells were mock-infected or infected with adenoviruses encoding HA-tagged PIP5KIα, PIP5KIβ, or PIP5KIγ isoforms at the indicated multiplicity of infection (MOI). Cell lysates were harvested and western blotted using anti-HA antibody to detect PIP5KI expression. The expected masses are approximately 68 (PIP5KIα and PIP5KIβ) and 91 kDa (PIP5KIγ). (C) Densitometric quantitation of the western blot above using arbitrary units (au) normalized to PIP5KIβ MOI 125 demonstrates that PIP5KIβ expression at different MOIs is linear and that expression levels of all three isoforms at MOI 125 are similar.

The subcellular localization of HA-tagged PIP5KI isoforms in mCCD cells was examined by indirect immunofluorescence. In non-polarized cells, all three isoforms localized largely to the cell surface and internal structures, consistent with previous reports (39-40, 44)(Figure 2.2A). In contrast, in polarized cells grown on permeable supports, PIP5KI isoforms were differentially distributed to distinct surface domains. As previously observed (8, 145), PIP5KIβ was strikingly localized to the apical surface (Figure 2.2B). In contrast, PIP5KIα and PIP5KIγ are found primarily at the basolateral domain with minimal localization to the apical domain (Figure 2.2B). This is consistent with a previous study that reported a lateral distribution of endogenous PIP5KIγ in MDCK cells (42). These differences in the localization of PIP5KIs in polarized cells suggested that individual isoforms might differentially regulate PtdIns(4,5)P$_2$ synthesis at the apical and basolateral domains.

I also assessed the localization of endogenous PIP5KIβ to determine whether the apical distribution of HA-tagged PIP5KIβ reflected the true distribution of this isoform in polarized kidney cells. As shown in Figure 2.3A, endogenous PIP5KIβ in mCCD cells was also preferentially distributed to the apical surface, consistent with myresults using virally expressed PIP5KIβ. Similarly, endogenous PIP5KIβ was visualized in rat kidney cortex sections. In the kidney, the apical surface of cells faces the lumen, whereas the basolateral surface faces the interstitium. I found that in the rat kidney cortex sections PIP5KIβ was concentrated at the apical (lumenal) surface of proximal tubules and cortical collecting duct cells (Figure 2.3B and 2.3C, respectively).

I performed thin-layer chromatography (TLC) to test whether cells overexpressing the various PIP5KI isoforms had elevated levels of PtdIns(4,5)P$_2$. mCCD cells grown on plastic or permeable supports were infected with adenoviruses encoding TA and PIP5KI isoforms,

radiolabeled with ^{32}Pi, and anionic phospholipids were isolated and analyzed by TLC. Expression of each of the three isoforms significantly increased PtdIns(4,5)P$_2$ levels in nonpolarized cells (Figure 2.4A), confirming that the adenovirally-expressed enzymes are active. In contrast, only PIP5KIβ expression significantly increased PtdIns(4,5)P$_2$ levels in polarized mCCD cells. PtdIns(4,5)P$_2$ levels in cells overexpressing PIP5KIα also increased consistently, though this was not statistically significant over four experiments (Figure 2.4B). These data suggest that the PIP5KI isoforms have access to distinct pools of PtdIns(4,5)P$_2$ in polarized epithelial cells, consistent with their differential localizations to membrane domains.
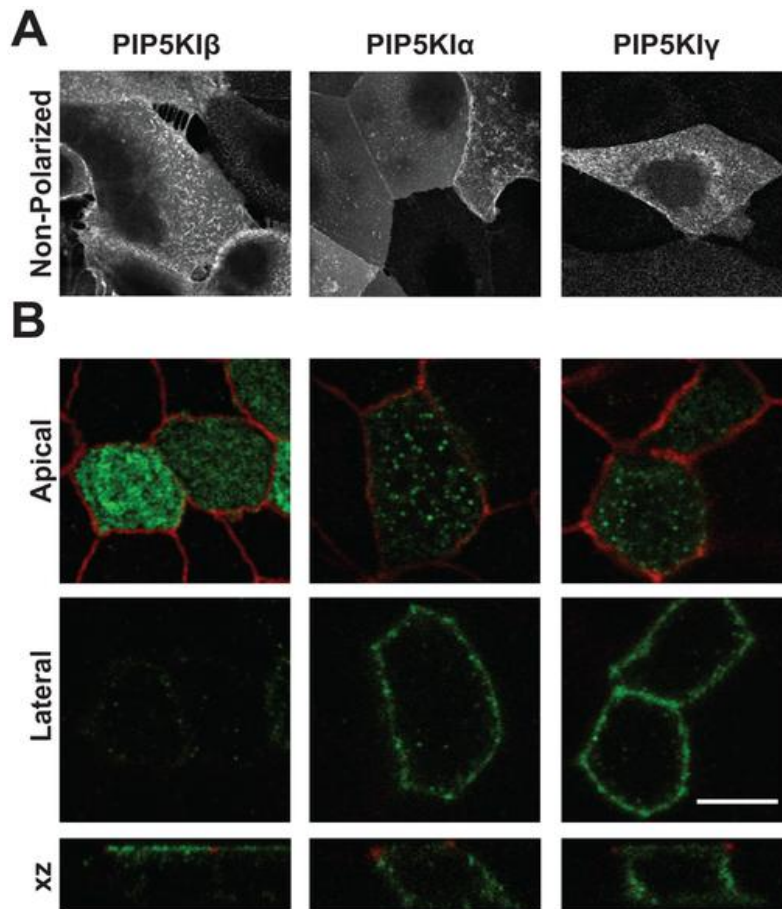
Figure 2.2 Localization of HA-tagged PIP5KI isoforms in polarized mCCD cells.

Mouse cortical collecting duct cells grown on (A) coverslips (non-polarized) or on (B) permeable supports were infected with adenovirus encoding PIP5KIβ, PIP5KIα or PIP5KIγ and processed for indirect immunofluorescence to visualize PIP5KIs using anti-HA epitope antibody [green in (B)]. Anti-ZO-1 antibody was included in filter-grown cells (red) to mark tight junctions. All isoforms are localized to the plasma membrane as well as intracellular punctate structures in nonpolarized cells. In contrast, PIP5KI isoforms are differentially distributed in polarized cells. Confocal sections acquired at the apical and lateral regions of cells are shown, as well as an xz reconstruction of the entire confocal stack. Whereas PIP5KIα and PIP5KIγ are found in a nonpolarized or lateral distribution, PIP5KIβ localizes almost exclusively at the apical surface. Scale bar: 10 μm.
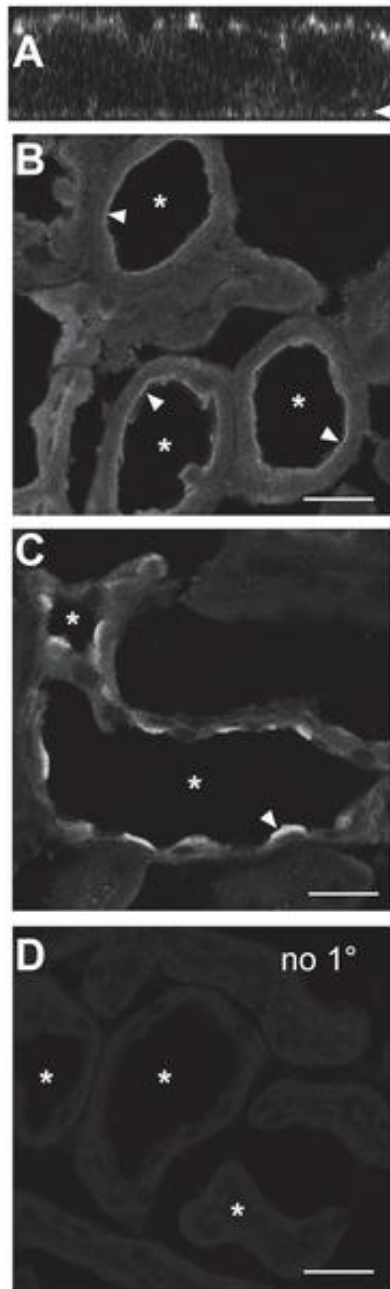
Figure 2.3 Endogenous PIP5KIβ localizes to the apical surface of kidney cells.

(A) Mouse cortical collecting duct (mCCD) cells cultured on permeable supports were fixed and processed for indirect immunofluorescence to detect endogenous PIP5KIβ, which localizes predominately to the apical surface. The arrowhead denotes the position of the filter. (B, C) 4 μm rat kidney cortex slices were fixed and stained to detect PIP5KIβ. The asterisks indicate the lumen. PIP5KIβ is enriched at the apical (lumenal) surface of (A) kidney proximal tubules and (B) collecting ducts. (D) A kidney section processed identically but without primary antibody shows minimal staining. Scale bar: 25 μm.
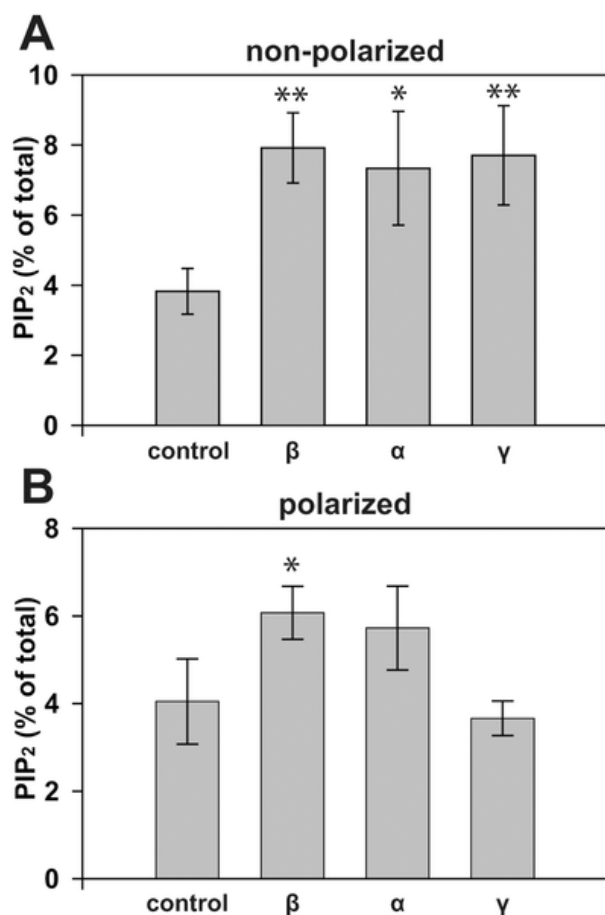
Figure 2.4 Effect of PIP5KI overexpression on PtdIns(4,5)P$_2$ levels in renal epithelial cells.

Non-polarized (A) or polarized (B) mCCD cells infected with either control adenovirus or virus encoding PIP5KIβ, PIP5KIα, or PIP5KIγ were radiolabeled with 32Pi for 4 h then acidic lipids collected and analyzed by TLC. PtdIns(4,5)P$_2$ was quantified as the percent of total acidic phospholipids recovered in each sample. Each graph represents the mean +/- SE of at least four experiments performed in duplicate. One way ANOVA with Bonferroni correction was performed to determine statistical significance (**p<0.01 *p<0.05). Whereas expression of each isoform increased cellular PtdIns(4,5)P$_2$ levels in nonpolarized cells, only PIP5KIβ had a significant effect on PtdIns(4,5)P$_2$ in polarized cells.

2.2.2 Overexpression of PIP5KIβ selectively stimulates apical endocytosis

Each of the three PIP5KI isoforms has been implicated in endocytosis in various non-polarized cell types (39-40, 42, 44). Because PIP5KI isoforms are differentially distributed in polarized cells, I sought to determine whether overexpressing individual isoforms would differentially affect endocytosis from the apical and basolateral domains. To this end, I measured the endocytosis of the polymeric immunoglobulin receptor (pIgR), which can be internalized from both plasma membrane domains of polarized cells (146). pIgR is synthesized in the endoplasmic reticulum, and transported through the Golgi complex, and then delivered to the basolateral surface before it is transcytosed to the apical surface (147). pIgR also recycles from both the apical and basolateral domains, so it can be used to study endocytosis at both surfaces (148). mCCD cells co-expressing pIgR and either PIP5KIα, PIP5KIβ, or PIP5KIγ were incubated with apically- or basolaterally-added ^{125}I-IgA and endocytosis of pre-bound IgA was monitored for 0-5 min. Overexpression of PIP5KIβ significantly and reproducibly stimulated the endocytosis of pIgR from the apical surface, but had no effect on basolateral endocytosis (Figure 2.5). In contrast PIP5KIα and PIP5KIγ had no effect on either apical or basolateral internalization of pIgR (Figure 2.5). These data suggest that endocytosis and PtdIns(4,5)P$_2$ synthesis at the apical surface of polarized cells is regulated primarily by PIP5KIβ.

The stimulation upon overexpression of PIP5KIβ suggests the possibility that production of PtdIns(4,5)P$_2$ is rate limiting for apical but not basolateral endocytosis. Apical endocytosis is known to proceed more slowly than basolateral endocytosis of many proteins that can be internalized from either membrane domain (7-11). Elevated levels of PtdIns(4,5)P$_2$ may selectively enhance recruitment of endocytic machinery to the apical surface of polarized cells

and/or alleviate steric barriers to endocytosis. However, it is also possible that PIP5KI isoforms do not elevate basolateral PtdIns(4,5)P$_2$ levels sufficiently to affect endocytic kinetics. The apical targeting signal in PIP5KIβ is unknown and I spent considerable effort without success attempting to mislocalize PIP5KIβ to the basolateral surface in order to test this directly. As an alternative approach, I tested whether overexpression of PIP5KIβ stimulated endocytosis of pIgR in nonpolarized cells, where changes in cellular PtdIns(4,5)P$_2$ levels were clearly evident. Nonpolarized cells maintain a rapid rate of constitutive pIgR endocytosis similar to the basolateral endocytic rate for this protein in polarized cells. As shown in Figure 2.6, endocytic kinetics of pIgR in non-polarized cells were not affected by overexpression of PIP5KIβ. Because PtdIns(4,5)P$_2$ has also been implicated in regulating exocytosis (145, 149-153) I also tested whether overexpression of PIP5KIβ affects pIgR recycling. As shown in Figure 2.7, I found no differences in either apical or basolateral pIgR recycling rates in cells overexpressing PIP5KIβ compared with control. I conclude that PtdIns(4,5)P$_2$ is rate limiting for apical but not basolateral endocytosis, and that elevation of PtdIns(4,5)P$_2$ levels does not appreciably stimulate endocytosis in nonpolarized cells.
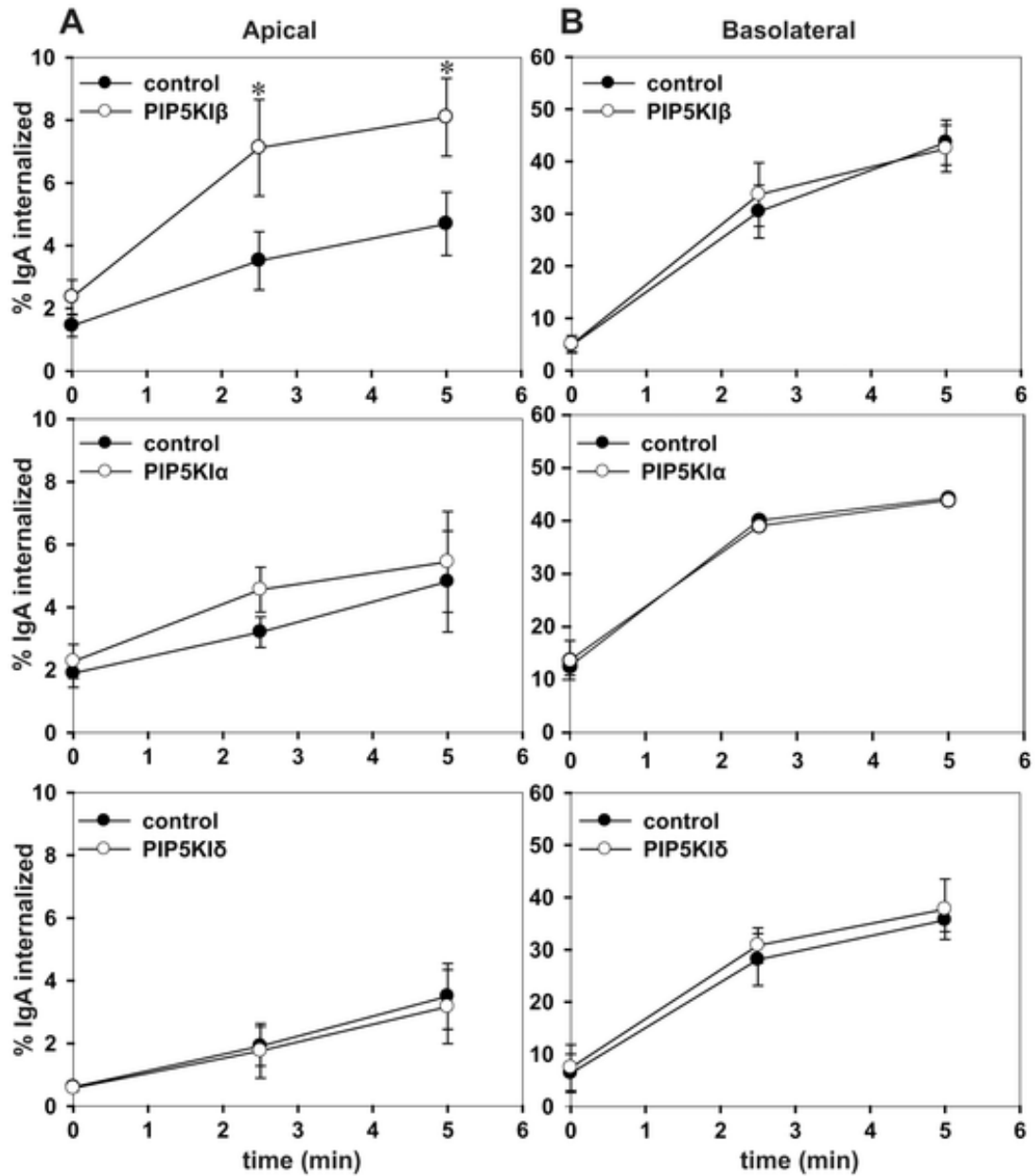
Figure 2.5 Apical endocytosis is selectively increased in cells overexpressing PIP5KIβ.

Internalization kinetics of ^{125}I-IgA from the apical (A) or basolateral (B) surface were assessed in polarized mCCD cells co-infected with adenovirus encoding the polymeric immunoglobulin receptor and either control adenovirus or adenovirus expressing PIP5KIβ, PIP5KIα, or PIP5KIγ. The graphs shows the percent of ^{125}I-IgA internalized over a five min time course. Each graph represents the mean +/- SE of at least three independent experiments performed in duplicate. *$p < 0.05$ by paired t-test.
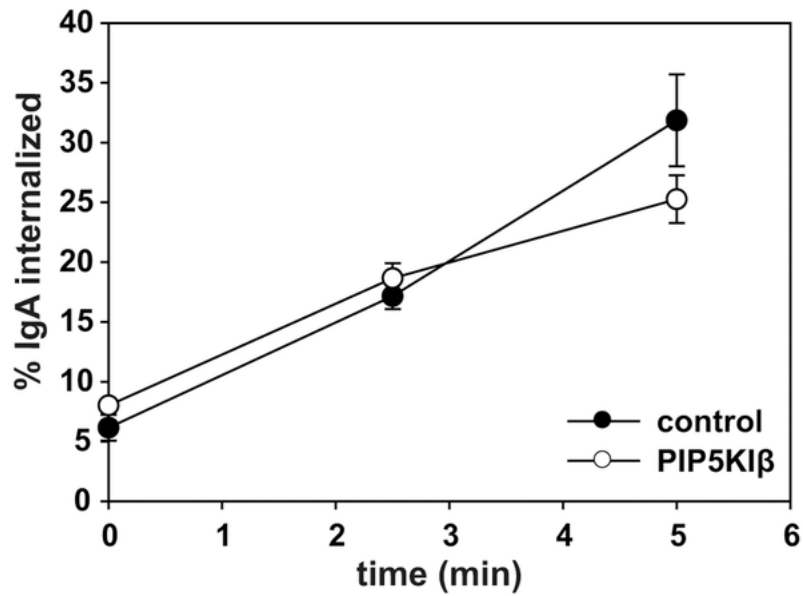
Figure 2.6 Endocytosis in non-polarized cells is unaffected by PIP5KIβ.

(A) Internalization kinetics of ^{125}I-IgA were measured in nonpolarized cells co-infected with adenovirus encoding the polymeric immunoglobulin receptor and either control or PIP5KIβ adenovirus. The graph shows the percent of internalized ^{125}I-IgA over a five min time course. The mean +/- range from one experiment performed in duplicate is shown. Similar results were obtained in three independent experiments.
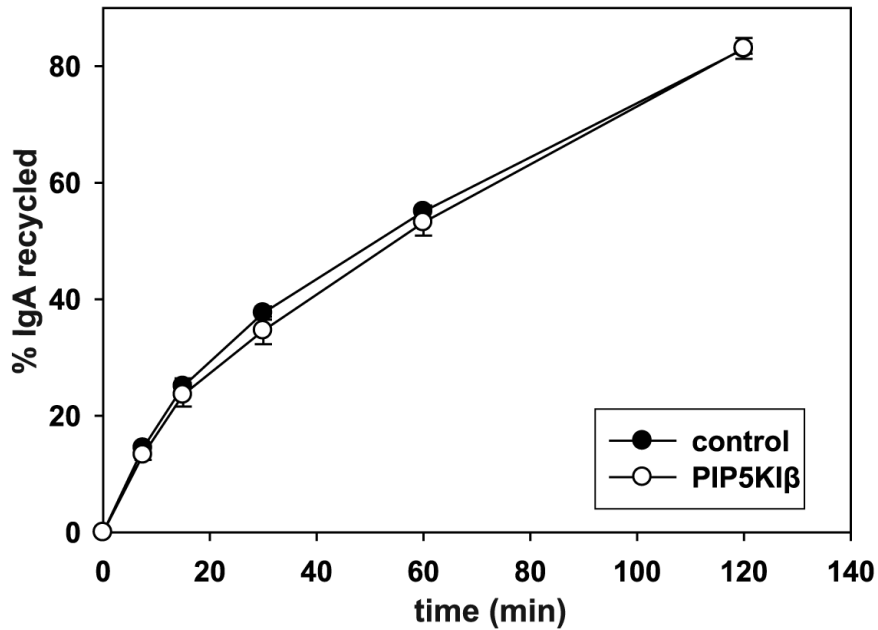
Figure 2.7 IgA Recycling is unaffected by PIP5KIβ.

Recycling of apically-internalized ^{125}I-IgA was quantified in polarized mCCD cells infected with adenovirus encoding pIgR and either control or PIP5KIβ expressing adenovirus. Recycling of IgA is not affected by PIP5KIβ. The graph shows the mean +/- SE of three experiments each performed in triplicate.

2.2.3 Increased cellular PtdIns(4,5)P$_2$ increases maturation rate of apical CCPs

PIP5KIβ may stimulate apical endocytosis generically, or could selectively enhance uptake of cargoes in an adaptor-selective manner. There is conflicting evidence for adaptor-selective effects of PtdIns(4,5)P$_2$ on endocytosis. Overexpression of PIP5KIβ was previously found to decrease ENaC currents in mCCD cells, and also decreased surface expression of the channel in *Xenopus* oocytes, suggesting that increased PtdIns(4,5)P$_2$ stimulates endocytosis of this epsin-dependent channel (8). In the same study, surface expression and current of the ARH-dependent channel ROMK were slightly elevated, suggesting that the stimulatory effect of PIP5KIβ on channel endocytosis may be selective for epsin-dependent cargoes (154). However, overexpression of PIP5KIβ stimulated endocytosis of another ARH/Dab-2-dependent apical protein, megalin, in HK-2 cells (155-157). Because epsin and ARH/Dab-2 bind to PtdIns(4,5)P$_2$ via ENTH and PTB domains, respectively, I asked whether these domains might engage PtdIns(4,5)P$_2$ with differing affinities. To this end, I purified recombinant PtdIns(4,5)P$_2$ binding domains of Dab2 and epsin and measured their relative affinity to PtdIns(4,5)P$_2$-containing liposomes using a sedimentation assay. As expected, both the ENTH domain and the PTB domain bound better to PtdIns(4,5)P$_2$-containing liposomes than to control liposomes lacking PtdIns(4,5)P$_2$ (Figure 2.8). Both domains had similar affinities for PtdIns(4,5)P$_2$, (~50 nM). The ENTH domain was previously reported to have a 23 nM affinity for PtdIns(4,5)P$_2$ containing liposomes (158). While the adaptor protein binding dose response curve showed apparently saturating kinetics, a significant fraction (60%) of the added ENTH protein was recovered in the supernatant, even at the highest concentrations added (Figure 2.9). When the unbound material in the supernatant was collected and tested for rebinding to liposomes, it bound with the same

affinity as the original preparation (not shown). This result suggests that PIP5KIβ-mediated increases in PtdIns(4,5)P$_2$ levels are unlikely to cause differential recruitment of distinct adaptors to the apical surface and instead have a generic stimulatory effect on apical endocytosis kinetics.

The stimulation of apical endocytosis by PIP5KIβ could be due to an increase in the number of apical CCPs or an increase in the maturation rate of individual apical CCPs. I therefore assessed whether either of these contributed to enhanced apical endocytosis in PIP5KIβ overexpressing cells. I used TIRF microscopy to determine the number of CCPs at the apical surface of MDCK cells overexpressing PIP5KIβ compared with control. MDCK cells were grown on filters and co-infected with adenovirus encoding epsin-GFP and either control adenovirus or adenovirus encoding PIP5KIβ. Epsin is known to colocalize with the vast majority (97%) of CCPs in HeLa cells (159). The cells were fixed, stained with anti-HA antibody to detect PIP5KIβ, and the filter was cut out and placed in a machined chamber containing an adjustable piston that positions the filter firmly against a coverslip for TIRF illumination. Epsin-GFP spots were identified and quantitated using Imaris software. Epsin-GFP spots did not colocalize with actin or with a diffuse cytosolic marker (RFP-tagged FKBP5), confirming that the spots represented CCPs rather than aberrations in the apical plasma membrane (not shown). As shown in Figure 2.10, the number of epsin-GFP spots detected was significantly decreased in cells overexpressing PIP5KIβ compared with control. These results suggest that the increase in the apical endocytosis of IgA upon overexpression of PIP5KIβ is not due to increased numbers of CCPs.
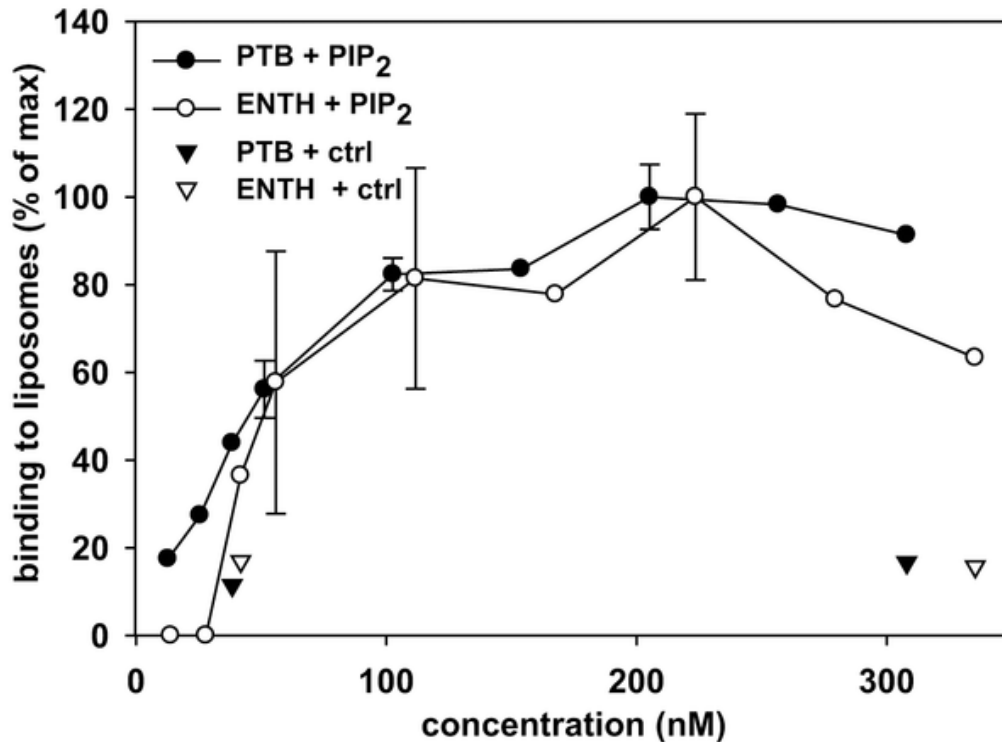
Figure 2.8 Recombinant ENTH and PTB domains bind to PtdIns(4,5)P$_2$-containing liposomes with similar affinities.

Increasing concentrations of PTB-GST or ENTH-GST (the PtdIns(4,5)P$_2$ binding domains of Dab2 and epsin, respectively) were incubated with control or PtdIns(4,5)P$_2$-containing liposomes at ambient temperature for 30 min. The liposomes were pelleted and aliquots of the supernatant and pellet were analyzed by Coomassie staining after SDS-PAGE. The protein recovery in the pellet was quantified by scanning densitometry. Neither domain bound significantly to control liposomes (triangles), and there is no significant difference in the dose dependence of ENTH or PTB binding to PtdIns(4,5)P$_2$-containing liposomes (circles). Data represent the combined results from three independent experiments performed using different protein concentrations. The mean +/- SE or range is plotted for data from multiple experiments.
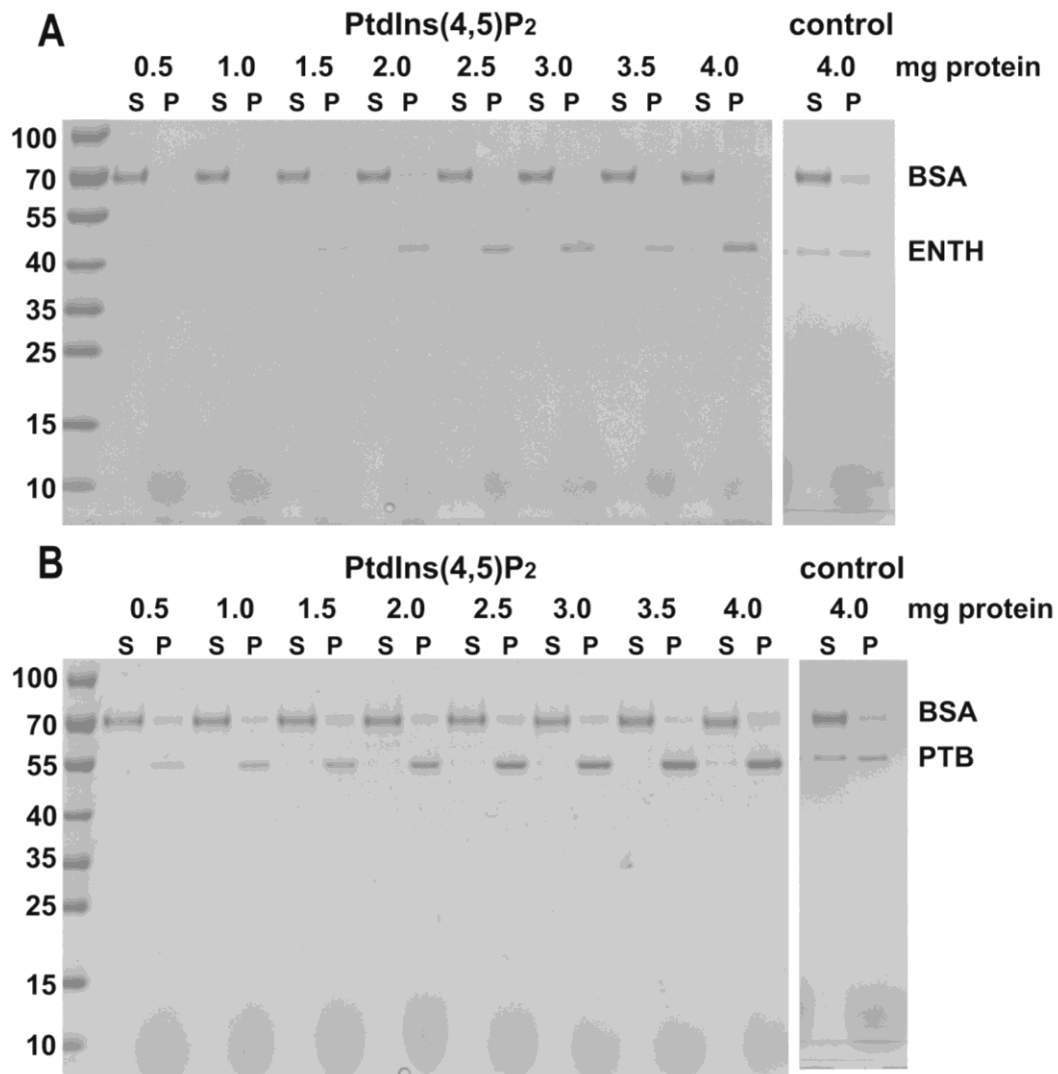
Figure 2.9 ENTH and PTB domain binding to PtdIns(4,5)P$_2$-containing and control liposomes.

Increasing concentrations of (A) ENTH-GST or (B) PTB-GST were incubated with control or PtdIns(4,5)P$_2$-containing liposomes at room temperature for 30 min. The liposomes were pelleted and aliquots of the supernatant and pellet (2.6% and 20% of total, respectively) were separated by SDS-PAGE and stained with Coomassie blue. ENTH and PTB both bind to PtdIns(4,5)P$_2$ containing liposomes in the pellet (P) fraction. ENTH and PTB are found in the pellet (P) and supernatant (S) fractions in control liposomes that do not contain PtdIns(4,5)P$_2$.

To quantitate CCP maturation, I fixed control or PIP5KIβ-overexpressing polarized MDCK cells and processed them for electron microscopy (EM). Blocks were sectioned perpendicular to the plane of the filter to visualize the apical and basolateral cell surfaces, and CCPs and vesicles identified and quantified as described in Methods. CCPs were classified as shallow (type I), invaginated (type II), or deeply invaginated (type III). Clathrin-coated vesicles within 1 micron of the membrane were classified as fully budded (type IV). Examples of each class and the distribution of apical and basolateral coated pits and vesicles within these classes are shown in Figure 2.11. Consistent with previous observations (9) I observed approximately 1.5 times more apical than basolateral CCPs per unit length of membrane in control cells (Table 2.1), however, the total number of pits identified was low, precluding rigorous statistical analysis. Nevertheless, the most striking difference I observed was a decrease in mature (Type III) pits at the apical surface of PIP5KIβ-overexpressing cells compared with control cells (Figure 2.11B). In combination with the TIRF data, this result is consistent with the interpretation that an increased rate of budding of apical CCPs may account for the stimulation of apical endocytosis I observed upon overexpression of PIP5KIβ in polarized kidney cells.
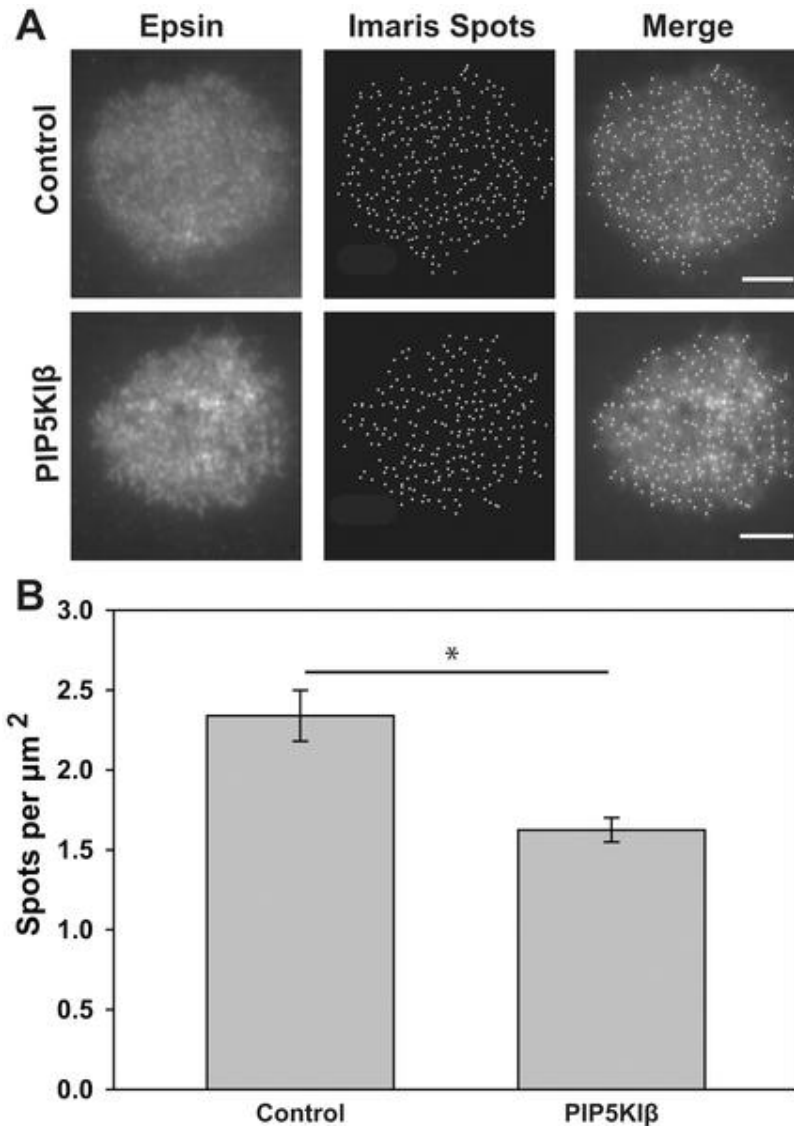
Figure 2.10 There are fewer apical CCPs in MDCK cells overexpressing PIP5KIβ.

MDCK cells were cultured on permeable supports and co-infected with adenovirus encoding epsin-GFP and either PIP5KIβ or control virus. Filters were fixed and processed to detect HA-tagged PIP5KIβ in order to determine which cells were overexpressing the kinase, then mounted in PBS for TIRF microscopy. (A) TIRF images of epsin-GFP in control and PIP5KIβ overexpressing cells are shown with corresponding detection of spots by Imaris. Scale bar: 5 μm. (B) Imaris analysis of TIRF data (n= 23 cells from three experiments) indicates that there is a decrease in epsin spots per square micron upon over expression of PIP5KIβ. Student's t-test was performed to assess statistical significance (*p<0.001).
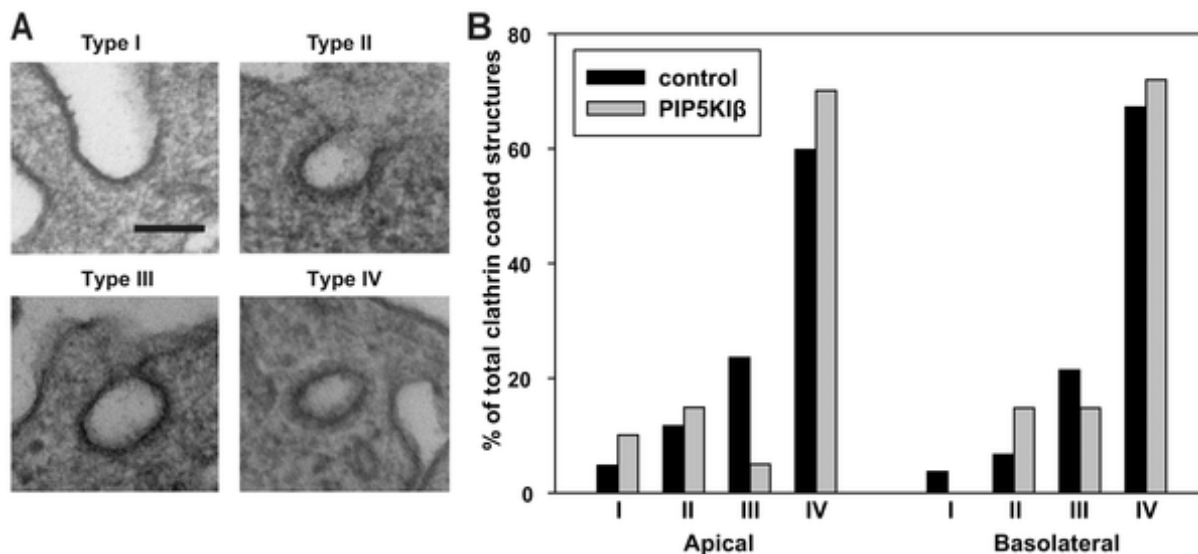
Figure 2.11 Apical CCP maturation is enhanced in PIP5KIβ-overexpressing cells.

MDCK cells cultured on permeable supports and infected with control adenovirus or adenovirus encoding PIP5KIβ were processed for electron microscopy. (A) Representative EM images show each of the stages of CCP maturation that were quantitated for analysis. Scale bar: 100 nm. (B) Analysis of data from 33 control cells and 35 PIP5KIβ-overexpressing cells shows a decrease in the frequency of type III CCPs upon overexpression of PIP5KIβ.

Table 2.1 Quantitation of clathrin coated structure distribution in MDCK cells.

MDCK cells cultured on permeable supports were infected with control or PIP5KIβ adenovirus and processed for electron microscopy. Clathrin coated structures were classified as shallow (type I), invaginated (type II), deeply invaginated (type III), or internalized and within one micron of the plasma membrane (type IV). Listed are the total number of clathrin coated structures counted of each type and the total length of membrane analyzed.

	Apical		Basolateral	
	Control	**PIP5KIβ**	**Control**	**PIP5KIβ**
Class I	2	3	1	0
Class II	5	5	2	9
Class III	9	2	6	5
Class IV	26	22	20	32
Total	42	32	29	46
Membrane length (μm)	1377	1585	1469	1408

39

2.3 DISCUSSION

Precise spatially and temporally regulated synthesis and conversion of phosphatidylinositol species are essential for their myriad functions in cellular homeostasis. Here I find that the three isoforms of PIP5KI, which together synthesize the majority of PtdIns(4,5)P$_2$ in cells, are differentially distributed along plasma membrane domains of polarized kidney cells and have access to distinct pools of substrate. Overexpression of PIP5KIβ, which is largely confined to the apical domain, selectively stimulated apical endocytosis of cargo. In contrast, basolateral endocytosis kinetics, which are faster than apical internalization rates, were unaffected by expression of any isoform. TIRF and EM imaging studies suggest that overexpression of PIP5KIβ increases the maturation efficiency of CCPs to generically stimulate apical internalization kinetics. Thus, availability of PtdIns(4,5)P$_2$ appears to be rate limiting for apical endocytosis. This finding has implications for understanding how apical endocytosis is regulated in response to physiological cues.

The localization of PIP5KIβ to the apical surface of mCCD cells and rat kidney tissue is consistent with previous reports which showed that overexpressed PIP5KIβ has an apical distribution in polarized kidney cells (8, 42, 145). PIP5KIγ localizes to the basolateral surface in polarized kidney cells, consistent with previous reports (42), as does PIP5KIα. While the signals that determine the distinct distributions of PIP5KI isoforms are not known, the differential localization of these enzymes suggests that they have different and non-redundant functions in polarized cell trafficking and/or signaling. In support of this, whereas overexpression of each of the three PIP5KI isoforms increased PtdIns(4,5)P$_2$ levels in non-polarized kidney cells, only

PIP5KIβ overexpression significantly affected PtdIns(4,5)P$_2$ levels in polarized cells. This suggests that PIP5KIα and PIP5KIγ cannot access the same substrate pools as PIP5KIβ. This was not surprising, given that overexpressed PIP5KIγ and PIP5KIα tend to localize to the basolateral domain of polarized mCCD cells. Thus, PIP5KIβ appears to be the primary enzyme responsible for synthesis of this pool in mCCD cells.

The concept that PIP5KI isoforms synthesize functionally distinct pools of PtdIns(4,5)P$_2$ is not new (160). As evidence of this, PIP5KIγ knockout (KO) reduced PtdIns(4,5)P$_2$ levels in the mouse brain by 40%, whereas PIP5KIα or PIP5KIβ KO had no effect (150, 161). In contrast, there was no change in PtdIns(4,5)P$_2$ in bone marrow macrophages derived PIP5KIγ KO mice, but there was a decrease in PtdIns(4,5)P$_2$ in PIP5KIα or PIP5KIβ KO macrophages (162-163). Additionally, overexpression of PIP5KIβ in HeLa cells led to an increase in PtdIns(4,5)P$_2$ levels, whereas expression of PIP5KIα and PIP5KIγ had no effect on PtdIns(4,5)P$_2$ (39). Moreover, PIP5KIγ appears to be selectively required for localized synthesis of PtdIns(4,5)P$_2$ in the uropod of primary neutrophils (164). Thus, the ability of PIP5KI isoforms to access distinct pools of PtdIns(4)P$_2$ is apparently cell-type specific.

The requirement for PtdIns(4,5)P$_2$ during multiple steps of the endocytic process has long been known (165), and several groups have confirmed that rapid depletion of PtdIns(4,5)P$_2$ upon acute targeting of PtdIns(4,5)P$_2$ 5'-phosphatase domains profoundly inhibits endocytosis (46-48). However, the role of individual PIP5KIs in modulating endocytosis in nonpolarized cells remains unclear and data from different laboratories or approaches are not necessarily congruent. Overexpression of PIP5KIγ in experiments by Bairstow et al. enhanced transferrin uptake in MDCK cells grown on plastic (42), whereas another group reported that overexpression of either PIP5KIα or PIP5KIβ but not PIP5KIγ stimulated transferrin uptake and increased CCP number

41

in CV1 cells (39). The same study found that siRNA mediated knockdown of PIP5KIβ (but not PIP5KIα or PIP5KIγ) in HeLa cells inhibited transferrin internalization kinetics (39). In contrast, a more recent study found that overexpression of PIP5KIα slightly inhibited transferrin endocytosis while paradoxically increasing CCP initiation and size (166). In yet another study, truncation of the kinase domain of PIP5KIα but not PIP5KIβ inhibited endocytosis of EGF receptors in NR6 cells (40). These discrepancies could arise from differences in cell type, changes in expression of endogenous isoforms upon overexpression, or knockdown of the others (39, 42). Alternatively, constitutive endocytosis kinetics or substrate levels may differ between cell types.

I found that overexpression of PIP5KIβ but not PIP5KIα or PIP5KIγ stimulated apical endocytosis of IgA via the pIgR, whereas none of these enzymes altered basolateral internalization kinetics of the same cargo. This result is consistent with myobservation that despite their partial localization to the apical surface, overexpression of PIP5KIα or PIP5KIγ had no significant effect on cellular PtdIns(4,5)P$_2$ levels in polarized cells. Because overexpression of PIP5KIβ increased PtdIns(4,5)P$_2$ levels but had no effect on the kinetics of pIgR endocytosis in nonpolarized cells, I conclude that PtdIns(4,5)P$_2$ levels may be rate limiting at the apical surface. Endocytosis in non-polarized cells is similar to endocytosis at the basolateral surface as it has rapid kinetics and is relatively unaffected by actin depolymerizing reagents (49). I hypothesize that increased PtdIns(4,5)P$_2$ has a generic effect on apical internalization because (1) internalization of several other cargoes that engage distinct adaptors is apparently stimulated in cells overexpressing PIP5KIβ (8, 155) and (2) I found no difference in the affinity of adaptor protein PtdIns(4,5)P$_2$-binding domains for PtdIns(4,5)P$_2$-containing liposomes.

Many laboratories have observed that endocytosis of the same cargo protein proceeds more slowly from the apical than the basolateral surface of polarized cells, suggesting that clathrin mediated endocytosis may be constrained by morphological features of the apical surface (7-11). Apical CCP formation is confined to the base of microvilli, and the lipid composition or high membrane curvature at that site could impede membrane deformation or remodeling necessary for CCP invagination. Indeed, Roth and colleagues previously showed that CCP maturation proceeds more slowly at the apical surface compared with the basolateral domain (9). Moreover, the local concentration of actin within the subapical terminal web and in microvilli could impede recruitment of endocytic machinery components or vesicle formation or movement. Kirchhausen and colleagues recently demonstrated that the tension at the apical membrane is the reason for the actin-dependence of apical endocytosis (49). PIP5KIβ-mediated changes in apical PtdIns(4,5)P$_2$ levels could generically stimulate apical endocytosis by alleviating several of these impediments. Locally elevated levels of PtdIns(4,5)P$_2$ could enhance binding of endocytic components to apical CCPs. Alternatively or in addition, dynamin-mediated fission or clathrin-coated vesicle transport through the actin-rich terminal web might be stimulated (56, 167). Vesicle transport could be promoted through an increase in actin polymerization or myosin recruitment. My studies do not identify whether one or multiple steps in endocytosis are affected upon PIP5KIβ overexpression, but support the notion that CCP maturation occurs more rapidly under these conditions. Apical TIRF imaging revealed a significant decrease in the number of apical CCPs in PIP5KIβ overexpressing cells. Additionally, the EM analysis suggested that PIP5KIβ overexpression leads to a decrease in mature pits and an

increase in budded pits at the apical surface, consistent with my TIRF findings. Further studies will be required to determine which step(s) of endocytosis are stimulated upon increased PtdIns(4,5)P$_2$ levels.

3.0   VAMP7 AND APICAL EXOCYTOSIS

3.1   INTRODUCTION

Epithelial cells elaborate specialized domains, including the apical and basolateral surface and primary cilia, which have distinct protein and lipid compositions required for proper cell function. Maintaining these domains requires efficient and selective SNARE-mediated fusion of vesicles containing newly synthesized and recycling proteins with the proper target membrane. Multiple pathways exist to deliver newly synthesized proteins to the apical surface of kidney cells and the post-Golgi SNAREs, or VAMPs, involved in these distinct pathways have not been identified. VAMP7 has been implicated in apical protein delivery in other cell types, and I hypothesized that this SNARE would have differential effects on the trafficking of apical proteins known to take distinct routes to the apical surface in kidney cells.

3.2   RESULTS

3.2.1   Expression of VAMP isoforms in canine kidney cells

Multiple VAMPs, including VAMP1, VAMP2, VAMP3, VAMP4, VAMP5, VAMP7 and VAMP8 are expressed in rat kidney (168-172). Of these, VAMP1, VAMP2, VAMP4, VAMP5, VAMP7 and VAMP8 were readily detected by RT-PCR of RNA isolated from polarized MDCK cells (Figure 3.1A). Surprisingly, there is no sequence homologous to VAMP3 (cellubrevin) in the canine genome. Moreover, by RT-PCR I was unable to amplify message from MDCK mRNA using primers targeting a completely conserved sequence in human, mouse, rat, orangutan, chimpanzee, gorilla, and macaque VAMP3. As a positive control, I confirmed that these primers efficiently amplified VAMP3 in HEK cells (Figure 3.1B).
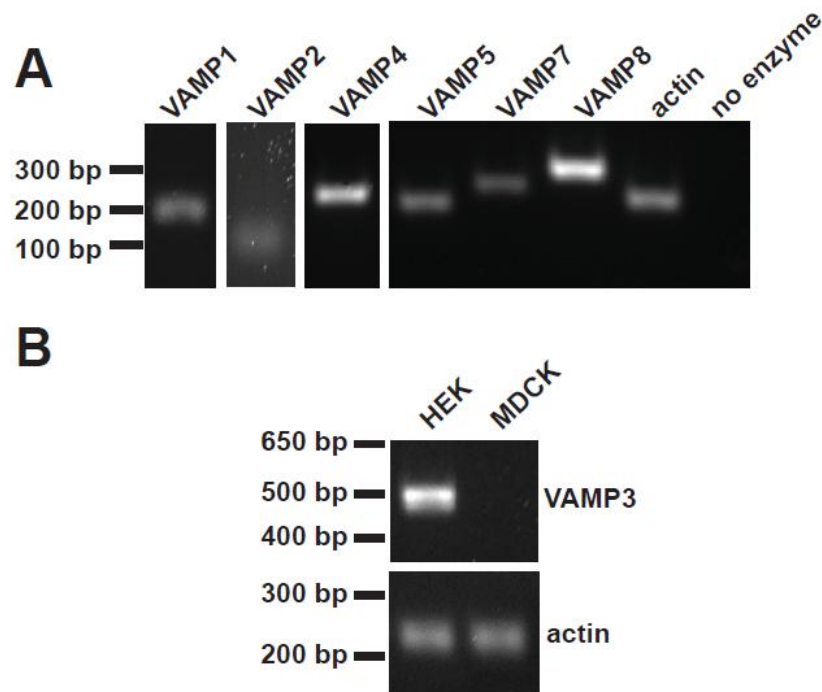
Figure 3.1 VAMP isoforms in MDCK cells.

(A) mRNA isolated from MDCK cells and converted to cDNA was subjected to PCR using primers designed to detect VAMP isoforms. VAMP1 (218 bp expected product), VAMP2 (101 bp), VAMP4 (244 bp), VAMP5 (216 bp), VAMP7 (261 bp), and VAMP8 (298 bp) were detected. (B) Primers designed against completely homologous regions of human, mouse, rat, orangutan, chimpanzee, gorilla, and macaque VAMP3 detected human VAMP3 (500 bp), but not canine VAMP3. Actin (231 bp) was detected as an additional control to ensure amplification of mRNA.

3.2.2 Subcellular localization of VAMP7 in MDCK cells

VAMP7 is associated with endosomes and lysosomes in many cell types, and I sought to confirm its localization in polarized MDCK cells. I was unable to detect endogenous VAMP7 in MDCK cells using commercially available antibodies, so I expressed low levels of tagged VAMP7 in these cells by transient transfection, then allowed the cells to differentiate on permeable supports prior to processing for immunofluorescence. Pearson's correlation coefficients were determined using Imaris software for each of these markers (Table 3.1). VAMP7 proteins modified by a cytoplasmic amino-terminal GFP tag (GFP-VAMP7) or by a lumenally-oriented carboxy-terminal HA epitope tag (VAMP7-HA) colocalized with one another when coexpressed, suggesting that neither tag disrupts the targeting of heterologously expressed VAMP7 (Figure 3.2A; Table 3.1). GFP-VAMP7 colocalized poorly with the Golgi marker giantin (Figure 3.2B; Table 1) or with markers of early endosomes (EEA1, GFP-Rab5; Figure 3.2C and 3.2D; Table 3.1) or the ARE (SNAP-Rab11a; Figure 3.2E; Table 3.1) in polarized cells. More colocalization was observed with the recycling endosome marker Rab4-GFP (Figure 3.2F; Table 3.1). The greatest extent of colocalization was observed with the lysosomal marker LAMP2 (Figure 3.2G; Table 3.1). I observed similar results in subconfluent MDCK cells (data not shown). The observed colocalization between VAMP7 and LAMP2 is consistent with previous studies, which reported that VAMP7 colocalizes with lysosomal markers Niemann-Pick C1, lysosomal glycoprotein 120, LAMP1, and CD63 (70-71, 80-85). VAMP7 was also shown to partially colocalize with the transferrin receptor [another marker of recycling endosomes (70, 82)].

Table 3.1 Colocalization analysis of VAMP7 and various organelle markers.

MDCK cells grown on transwells were transfected with VAMP7 constructs and co-transfected with tagged organelle markers, or stained for organelle markers. Imaris software was used to determine the Pearson's correlation coefficient between the markers. An R value of 1.0 would indicate perfect colocalization.

	Pearson's Correlation Coefficient
GFP-VAMP7 and VAMP7-HA	0.736 ± 0.108
GFP-VAMP7 and giantin	0.170 ± 0.060
GFP-VAMP7 and EEA1	0.151 ± 0.055
Rab5-GFP and VAMP7-HA	0.379 ± 0.188
Rab11a-SNAP and VAMP7-HA	0.351 ± 0.222
Rab4-GFP and VAMP7-HA	0.504 ± 0.099
GFP-VAMP7 and LAMP2	0.736 ± 0.108
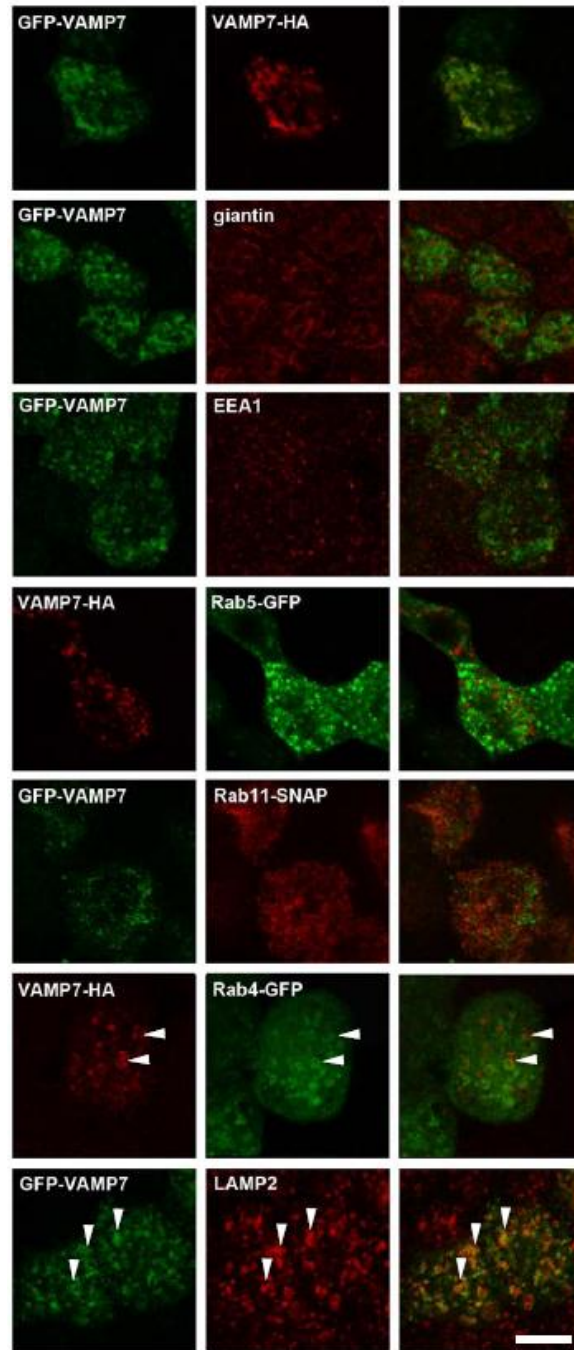
Figure 3.2 VAMP7 localization in polarized MDCK cells.

Polarized MDCK cells grown on transwells were transfected with GFP- or HA-tagged VAMP7 constructs and stained for the indicated endogenous proteins or co-transfected GFP- or SNAP-tagged organelle markers. (A) GFP-VAMP7 and VAMP7-HA colocalize with each other. Little colocalization is observed between VAMP7 and (B) giantin (Golgi), (C) EEA1 (early endosomes), (D) Rab5-GFP (early endosomes), or (E) Rab11a-SNAP. More extensive colocalization (marked by arrowheads) is observed between VAMP7 and (F) Rab4-GFP (recycling endosomes) and (G) LAMP2 (late endosomes and lysosomes).

3.2.3 VAMP7 knockdown has no effect on apical cargo delivery

Multiple pathways exist for newly synthesized proteins to reach the apical membrane of polarized cells (110). Endolyn traverses the Rab11-positive ARE *en route* to the apical surface, and is delivered to the apical surface via a pathway that requires the motor protein myosin Vb (113). In contrast, the lipid-raft-associated protein influenza HA is apparently excluded from the ARE (113). Soluble proteins also apparently enter the ARE but can exit via myosin Vb-dependent or independent pathways (111). Based on previous observations implicating VAMP7 in apical biosynthetic delivery (67-68), I hypothesized that VAMP7 may play a role in apical delivery of a subset of apical cargo in MDCK cells (111). To test my hypothesis I knocked down VAMP7 in MDCK cells and determined using biochemical approaches whether apical delivery of various membrane and secreted proteins known to take distinct routes to the surface is compromised. I tested the efficacy of multiple siRNAs targeting canine VAMP7 using RT-PCR to estimate the extent of knockdown. Of these, I selected a siRNA that consistently achieved ~80% knockdown of VAMP7 mRNA (Figure 3.3A). The efficiency of knockdown was confirmed by qPCR (not shown). Cells transfected with control or VAMP7 siRNA were plated on permeable supports for four days prior to quantitating the effect of knockdown on the kinetics of surface delivery using a pulse chase approach as described in Materials and Methods. Knockdown of VAMP7 had no effect on apical delivery of the lipid-raft associated protein influenza HA, which bypasses the ARE *en route* to the surface [Figure 3.3B, (113)], Similarly, I observed no effect of VAMP7 knockdown on apical delivery kinetics of the glycan-dependent protein endolyn, which traffics through the Rab11-positive ARE and is delivered to the apical surface in a myosin Vb-dependent manner [Figure 3.3C, (113)]. Additionally, I observed no

effect on the apical secretion of Ensol, a truncated version of endolyn that transits the ARE but unlike endolyn, does not require Myosin Vb for apical delivery [Figure 3.3D, (111)]. VAMP7 knockdown also had no effect on the kinetics or polarity of delivery of two other apically-destined proteins [the multiligand receptor megalin and secreted glycosylated growth hormone (111, 173); data not shown].
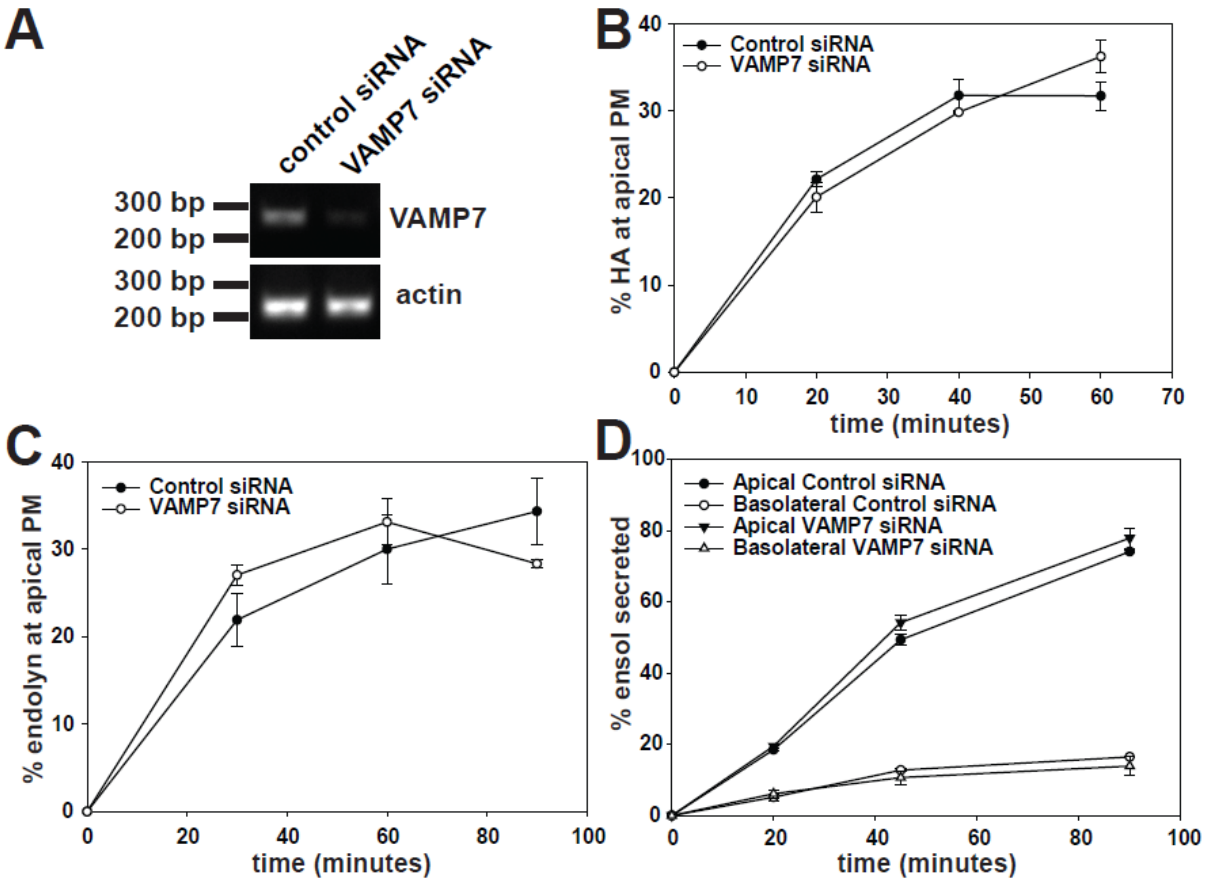
Figure 3.3 Knockdown of VAMP7 has no effect on apical secretion of lipid-raft associated, non-lipid-raft associated or secreted cargo.

(A) MDCK cells were transfected with an siRNA targeting VAMP7, and knockdown after 4 days was assessed using RT-PCR. A representative gel is shown. I routinely observed approximately 80% knockdown using this oligonucleotide. (B) The kinetics of HA (a lipid-raft associated protein) delivery to the apical surface of MDCK cells transfected with control or VAMP7 siRNA were quantitated using a cell surface trypsinization assay as described in Methods. Results from a representative experiment performed in duplicate are plotted (mean +/- range). Similar results were obtained in three experiments. (C) Endolyn (a non-lipid raft associated protein) delivery to the apical surface of MDCK cells transfected with control or VAMP7 siRNA was quantitated using a surface biotinylation assay as described in Methods. The results are a representative experiment (mean +/- range) of two experiments. (D) Ensol (a secreted protein) apical and basolateral secretion was measured in control and VAMP7 knockdown cells as described in Methods. A representative experiment (mean +/- range of duplicate samples) is shown. Similar results were obtained in five experiments.

3.2.4 VAMP7 knockdown decreases cilia length and frequency

The primary cilia of polarized kidney cells are specialized apical structures believed to function as mechanosensors that sense changes in flow to modulate downstream signaling pathways (174). Although little is known about how proteins traffic to this compartment, some ciliary proteins are thought to be delivered to the apical plasma membrane prior to reaching the primary cilium (175). Transport to the ciliary membrane may then occur by lateral diffusion across a septin barrier (142, 176). Because one of the VAMP7 cognate SNAREs, syntaxin-3, was found to be involved in ciliogenesis (132) I asked whether VAMP7 also has a role in this process. To this end, I transfected MDCK cells with control or VAMP7 siRNA, plated the cells on permeable supports, and processed them after four days for indirect immunofluorescence to detect the cilia marker acetylated tubulin (177). Images of randomly selected fields were acquired using an epifluorescence microscope, and cilia length and the percent of cells elaborating a primary cilium were quantified in randomly selected fields using ImageJ. As shown in Figure 3.4 (panels A, C, E), I found a statistically significant decrease in the median length of cilia in cells depleted of VAMP7 compared with control cells (Figure 3.4 C,E). Additionally, the fraction of cells expressing a primary cilium was significantly decreased (Figure 3.4 B,D). Similar results were obtained in the rat neuronal cell line PC-12 (Figure 3.5). In contrast, knockdown of VAMP8 had no effect on either cilia length or frequency (Figure 3.4 A,D).

To confirm that the changes I observed were due to a specific consequence of VAMP7 depletion rather than to an off-target effect of the siRNA oligonucleotide, I determined the effect on ciliogenesis of a second siRNA oligonucleotide (VAMP7 #2) that targets a different region of VAMP7 and knocks down the protein with lower efficiency (~50%, data not shown).

Transfection of MDCK cells with the VAMP7 #2 siRNA also led to a decrease in cilia length and frequency, but to a lesser extent than the primary siRNA, consistent with the reduced knockdown efficiency of this oligonucleotide (Figure 3.4B, D). Together, these data suggest that knockdown of VAMP7 causes a selective decrease in both cilia length and frequency.

Changes in cilia length have been linked to alterations in cell cycle and proliferation (136). Thus, I asked whether the effect of VAMP7 depletion on ciliogenesis could be due to changes in cell proliferation (143). Indeed, overexpression of the cytosolic fragment of VAMP7 has been shown to inhibit cytokinesis in BSC1 cells, resulting in multiploidy (178). My studies were performed using differentiated, superconfluent MDCK cells, the majority of which should be quiescent. To ensure quiescence, I serum starved MDCK cells transfected with control or VAMP7 siRNA for 48 h prior to quantifying cilia length and frequency. Similar to my normal conditions, knockdown of VAMP7 in starved cells resulted in a decrease in both of these parameters (data not shown). Additionally, to confirm that VAMP7 does not alter proliferation in my system, I quantitated the number of nuclei per field in control and VAMP7 knockdown cells by DAPI staining. In six experiments, I observed no significant difference (control average = 183 +/- 14 cells/field, VAMP7 KD average = 186 +/- 6 cells/field). Together, these data suggest that the effect of VAMP7 knockdown on ciliogenesis is not due to effects on the cell cycle.
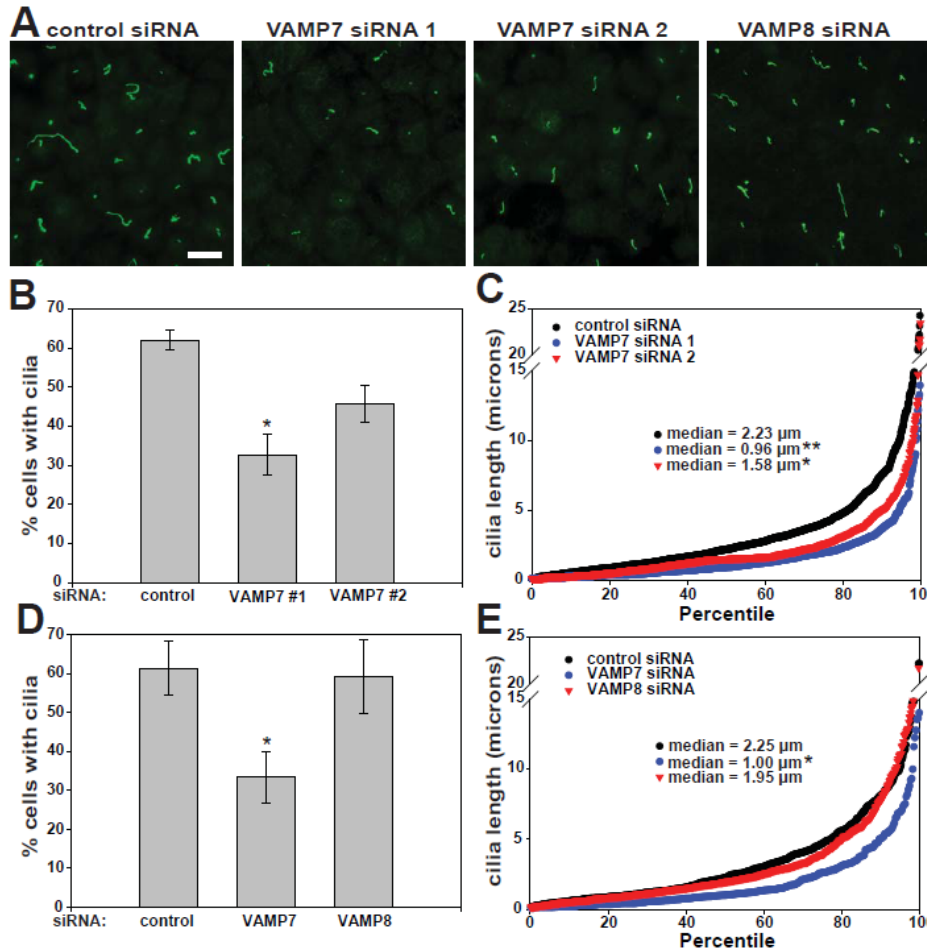
Figure 3.4 VAMP7 knockddown decreases cilia frequency and cilia length in MDCK cells.

(A) MDCK 2001 cells were transfected as indicated with control siRNA, our standard VAMP7 siRNA (VAMP7 #1), a less effective VAMP7 targeting sequence (VAMP7 #2), or VAMP8 siRNA. Cells were cultured for four days on permeable supports, then fixed and processed for indirect immunofluorescence to detect acetylated tubulin and cell nuclei. Representative fields acquired using epifluorescence microscopy are shown. Scale bar = 10 μm. (B, D) The number of cells in multiple fields was determined using DAPI nuclear stain and used to quantify the fraction of cells with a primary cilium in each sample. The average of three experiments is plotted (mean +/- SEM); *p < 0.05 compared to control using one-way ANOVA with Bonferroni correction. (B) Control n=1,907; VAMP7 n=1,747; VAMP7 #2 n=1,608 cells. (D) Control n=1,040, VAMP7 n=1,169, VAMP8 n=1,049 cells. (C, E) Cilia lengths in multiple fields were measured using ImageJ software, then sorted by length in ascending order and graphed by percentile (100th percentile= longest cilium in each sample). Each point on the graph represents the length of an individual cilium. (C) There was a statistically significant reduction in cilia length in cells transfected with VAMP7 #1 and VAMP7 #2 siRNAs, as assessed by comparing the medians from four experiments (*p < 0.05, **p < 0.01 using one-way ANOVA with Bonferroni correction). (E) There was a statistically significant reduction in cilia length in VAMP7 depleted cells, as assessed by comparing the medians from three experiments (*p < 0.05 using one-way ANOVA with Bonferroni correction).

56
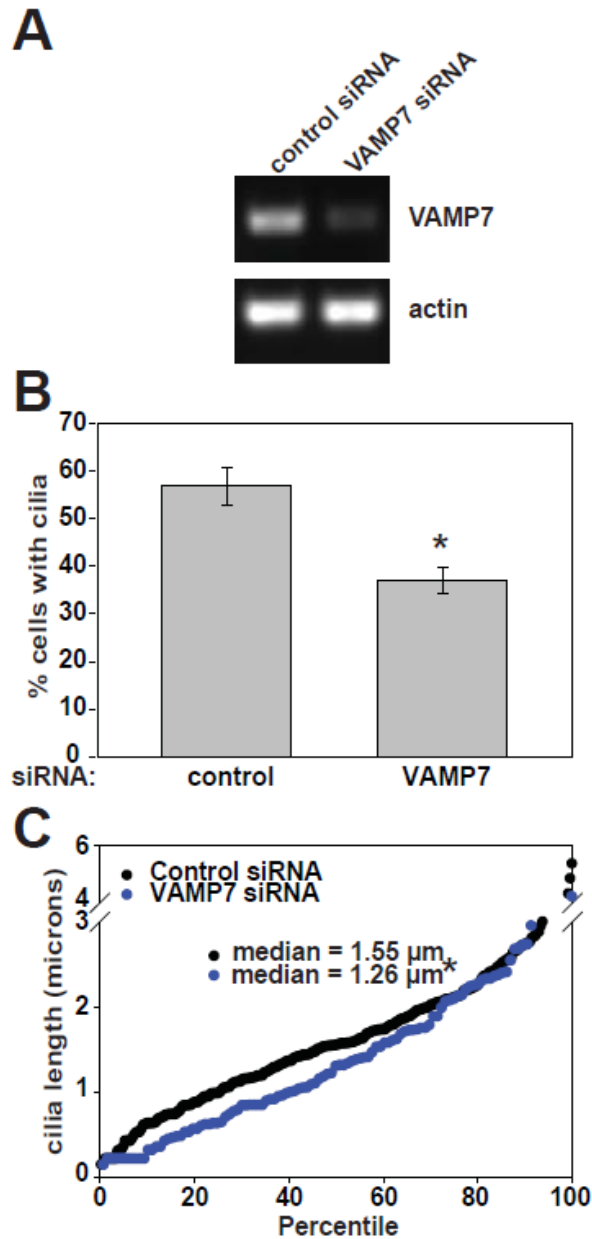
Figure 3.5. Cilia length and frequency in PC-12 cells.

PC-12 cells grown for 1 day after transfection were serum starved for 24 h then harvested for RT-PCR or fixed and stained for acetylated-tubulin and imaged on an epifluorescence microscope. (A) RT-PCR was used to estimate knockdown and about 70% reduction in mRNA was consistently achieved.). (B) The number of cilia was counted and the number of cells was determined by DAPI staining. The percent of cells with cilia was significantly decreased in three experiments (*$p < 0.05$ assessed by t-test). Control cells n=586, VAMP7 knockdown cells n=468. (C) Cilia were counted and measured using ImageJ software. Cilia lengths were sorted by length in ascending order and graphed by percentile as in Figure 3.4. The cilia length is significantly reduced by VAMP7 knockdown in three experiments (*$p < 0.05$ determined by Mann-Whitney Rank Sum Test).

3.2.5   VAMP7 expression modulates lysosome size

VAMP7 has previously been shown to play a role in the delivery of cargo from endosomes to lysosomes. Inhibition of VAMP7 function decreased EGF degradation in HeLa and reduced delivery of internalized dextran and BSA to lysosomes in MDCK cells and NRK cells, respectively (63, 71, 86). To test whether VAMP7 is important for lysosome biogenesis in MDCK cells, I modulated VAMP7 levels by overexpression of GFP-VAMP7 or by siRNA-mediated knockdown and examined the consequences on lysosome size. Overexpression of VAMP7 led to enlargement of LAMP2-positive organelles (Figure 3.6A, 3.6C) and reduced their number by 68 percent (data not shown). In contrast, knockdown of VAMP7 caused a reduction in the average volume of LAMP2-positive structures (Figure 3.6A, 3.6C), but increased the number of LAMP2 structures by 138 percent (data not shown). These data suggest that, similar to its role in other cell types, VAMP7 is involved in delivery to lysosomes in MDCK cells.
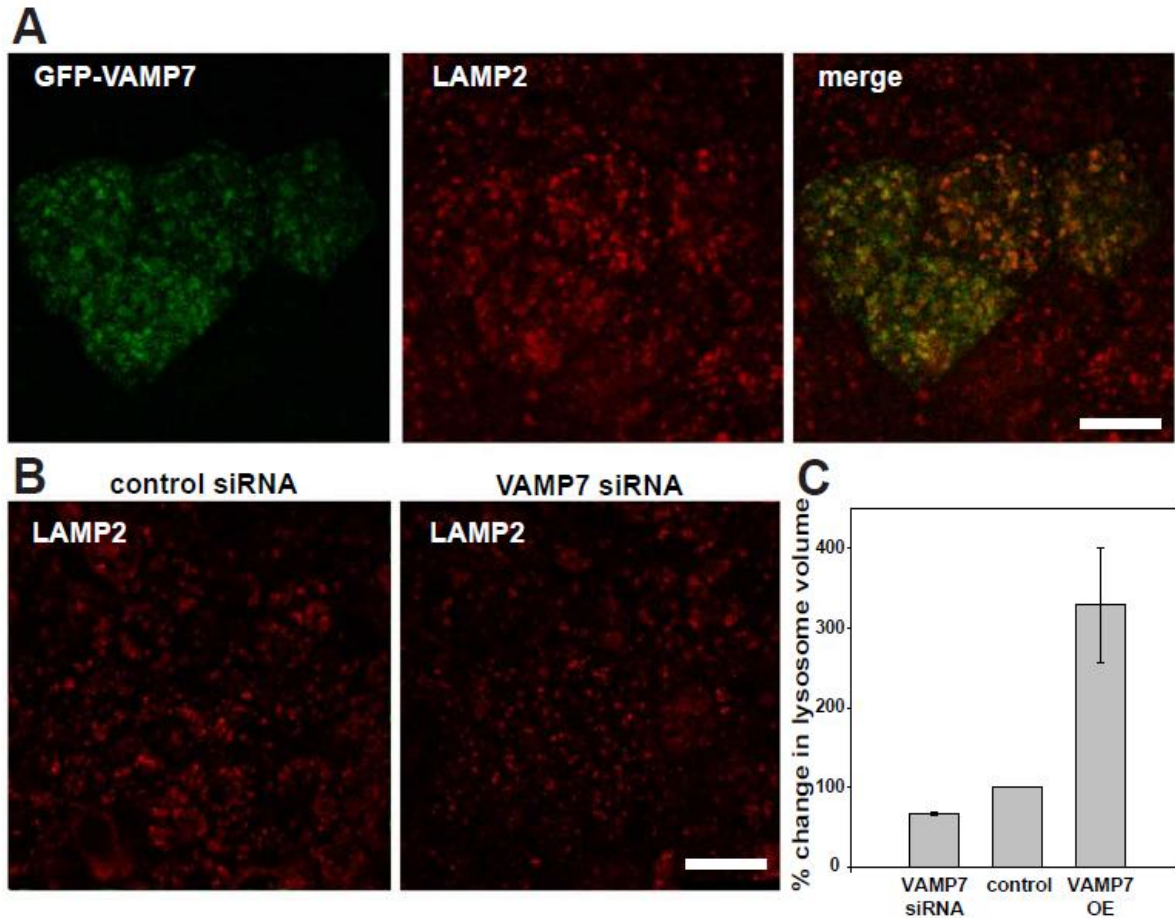
Figure 3.6 VAMP7 knockdown and overexpression alters lysosome size.

MDCK cells were transfected with cDNA encoding GFP-VAMP7 (A) or with control or VAMP7 siRNA (B) and processed for immunofluorescence to detect LAMP2 after four days. (C) Percent change +/- range of lysosome volume was quantitated using Imaris software as described in Methods. Compared to cells transfected with control siRNA, cells treated with VAMP7 siRNA had smaller LAMP2-positive structures compared to control. In contrast, VAMP7 overexpression (OE) led to an enlargement of LAMP2-positive structures. 10 fields from two experiments were quantitated.   Scale bars = 10 μm.

3.2.6 Perturbing lysosomes has no effect on cilia

I considered the possibility that the consequences of VAMP7 knockdown on lysosomal size/function and on ciliogenesis could be directly linked. In support of the latter possibility, siRNA mediated depletion of a protein implicated in the delivery of EGF to lysosomes (PTPN23) was also shown to result in fewer cilia in retinal epithelial cells (179-180). To test whether there is a connection between lysosome dysfunction and aberrant ciliogenesis, I examined cilia length in an MDCK model for lysosomal storage disease. Fabry disease is caused by mutations in the lysosomal enzyme α-gal A that prevents normal catabolism of globotriaosylceramide [Gb3; (181)]. Transfection of MDCK cells with an siRNA targeting α-gal A resulted in efficient knockdown of mRNA as assessed by PCR (89% reduction; Figure 3.7A) as well as in the dramatic increase in accumulation of Gb3 (measured using the anti-Gb3 antibody CD77; Figure 3.7B). VAMP7 levels in α-gal A knockdown cells were not different from control, as confirmed by qPCR (1.34 fold change; data not shown). α-gal A knockdown led to a 167% increase in lysosome volume (Figure 3.7C; data not shown). Neither cilia length (Figure 3.7D) nor frequency (Figure 3.7E) was significantly altered in α-gal A-depleted cells compared with controls, suggesting that there is no direct link between disrupted lysosome function and ciliogenesis.
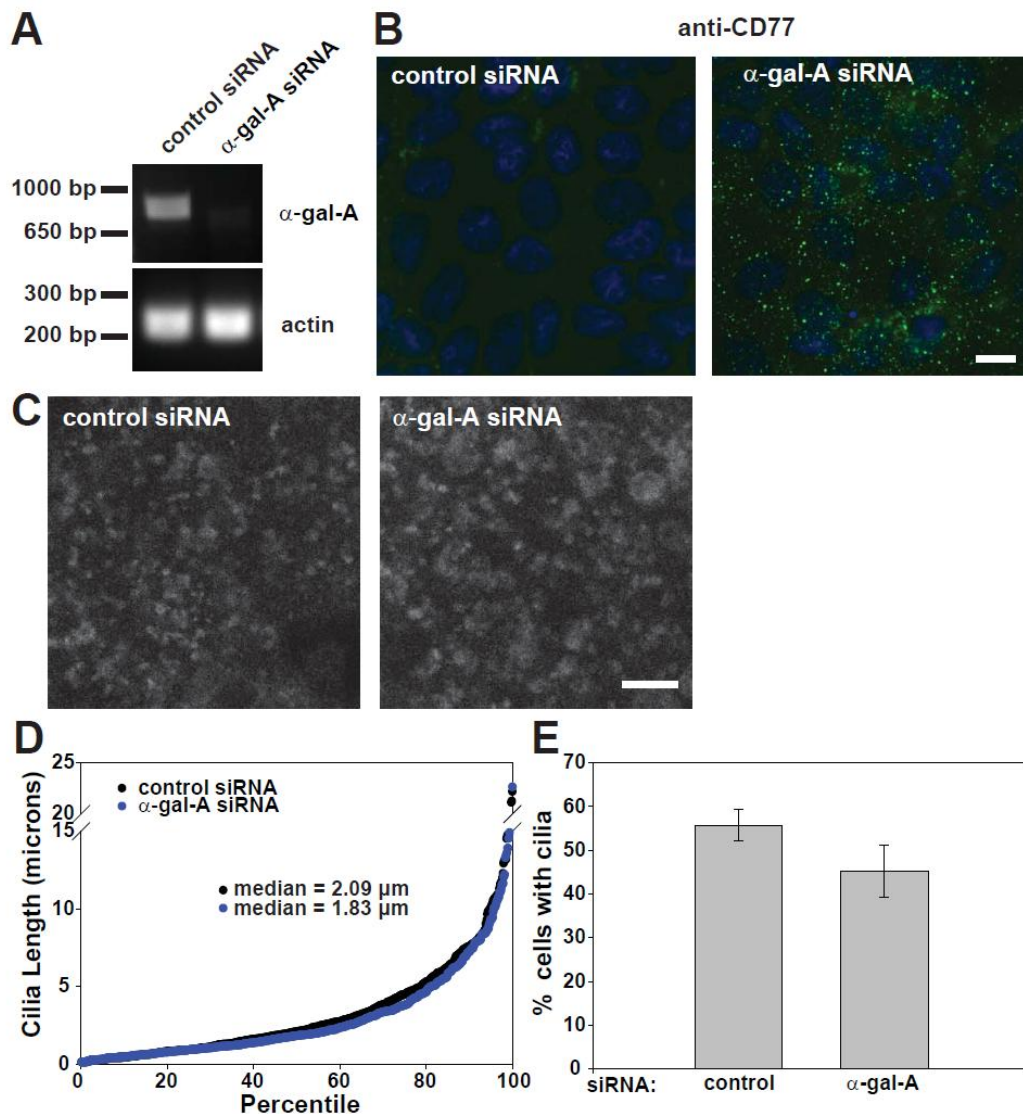
Figure 3.7 Perturbing lysosomes has no effect on ciliogenesis.

MDCK cells were transfected with control or α-gal A siRNA and cultured for four days on permeable supports, then harvested for (A) RT-PCR (expected products are 898 bp for α-gal A and 231 bp for actin) or (B-E) processed for immunofluorescence. (B) Knockdown of α-gal A caused a dramatic cellular accumulation of its substrate Gb3, as shown by indirect immunofluorescence using the anti-Gb3 antibody CD77. Scale bar = 10 μm. (C) Knockdown of α-gal A lead to an increase in late-endosome/lysosome size, and a decrease in the number of these structures, shown by indirect immunofluorescence of LAMP2. Scale bar = 5 μm. (D) Cilia were detected using anti-acetylated tubulin antibody, and cilia from random fields were measured and counted using ImageJ. The cilia were sorted by length in ascending order and graphed by percentile as in Fig. 4. (E) The number of cilia in each field was divided by the number of nuclei (identified using DAPI staining) and the mean +/- SEM of three experiments is shown. There is not a significant difference in cilia length or percent of cells with cilia in control and α-gal A siRNA transfected cells as assessed by t-test of the medians in three experiments. Data represent measurements from 1,535 cells for control siRNA and 1,407 cells for α-gal A siRNA-treated cells. Scale bar = 10 μm.

3.2.7   VAMP7 knockdown leads to aberrant cyst morphology

Many proteins that have been implicated in ciliogenesis also have a functional effect on cyst formation (104, 132, 177, 182-185). Thus, I tested whether knockdown of VAMP7 affects the formation of hollow cysts when MDCK cells are grown in a three-dimensional basement membrane Matrigel matrix for six days. Cells transfected with control siRNA predominantly formed cysts with a single hollow lumen (Figure 3.8A, 3.8B). In contrast, knockdown of VAMP7 led to a significant decrease in the number of normal lumens and an increase in the number of cysts with abnormal cysts with either no lumen or with multiple lumens (Figure 3.8A, 3.8B), though the majority of abnormal cysts had filled lumens. Knockdown of another R-SNARE, VAMP8, had no effect on cystogenesis, indicating that the effect is specific to VAMP7 (Figure 3.8A, 3.8B).   Additionally, α-gal A knockdown showed no change in cystogenesis indicating that the effect of VAMP7 on cystogenesis is independent of its effects on lysosome fusion. This suggests that the effect of VAMP7 knockdown on cilia length has functional consequences on lumen formation.
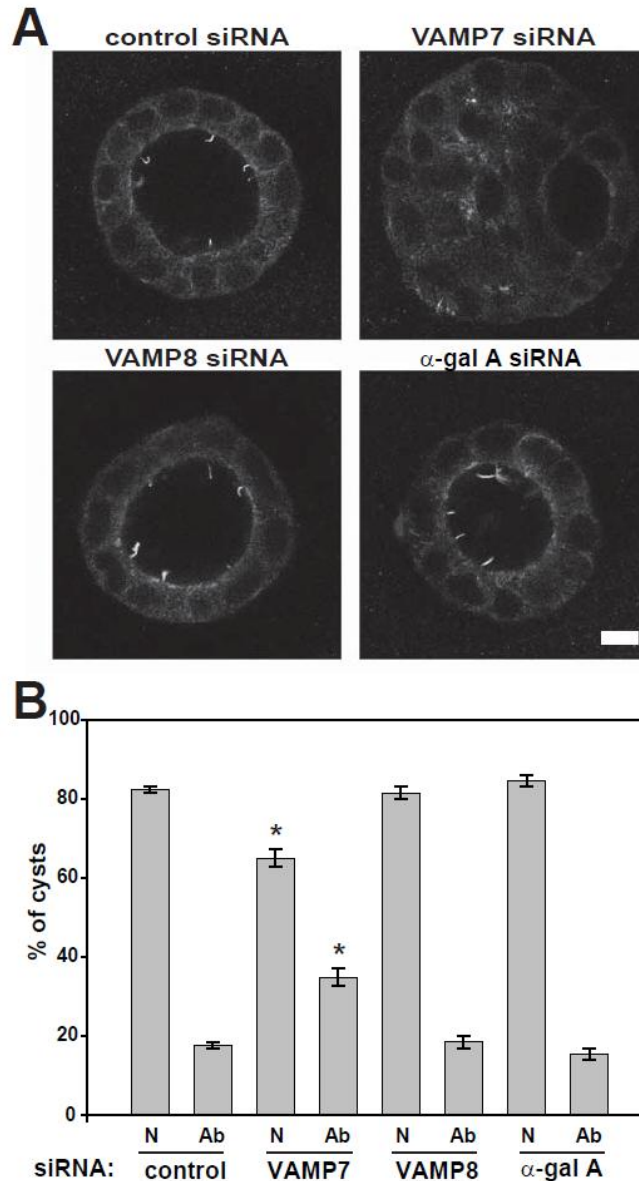
Figure 3.8 VAMP7 knockdown disrupts cyst morphology.

MDCK cells were transfected with control, VAMP7, VAMP8 or α-gal A siRNA as indicated, then trypsinized and resuspended in basement membrane matrix the following day. Six days later the cells were fixed and processed for immunofluorescence with anti-acetylated tubulin antibody to detect cilia. Confocal imaging revealed normal hollow lumens and cells with cilia projecting into the lumen in control, VAMP8 or α-gal A siRNA treated cells. However, transfection with VAMP7 siRNA led to an increase in the fraction of abnormal cysts with either filled lumens or multiple lumens. Representative examples are shown in (A). (B) One hundred cysts from each siRNA treatment were classified as normal (N) or abnormal (Ab) in three experiments. VAMP7 knockdown led to a significant increase in the number of abnormal cysts (*$p<0.001$ using one-way ANOVA with Bonferroni correction).

3.3   DISCUSSION

Individual SNARE proteins localize to distinct plasma membrane subdomains of polarized epithelial cells to provide specificity in vesicle fusion with these domains. Here, I investigated the role of VAMP7 in lysosomal and apical delivery in MDCK cells. I found that VAMP7 is predominantly localized to late-endosomes and lysosomes, and is partially associated with recycling endosomes. Both VAMP7 knockdown and overexpression altered the size and number of LAMP2-positive compartments, consistent with previous reports demonstrating a role for this SNARE protein in late-endosome-to-lysosome fusion. Though VAMP7 has been previously implicated in apical trafficking in several epithelial cell types, I observed no effect of VAMP7 knockdown on the delivery of a number of cargoes known to take distinct routes to the apical surface in MDCK cells. However, I did observe a significant reduction in the fraction of cells expressing a primary cilium as well as a decrease in mean cilia length upon VAMP7 knockdown. My results suggest that VAMP7 plays an important role in delivery to lysosomes and ciliogenesis in MDCK cells, but is not essential for surface delivery of apical proteins.

Using PCR, I found that mRNAs for the R-SNAREs VAMP1, VAMP2, VAMP4, VAMP5, VAMP7, and VAMP8, but not VAMP3 (cellubrevin) are endogenously expressed in MDCK cells. Curiously, there is no VAMP3 ortholog in the canine genome, nor was I able to detect VAMP3 mRNA by PCR using primers targeting highly conserved regions in multiple other species. VAMP3 is thought to play a role in polarized trafficking in rat kidney cells and hepatocytes (170, 172, 186). Endogenous VAMP3 localizes to the basolateral surface of hepatocytes, and follows the transcytotic pathway to the apical surface, suggesting it may be

involved in apical targeting in these cells (186). VAMP3 localizes to the subapical region of rat kidney cells and tetanus toxin, which cleaves VAMP1, VAMP2, and VAMP3, was shown to disrupt cAMP stimulated apical surface expression of the Na-K-2Cl cotransporter in the thick ascending limb of rat kidneys (172). Additionally, vesicles containing VAMP3 and the apical channel, aquaporin-2, were observed in the rat kidney (187). In contrast, heterologously expressed VAMP3 localized to the basolateral surface in MDCK cells (124) but was shown to access both apical and basolateral surface domains. Addition of tetanus neurotoxin caused mistargeting of basolateral proteins to the apical surface in MDCK cells, that could be rescued by expression of VAMP3 (124). Based on these data, I suggest the possibility that VAMP1 and/or VAMP2 are likely involved in basolateral trafficking in canine cells but that exogenous VAMP3 can compensate for loss of their function.

VAMP7 is unique among VAMPs in that it has an N-terminal extension of 120 amino acids termed the longin domain. There are two additional R-SNAREs with longin domains: Ykt6, and Sec22 (79). Intriguingly, these three longin domain-containing VAMPs are the only R-SNAREs that are conserved in all eukaryotes, suggesting that the longin domain may have essential functions in trafficking (79). Consistent with previous reports (63, 70-71, 80-86, 188), I found that VAMP7 localizes predominantly to LAMP2-positive structures that include late endosomes and lysosomes. VAMP7 localization to these compartments is mediated by the interaction of its longin domain with the adaptor protein AP-3 (82, 86, 189). AP-3 has also been implicated in the surface delivery of VSV-G (190), and in LAMP1, lysosomal integral membrane protein II and CD63 delivery to lysosomes (191-192). Although VAMP7 has been previously implicated in apical trafficking (60, 67-68) I observed no changes in the apical delivery of a number of proteins that take different routes to the surface. This is in contrast to

published data in MDCK cells showing that adding antibody against VAMP7 to permeabilized cells reduced the TGN to apical surface transport of HA (60). It is conceivable that sufficient VAMP7 remains after knockdown to enable apical delivery or that another VAMP with redundant function also operates in these pathways. Indeed, functional redundancies have made it difficult to sort out the SNAREs involved in a given transport pathway. For example, neither individual knockdown of VAMP1, VAMP2, VAMP3, VAMP4, VAMP5, VAMP7, or VAMP8, nor combined knockdown of VAMP3, VAMP4, VAMP7, and VAMP8 affected the exocytosis of growth hormone in neuronal C1 cells (193). In other instances, the role for a given VAMP in a particular trafficking step became evident only when the need for transport was exacerbated. For example, constitutive mucin secretion is normal in the lung of the VAMP8 knockout mouse, whereas a defect in mucous secretion could be observed after stimulation with IL-13 (194). It may be necessary to deplete multiple VAMPs or to somehow stress the secretory pathway upon VAMP7 knockdown in order to observe a defect in apical trafficking in MDCK cells.

The primary cilium is a specialized subdomain of the apical surface. My data show that VAMP7 plays an important role in ciliogenesis; however, I do not yet know its role in this process. The cilium is too narrow to accommodate transport vesicles and diffusion of proteins into the cilium is restricted by a large protein complex at the transition zone (195-197). Delivery of transmembrane proteins to the cilium is thought to happen in one of two ways. Some ciliary proteins are inserted first in the apical plasma membrane and then laterally cross the transition zone into the periciliary base, as has been observed for the Sonic hedgehog receptor, Smoothened (142). Alternatively (or in addition), some proteins are delivered directly to the periciliary base (176). From this region, membrane proteins are transported into the cilium by intraflagellar transport (IFT) mediated by IFT protein complexes that also contain motor proteins

(143). Future studies will be necessary to determine whether VAMP7 facilitates the transport of ciliary proteins to the apical surface and/or directly to the periciliary base.

Several known interacting partners for VAMP7 may contribute to its role in ciliogenesis. Similar to VAMP7, loss of its interacting partner syntaxin-3 has been shown to disrupt ciliogenesis (131-132). Another VAMP7 partner, SNAP25 (the neuronal-specific homolog of the ubiquitous SNAP23) localizes to cilia and has also been implicated in ciliogenesis (61, 131). It is not known whether SNAP23 is involved in ciliogenesis. Additionally, AP-3, which binds to the longin domain of VAMP7, also interacts with Septin-7, a cytoskeleton-associated GTPase localized at the ciliary base (195, 198). This interaction may localize VAMP7 to its site of function in ciliogenesis, in addition to its role in localizing VAMP7 to endosomes and lysosomes (82, 86, 189). Septin-7 knockdown caused a decrease in cilia length and number (198), suggesting that this septin may function in ciliary delivery at the transition zone. Future studies could confirm whether these proteins function together with VAMP7 to promote ciliogenesis.

Although defects in ciliogenesis and aberrant cyst formation are not conclusively linked, there are numerous studies that suggest a connection between these processes (104, 132, 177, 182-183). Loss of the VAMP7 cognate SNARE syntaxin-3 leads to defects in cilia length and in cyst morphology (184-185), though one study observed no effect of synatxin-3 knockdown in the latter process (132). It is conceivable that VAMP7 and syntaxin-3 pair during the processes of lumen formation. Future studies could confirm the link between ciliogenesis and cystogenesis.

My data suggest that there is not a direct connection between the effects of VAMP7 knockdown on lysosomal function and on the defects in ciliogenesis and cystogenesis that I observed. Knockdown of α-gal A, deficient in the lysosomal storage disorder Fabry disease, led to the cellular accumulation of Gb3 but caused no defect in ciliogenesis. This is consistent with

data showing that the pharmacological inhibitor concanamycin A, which blocks lysosomal acidification, had no effect on cilia length (180). However, knockdown of PTPN23, a protein tyrosine phosphatase implicated in delivery of EGF to lysosomes, was previously shown to decrease the fraction of cells elaborating a primary cilium (179-180). PTPN23 knockdown also led to decreased levels of transferrin receptor at the surface, likely due a recycling defect (180). It is possible that the effect of PTPN23 knockdown on ciliogenesis is related to its function in endosomal sorting rather than trafficking to lysosomes (180). This is an intriguing possibility considering that I found VAMP7 partially colocalized with Rab4-positive recycling endosomes, and a number of proteins involved in recycling have been implicated in ciliogenesis (179).

Together, my data suggest that protein delivery to cilia and lysosomes in MDCK cells is more heavily reliant on VAMP7 function compared with other pathways in which VAMP7 may be also involved. My studies do not reveal the precise role of VAMP7 in ciliogenesis, but support the idea that its functions in ciliogenesis and cystogenesis are independent of its role in lysosomal fusion. Further studies will be required to determine which step(s) in ciliogenesis require VAMP7.

4.0 FUTURE DIRECTIONS

4.1 THE FUNCTION OF PIP5KIB IN APICAL ENDOCYTOSIS

My studies raise new questions about the role of $PtdIns(4,5)P_2$ and PIP5KIβ in apical endocytosis. Future studies could address how $PtdIns(4,5)P_2$ modulates apical endocytosis and the physiological relevance of increasing or decreasing surface $PtdIns(4,5)P_2$ levels as a way to regulate polarized endocytosis.

I found no significant effect of overexpression of PIP5KIα and PIP5KIγ on endocytosis in polarized cells yet they are both active in non-polarized cells. This raises the question of whether basolateral endocytosis is not limited by $PtdIns(4,5)P_2$ levels. To address this, I could mistarget PIP5KIβ to the basolateral surface and measure the rate of endocytosis compared to control. However, this is challenging at present because the targeting signal is not known. A previous student, Shanshan Cui, tried to elucidate the targeting mechanism of PIP5KIβ without success. Dr. Cui found that neither the kinase domain nor $PtdIns(4,5)P_2$ were required for the apical localization of PIP5KIβ (199). However, it seemed that binding to lipid rather than proteins may be important for PIP5KIβ localization as increases in PIP5KIβ expression did not saturate its localization to the apical surface (199).

$PtdIns(4,5)P_2$ plays multiple roles in endocytosis. My data suggest that the increase in endocytosis upon overexpression of PIP5KIβ is due to an increase in the rate of maturation of

clathrin-coated pits. However, I do not know which specific step(s) in this process is stimulated. PtdIns(4,5)P$_2$ is involved in recruitment of clathrin adaptors and fission components, PtdIns(4,5)P$_2$ modulates actin dynamics as well as motor proteins. Any or all of these steps could potentially lead to an increased rate of endocytosis. One way to investigate this in more depth would be live-cell TIRF imaging. Looking at rate of appearance or disappearance of fluorescent actin, adaptors, and clathrin (52, 200-202) could be used to test effects of PIP5K overexpression in these steps.

My data showed that changes in PIP5KIβ lead to increases in apical endocytosis. This opens possibility that physiological modulation of PIP5K activity may be a way to acutely stimulate this process. There are a number of signaling proteins that have been shown to increase PIP5KI activity, such as Wnt (203) and PKA (204). It is not known whether endocytosis is stimulated in a PIP5KI dependent manner upon activation of these pathways. The rate of endocytosis could be monitored after activation of these pathways. If stimulation of endocytosis is observed, then PIP5KI isoforms could be knocked down to determine whether this inhibits stimulation of endocytosis. This would suggest that the signaling pathway acted upstream of PIP5KI to modulate endocytosis.

Although my work focused on how increased levels of PtdIns(4,5)P$_2$ synthesis affect endocytosis, it is likely that decreases in PtdIns(4,5)P$_2$ levels also modulate this process. One physiologically-relevant effect on PtdIns(4,5)P$_2$ in endocytosis may be GPCR signaling. For example, the purinergic receptor P2Y is expressed at the lumenal surface of renal cells. Upon activation of the P2Y receptor, the α and βγ subunits of the heterotrimeric G proteins dissociate and α goes on to stimulate PLC. Activated PLC cleaves PtdIns(4,5)P$_2$ into the 2nd messengers diacylglycerol and inositol trisphosphate. Diacylglycerol and inositol trisphosphate activate

70

protein kinase C and the release of calcium from intracellular stores, respectively. Carvou *et. al.* showed that stimulation of the P2Y receptor with ATP induces inositol phosphate production at 10 μM and plateaus around 300 μM in renal epithelial cells (34). PtdIns(4,5)P_2 hydrolysis mediated by GPCRs could affect endocytic processes. Indeed, PtdIns(4,5)P_2 hydrolysis leads to decreased endocytosis and decreased ENaC open probability (8, 205). One way to measure acute changes in endocytosis would be to monitor current in cells expressing a β-ENaC construct which contains mutations that increase the open probability and cause insensitivity to the ENaC inhibitor amiloride. Any changes observed in current would be due to endocytosis, rather than gating, of the channel.

I found that clathrin adaptors ARH and epsin have approximately the same affinity for PtdIns(4,5)P_2–containing liposomes *in vitro*. There could differences in recruitment *in vivo* due to interactions with other proteins. Additionally, decreases in PtdIns(4,5)P_2 may have different effects on recruitment of individual clathrin adaptors. During GPCR signaling events that lead to the hydrolysis of PtdIns(4,5)P_2, internalization of insulin was diminished but β2 glycoprotein I continued to internalize (34). These differences could be due to an effect on adaptor recruitment. Live-cell TIRF imaging could be used to visualize differences in adaptor recruitment upon decreasing PtdIns(4,5)P_2. However, for optimal quantitation of adaptor recruitment it would be best to have tagged genome-edited cell lines, as overexpression of clathrin and clathrin adaptors can affect dynamics of internalization (201-202).

4.2   THE ROLE OF VAMP7 IN APICAL EXOCYTOSIS

My studies raise new questions about the mechanism and functional significance of the role of VAMP7 in ciliogenesis. Future studies will determine the VAMPs involved in the diverse trafficking routes observed in kidney cells.

My data suggest that VAMP3 is not present in canine cells. Although VAMP3 has been implicated in basolateral trafficking, I do not know which VAMP is involved in this pathway in MDCK cells. Tetanus neurotoxin, which cleaves VAMP1, VAMP2 or VAMP3, caused mistargeting of basolateral proteins to the apical surface of MDCK cells (124). This suggests that VAMP1 or VAMP2 would be good candidates for a role in basolateral trafficking. Knockdown of these VAMPs would indicate if one or both is involved in this pathway.

I sought to identify the VAMPs involved in the diverse trafficking pathways to the apical surface in polarized cells. However, I found that VAMP7 [a likely candidate for a role in apical trafficking (60, 67-68)] knockdown had no effect on the trafficking of five apical proteins known to take distinct routes to the surface. Possibly, there was sufficient VAMP7 remaining after knockdown to promote apical delivery. To achieve better knockdown, an inducible lentiviral shRNA stable cell line could be generated. Alternatively, a redundant VAMP may be functioning in this pathway. Combinatorial knockdown of multiple VAMPs would elucidate the presence of a redundant VAMP. As observed for VAMP8 (194), it may be necessary to stimulate the biosynthetic pathway to see changes in apical delivery upon VAMP7 knockdown. Overexpression of PIP5KI stimulated the kinetics of apical delivery of the lipid-raft protein, hemagglutinin (145). This may be a way to determine the VAMPs involved in delivery of lipid-raft associated proteins. However, it could prove difficult to stimulate the delivery of other biosynthetic pathways in which a mechanism for stimulation has not been identified.

72

The observation that knockdown of VAMP7 leads to a decrease in cilia frequency and length is surprising considering that the VAMP7 knockout mice have no phenotype commonly associated with ciliopathies. Also, polymorphisms in the *SYBL1* gene lead to bipolar disorder, which has not been linked to ciliary defects. One reason for this discrepancy could be differences in VAMP expression. It is conceivable that there may be varying levels of VAMP gene expression in different species, different organs, or different stages in development. For example, VAMP7 might be critical for ciliogenesis in the canine but not murine kidney. qPCR analysis or Western blotting of multiple cell types and developmental stages could be used to determine differences in gene expression and protein levels of VAMPs.

Alternatively, bipolar disorder could represent a novel ciliopathy. Specific dopamine and serotonin receptors that are implicated in bipolar disorder signaling localize to the primary cilia of neurons (206-208). Reduction of DISC1 (disrupted in schizophrenia), which is implicated in schizophrenia and bipolar disorder, leads to a decrease in the number of cilia in fibroblasts and neuronal cells (206). Additionally, a recent paper suggested that spinocerebellar ataxia type 11, a neurodegenerative disorder, may also be a novel ciliopathy (209). VAMP7 interacts with syntaxin-3 (67) as well as with the Qbc-SNARE SNAP25 (87, 90), which have both been implicated in ciliogenesis (61, 131-132). Interestingly, SNAP25 levels are altered in patients with schizophrenia (210-212) as well as bipolar disorder (210). Considerable research would need to be done to implicate bipolar disorder as a ciliopathy. Determining cilia length in the neurons of control versus VAMP7 knockout mice might provide a clue as to whether the VAMP7 knockout mouse anxiety phenotype could correspond to cilia length.

Although I found a role for VAMP7 in ciliogenesis, I do not yet know which step in the process VAMP7 regulates. There is evidence for a Rab-GTPase cascade in ciliogenesis.

Rab11a was observed to concentrate near the base of the cilium (127). Rab11 stimulates the GEF activity of Rabin8 (127), which leads to the localization of Rab8 to the base of the cilium (213). If VAMP7 associated with Rab11 or Rab8 vesicles, this would suggest a role for VAMP7 in early or late ciliogenesis, respectively. However, the studies of Rabs in ciliogenesis were conducted in retinal epithelial cells and it is not known whether this pathway is conserved in kidney cells.

5.0   MATERIALS AND METHODS

5.1   RT-PCR AND QPCR

Ambion RNAqueous phenol-free total RNA isolation kit was used to extract RNA. One μg of

RNA, 2 μl of Oligo(dT)Primer (Ambion) and nuclease-free water in a total volume of 12 μl was

mixed gently, heated for 3 min at 72°C, and placed immediately on ice. After centrifuging

briefly, 2 μl of 10x RT buffer (Ambion), 2 μl 2.5mM dNTP mix (Invitrogen), 0.5 μl of RNAse

inhibitor (Ambion), 0.5 μl Moloney Murine Leukemia Virus Reverse Transcriptase (MMLV-RT;

Ambion) enzyme (or water for control), and 2 μl nuclease-free water were added and the sample

was incubated at 42°C for 1 h, followed by 92°C for 10 min to inactivate the RT enzyme. A 3 μl

aliquot of this reaction was mixed with 2.5 μl of 10 μM sense and antisense primers, 5 μl of 10x

PCR buffer, 0.5 μl of enzyme (GeneAmp High Fidelity), 5 μl of DMSO, and 26.5 μl of PCR

grade water, placed into a 0.6 ml thin walled tube, and incubated in a Bio-Rad thermocycler. The

cycle started at 95°C for 1 min and the following steps were then repeated 25 times: 95°C for 30

sec, 58°C for 30 sec, 72°C for 30 sec, followed by a single incubation at 72°C for 5 min and a

hold at 4°C. Fifteen μl of the reaction mixture was electrophoresed on a 2% agarose gel. The

primer sequences used were as follows: actin 5'-ACCTTCAACTCCATCATGAAG-3' and 5'-

CTGCTGGAAGGTGGACAG-3', mouse PIP5KIα 5'-CACTGTCTCCCCTTCCTCTG-3' and

5'-AGGAACAATGTCCAGCCAGT-3', mouse PIP5KIβ 5'-AACTTCCCCCACTGCAGAAT-

3' and 5'-GTCTTCATGGTCAGCAAGCA-3', mouse PIP5KIγ 5'-AAGGAGGAGGGTGCAGGAGT-3' and 5'-GGGAGGGAGAACAAGGTT-3', canine VAMP1 5'-ACAGCAAACCCAGGCACAAGTGG-3' and 5'-TGGCACAGATAGCTCCCAGCAT -3', canine VAMP2 5'-TGGAGCGGGACCAGAAGCTGT-3' and 5'-TTTGCGCTTGAGCTTGGCTGC-3', highly conserved VAMP3 5'-TGCTGCCACTGGCAGTAATC-3' and 5'-AGGCACTGTGCAAAATGTGG-3', canine VAMP4 5'- ACCGCGCTTGATTTGGTGACA-3' and 5'-GGCAAAACAGAGGCTGGTTATCTGC-3', canine VAMP5 5'-GCTCCACATGCCCAGGACGC-3' and 5'-TGCCCTCAAGGGCCAGTCTGT-3', canine VAMP7 3'-AGTGGTGGAGACTCAAGCCCA-5' and 5'-ATCCACCACAGAGAGGTGACACA -3', canine VAMP8 5'-TTTCGCCACCCATGCCATCCC-3' and 5'-ACCGGCCACCATCAGTGTCCT-3', rat VAMP7 5'-GTTGCCAGGGGAACCACTAT-3' and 5'-GCCAGAACGCTCGAAAACTC-3', and α-gal A 5'-TGTGCAACGTTGACTGCCAAGAAG-3' and 5 '-TCCTGCAGGTTTACCATAGCCACA-3'. For qPCR RNA was extracted and converted to cDNA. Express SYBR-GreenER Kit (Invitrogen) was added to triplicate samples of cDNA and primers. SYBR-Green illumination was detected by a 7900HT Fast Real-Time PCR System with thermal cycling controlled by SDSv2.3 software (Applied Biosystems). The primer sequences used for qPCR were as follows: actin 5'-GATCAAGATCATCGCACCCC-3' and 5'-ACAGTCCGCCTAGAAGCATT-3', canine VAMP7 5'-GGAGGATTTTGAACGTTCCCG-3' and 5'-GATGCTTCAACTGTGCAGCC-3', canine VAMP8 5'-GATCTGGAAGCCACATCGGA-3' and 3'-GTGGCGAAAAGCACGATGAA-3', canine

76

CathepsinD 5'-CACTGAAGGTTTCGCAAGGC-3' and 5'-AACACGGTGTAGTAGCAGCC-3', α-gal A 5'-TCTTGGCCTGGACATCTTCT-3' and 5'-TCACTAGCATATCTGGGTCGT-3'.

5.2   DNA AND RECOMBINANT ADENOVIRUSES

Constructs encoding the glutathione S transferase (GST) tagged phosphotyrosine binding (PTB) domain of mouse Dab2 (residues 1–205) (214) and the GST tagged epsin N-terminal homology (ENTH) domain of rat epsin (residues 1–162) were provided by Dr. Pietro de Camilli (via Dr. Linton Traub) (215). Rat Epsin-GFP was a gift from Dr. Pietro De Camilli (via Dr. Linton and the GFP tag was made monomeric by our lab by mutating position A206K. Epsin-GFP and was subcloned into the pAdtet vector. In this manuscript, I use the accepted convention of human nomenclature for murine PIP5KIβ and PIP5KIα, but note that our previous publications used the reverse mouse nomenclature (8, 42, 145). Recombinant adenoviruses were generated from epsin-GFP and PIP5KI isoforms as described previously (145, 216-217). Generation of control non-expressing (M2-Rev) and transactivator adenoviruses was described previously (218). Transactivator is required for expression from our doxycycline-repressible adenovirus constructs and was provided by co-infection of transactivator-expressing adenovirus or by using cells that stably express transactivator (see below). Generation of replication-defective recombinant adenoviruses encoding influenza HA, endolyn, and Ensol are described in (111, 216-217, 219) GFP-VAMP7 was kindly provided by Sergio Grinstein. VAMP7-HA was generated from full length human VAMP7 pCMV Sport6 cDNA (Thermo Scientific clone ID 6503665). The open reading frame was amplified using PCR with 5'-CACCATGGCGATTCTTTTTGCTGTTGTTGC-3' and 5'-

CTAAGCGTAGTCTGGGACGTCGTATGGGTATTTCTTCACACAGCTTGG-3' primers and inserted using pcDNA3.1-TOPO kit (Invitrogen). Rab4-GFP and Rab5-GFP were a gift from Jim Goldenring. Rab11a from Jim Goldenring was SNAP tagged by PCR amplified then subcloned into the BamHI and XhoI sites of pSNAP-tag(m) vector using the following primers: 3'-TAG GGATCCATGGGCACCCGCGACGACGA-3' and 5'-CTAGCTCGAG CTAGATGTTCTGACAGCACT-3'.

5.3   CELL CULTURE AND ADENOVIRAL INFECTION

mpkCCDc14 cells (mCCD cells) derived from the cortical collecting ducts of SV40 transformed mice (220) were provided by Dr. A. Vandewalle via Dr. John Johnson. Cells were cultured in Dulbecco's modified Eagle's medium (DMEM)/Ham's F12 with 5 μg/mL insulin, 0.02 μg/mL dexamethasone, 0.01 μg/mL selenium, 5 μg/mL transferrin, 2mM L-glutamine, 10-9 M triiodothyronine, 20mM HEPES, 2.2 % D-glucose, 2% FBS, 100 units/mL penicillin, 100 μg/mL streptomycin. For adenoviral infection, mCCD cells were cultured for three days on 12-mm Transwells (0.4-μm pore; Costar, Cambridge, MA), rinsed extensively with PBS and incubated for 1 h at 37°C on 50 μl drops of PBS containing recombinant adenoviruses and 150 μl of PBS/virus on the apical surface of the Transwell, using a total multiplicity of infection (MOI) of 125. Recombinant adenovirus encoding the constitutive expression of the tetracycline-repressible transactivator at a MOI of 50 was included in all experiments to enable doxycycline (DOX) repressible synthesis of HA-tagged PIP5KI isoforms. For endocytosis experiments adenovirus encoding the rabbit polymeric immunoglobulin receptor (pIgR) was also included at a MOI of 50. Following infection, mCCD cells were incubated in complete media supplemented with 20

ng/ml DOX for 24 h. Subsequently, cells were rinsed in complete media and incubated for 16 h in the absence of DOX to allow for expression of PIP5KI constructs. Where indicated, experiments were performed using Madin-Darby canine kidney (MDCK) T23 cells, which stably express pIgR as well as the tetracycline transactivator. These cells were cultured in Minimum Essential Medium (Sigma) supplemented with 10% FBS. Filter-grown cells were infected for 1 h at 37°C with 150 μl of PBS/virus added to the apical surface of the Transwell, using a MOI of 125 for control and PIP5KIβ virus and a MOI of 10 for epsin-GFP virus. Cells were used for experiments the day after infection. PC-12 cells, generously provided by Manojkumar Puthenveedu, were grown in DMEM with 5% FBS and 10% horse serum. MDCK T23 cells were used for delivery assays and the MDCK T23 parental cell line MDCK 2001 was used for experiments measuring cilia length.

5.4 INDIRECT IMMUNOFLUORESCENCE

Cells were fixed with 4% paraformaldehyde in 100 mM sodium cacodylate pH 7.4 at 37°C for 15 min, quenched in PBS with 20 mM glycine and 75 mM NH$_4$Cl for 5 min, permeabilized using 0.1% TritonX-100 in the quench solution for 10 min with gentle shaking, and blocked in PBS with 1% BSA and 0.1% saponin for 1 h at ambient temperature. Virally expressed PIP5KI isoforms were detected using anti-HA epitope tag antibody (Covance; 1:500). Rat anti-ZO-1 hybridoma R40.76 culture supernatant was used to detect ZO-1 (221). Rhodamine-Phalloidin (Life Technologies; 1:500) was used to visualize actin. Polyclonal anti-giantin was a gift from Adam Lindstedt, EEA1 (BD; 1:1000), LAMP2 AC-17 was a gift from E. Rodriguez-Boulan, anti-HA tag (Covance; 1:500) was used for HA tagged proteins. TMR-STAR (New England

Biolabs; 3 μM final concentration) was used to label SNAP tagged proteins. AlexaFlour conjugated secondary antibodies were from Invitrogen and used at 1:500. Samples were mounted in ProLong Gold Antifade with DAPI (Invitrogen). Confocal images were acquired on a Leica SP5 confocal microscope (100x/1.5 NA objective) and processed using Adobe Photoshop. To determine Pearson's Correlation Coefficient, confacal stacks were opened in Imaris and a median filter (3x3x1) was applied. Images were subjected to automatic thresholding using the method from (222). A region of interest was selected for calculation of colocalization using the Imaris Coloc function.

5.5   IMMUNOFLUORESCENCE OF RAT KIDNEY SECTIONS

Rat kidney cryosections (4-μm thick) were obtained from Dr. Nuria Pastor-Soler and processed as described in (223). Briefly, sections were fixed, then rehydrated in PBS for 30 min and treated with 1% SDS for 4 min, washed with PBS and then blocked with 1% BSA. Sections were then incubated with PIP5KIβ antibody (Abnova; 1:100) for 75 min, washed with high-salt PBS (2.7% NaCl), followed by PBS, and then incubated with secondary antibody Alexa-Flour 488 (Life Technologies; 1:400) for 1 h. The wash steps were repeated then the sections were mounted in Vectashield (Vector labs). Slides were imaged on a Leica SP5 confocal microscope.

5.6   QUANTITATION OF CELLULAR PTDINS(4,5)P$_2$

Cells were labeled with ^{32}P-orthophosphate, and phospholipids were extracted and analyzed by thin layer chromatography (TLC) essentially as described in (8). Briefly, mCCD cells plated in 12-well Transwells or on plastic were co-infected with adenoviruses encoding TA (MOI 50) and the indicated PIP5KI isoform (MOI 125). The cells were incubated for 30 min in phosphate- free DMEM and then for an additional 15 min in PBS with 1 mM MgCl$_2$ prior to radiolabeling for 4 h with 40 μCi/ml ^{32}P-orthophosphate. Next the cells were trypsinized, 1 ml of chloroform:methanol:1N HCl (4:3:3) was added to the pelleted cells, and the mixture was vortexed and centrifuged at 1500 rpm for at 4°C for 7 min. The organic phase was collected and washed twice with an equal volume of MeOH:1N HCl (1:1). Radioactivity in aliquots was counted using a scintillation counter, and equal counts/min of each sample were spotted onto oxalate-treated Silica gel 60 TLC plates (EM Science) and developed in 1-propanol:2M acetic acid (65:35). Authentic lipid standards (Avanti Polar Lipids) were included on all plates. Radiolabeled products were visualized and quantified using a phosphorimager. The percent of total was quantified by dividing the intensity of the PtdIns(4,5)P$_2$ spot relative to the total acidic phospholipids (phosphatidic acid, phosphatidylinositol, phophatidylinositol phosphate, and phosphatidylinositol 4,5-bisphosphate).

5.7   ENDOCYTOSIS OF IGA

Human polymeric IgA (Nordic) was iodinated as described in (224-225). Approximately 2 mCi Na^{125}I (Perkin-Elmer) was used to iodinate 40 μg of IgA in a final volume of 600 μl. mCCD

cells were plated in 12-well Transwells and infected with pIgR, TA, and PIP5KIβ, PIP5KIα or PIP5KIγ adenovirus as described above. The next day each Transwell was incubated with approximately 160 ng ^{125}I-IgA for 1 h in media MEM/BSA (MEM, HBSS, 0.6% BSA, 20 mM HEPES, pH 7.4) on ice, then washed extensively with ice cold media MEM/BSA to remove unbound radioligand. The cells were then incubated in pre-warmed media at 37°C for 0, 2.5, or 5 min, then rapidly chilled. To remove ^{125}I-IgA from the cell surface, cells were incubated for 30 min at 4°C with 100 μg/ml L-1-tosylamide-2-phenylethylchloromethyl-ketone-treated trypsin (Sigma), then stripped with 150 mM glycine buffer, pH 2.3 for 15 min at 4°C. Filters were cut out of their plastic inserts and cell-associated radioactivity was counted using a gamma counter (PerkinElmer) Internalized ^{125}I-IgA was quantitated relative to total ^{125}I-IgA (recovered in the cells, trypsin and glycine strips, and the incubation medium).

5.8   RECYCLING OF IGA

Recycling assays were performed essentially as described in (226). Briefly, mCCD cells were co-infected with pIgR, TA, and PIP5KIβ adenovirus. The following day cells were incubated with ^{125}I-IgA at 37°C for 45 min in MEM/BSA. Cells were extensively washed using cold MEM/BSA on ice, then pre-warmed MEM/BSA was added to the apical and basolateral chambers and cells were kept in a 37°C water bath. At each time point the media was collected and replaced with fresh media. After the last time point the filters were removed from their inserts and radioactivity in each media and filter sample was determined using a gamma counter and the fraction of IgA recycled at each time point was quantitated.

5.9   PROTEIN PURIFICATION

GST fusion proteins were expressed in *E. Coli* BL21 cell cultures at 37°C until log phase (OD600=0.6), at which time the cultures were transferred to ambient temperature and isopropyl-1-thio-β-D-galactopyranoside (100 μM) was added. After 3 h of shaking, the culture was centrifuged at 12,000g for 10 min at 4°C then stored at -80°C overnight. The frozen tubes were thawed on ice and the pellets were resuspended in sonication buffer (50 mM Tris-HCl, pH 8.0, 300 μM NaCl, 0.2% Triton X-100, 10 mM β-mercaptoethanol) with 1mM PMSF. The cell suspension was sonicated (Fisher Scientific Sonic Dismembranator Model 100) five times for 30 sec with 30 sec breaks on ice in between. Homogenates were then centrifuged at 40,000g for 20 min at 4°C and supernatants were loaded onto PBS-washed glutathione Sepharose beads and rotated end-over-end for 2.5 h at 4°C. GST proteins were eluted with 1 mL of glutathione elution buffer (25 mM Tris-HCl, pH 8.0, 250 mM NaCl, 10 mM glutathione) plus 5 μM DTT for 10 min on ice with gentle rocking. Samples were centrifuged at 400g for 4 min, and the supernatants collected. The elution process was repeated a total of three times, and the eluates were combined and dialyzed in a Slide-A-Lyzer (Pierce) overnight in 1.5 L of PBS at 4°C. Fresh PBS was added the next morning and the protein was extracted and quantified 7 h later and stored at -80°C.

5.10   LIPOSOME BINDING

Liposomes were prepared as described in (214) with 10% PtdIns(4,5)P$_2$. Varying amounts of ENTH or PTB GST fusion proteins were added to 20 μl incubation buffer (25 mM HEPES–KOH, pH 7.2, 125 mM potassium acetate, 5 mM magnesium acetate, 2 mM EDTA, 2 mM

EGTA, 1 mM DTT, 0.1 mg/ml BSA), 10 µl BSA (2mg/mL), 20 µl liposomes, and dH$_2$O in a final volume of 200 µl. Samples were incubated at ambient temperature for 30 min and then centrifuged at 20,000g for 15 min at 4°C. Aliquots of each supernatant and pellet (2.6% and 20% of total, respectively) were electrophoresed on SDS–PAGE gels and the gels were stained with Coomassie Blue. Images of the stained gels were acquired using a Bio-Rad Gel Doc XR+ and Image Lab software was used to measure the intensity of the supernatant and pellet fractions. The total protein recovered at each concentration was normalized to a standard curve generated from the intensities of the supernatant plus pellet fractions (each normalized to total input). To determine percent of protein bound to liposomes, the intensity of the normalized pellet fraction was divided by the normalized total protein values.

5.11   TOTAL INTERNAL REFLECTION FLUORESCENCE IMAGING

MDCK cells were grown on permeable supports and processed for immunofluorescence described above. The filters were cut out of their inserts and inverted onto a coverslip. Cells were imaged using a Nikon Eclipse Ti automated inverted microscope outfitted for total internal reflection fluorescence (TIRF) imaging and a 100x 1.49 NA TIRF objective. Solid-state lasers of 488, 561, and 647 nm were used as light sources. Images were acquired with an iXon+ 897 EM-CCD camera driven by iQ (Andor LLC). The depth of field of illumination was about 150 nm. Imaris (Bitplane Scientific Software) was used to quantitate the number of epsin spots per cell. The expected spot size was set to 0.3 µm and the threshold was set automatically to determine the number of spots in each frame. The area of each cell was determined using ImageJ software (NIH) to calculate the number of spots per square micron.

5.12   ELECTRON MICROSCOPY

MDCK cells cultured on filters were infected with control or PIP5KIβ adenovirus then fixed in 2.0 % (v/v) glutaraldehyde and 2.0 % (v/v) paraformaldehyde in 100 mM sodium cacodylate buffer, pH 7.4 for 30 min at 37˚ C. The tissue was then post-fixed in reduced 1.5 % (v/v) OsO_4, *en bloc* stained overnight in 0.5% (v/v) uranyl acetate, dehydrated in alcohol, and embedded in epon. The tissue was sectioned using a diamond knife (Diatome USA, Hatfield, PA), and sections, silver in color, were stained with lead citrate, viewed in a JEOL 100CX transmission electron microscope, and images acquired using an L9C Peltier-cooled TEM camera system (Scientific Instruments and Applications, Inc.; Duluth, GA). Representative digital images were imported into Adobe Photoshop CS4 (Adobe Systems Inc.; San Jose, CA), the contrast was corrected, and composite images were generated using Adobe Illustrator CS4 (Adobe Systems Inc.).

To quantify the number of clathrin-coated structures per μm of apical or basolateral membrane I used our previously described methods (227). Briefly, random epon blocks were sectioned perpendicular to the length of the epithelium to obtain vertical sections. At least 35 randomly chosen cross sections of MDCK apical or basolateral membrane were photographed at 27,000 X and then printed. For each image a grid of cycloidal arcs (see grid C3 228)] was placed over the image and the number of intersections of plasma membrane (I_P) with the grid, and the number of the following clathrin-coated structures (Q_{CCS}) was recorded: those with only a small amount of membrane curvature (shallow coated pits); those with a significant curvature, but lacking a discernable neck (invaginated pit); those with significant curvature and attached to the surface by a neck structure (deeply invaginated pits), and coated vesicles within 1 μm of the

surface. The following formula was used to estimate the boundary length of apical or basolateral plasma membrane in each image (B_{Lp}) (229):

$$B_{Lp} = A_{grid} \acute{\ } L_{Ap}$$

$$L_{Ap} = \frac{p}{2} \cdot \frac{I_p}{l_{lp}}$$

where A_{grid} is equal to the calibrated area of the cycloid grid, which was 32.96 µm^2 in our experiments, L_{Ap} is equal to the length of plasma membrane per unit area (units of µm/µm^2), and l_{lp} is equal to the calibrated length of line probe, which was 44.4 µm in our experiments. To estimate the number (Q) of each of the clathrin-coated structures (CCS) per length of plasma membrane the following formula was used:

$$CCS / length = \frac{Q_{CCS}}{B_{Lp}}$$

5.13   SIRNA OLIGOS AND TRANSFECTION

MDCK cells were trypsinized (day 1) and plated to be ~80% confluent the next day (~3 x 10^6 cells in a 10 cm dish). On day 2, transfection reagents were prepared while the cells were trypsinized. For each sample, 75 pmol of siRNA oligo (Sigma) was added to 62.5 µl OptiMEM (Invitrogen). Lipofectamine (Invitrogen; 3.75 µl in 62.5 µl OptiMEM) was added and the mixture was incubated for 20 min. The cells were collected and resuspended at a concentration of 2.4 x 10^6 cells/mL. Cells (330 µl) were mixed with 125 µl of siRNA/Lipofectamine/OptiMEM

and plated on each Transwell. Cells were used for experiments on day 6. PC-12 cells were transfected on day 1 using AMAXA electroporation; 2×10^6 cells were mixed with 200 pmol siRNA and electroporated with program U-029, then plated onto coverslips in four wells of a 12-well dish. The next day, the cells were transfected again using RNAiMAX (Invitrogen) following the manufacturer's protocol. On day 3 the cells were serum starved, and the following day they were processed for immunofluoresence or RT-PCR. The siRNA target sequences are as follows: control (firefly luciferase) 5'-GAAUAUUGUUGCACGAUUU-3', VAMP8 canine 5'-CCACATCGGAGCACTTCAA-3', VAMP7 canine 5'-GAAGAGGTTCCAGACTACA-3', VAMP7 rat 5'-GAAGAGGTTCCAGACCACA-3', VAMP7b 5'-GTGGAGGAAACTTCCTGGAG-3', α-gal-A 5'-GATAGATCTGCTGAAATT-3'.

5.14   PULSE CHASE

MDCK cells were plated onto transwells on day 1 and on day 4 they were infected with adenovirus encoding megalin, ensol or gGH at an MOI of 50, endolyn at an MOI of 100, or HA at an MOI of 25 as described above. On day 5, cells were rinsed with DPBS^{++} and starved with warm media A (cysteine-free, methionine-free MEM with 0.35 g/liter NaHCO$_3$, 10 mM MES, and 10 mM HEPES, pH 7.0) for 30 minutes in a 37 degree water bath. Then transwells filters were incubated on a 50 µl drop of ^{35}S Easy Tag (2.5 µl/well) or ^{35}S-cysteine for endolyn and ensol (5 µl/well) for a pulse at 37 degrees. Then the cells were rinsed once time with warm media A. Then media with cysteine and methionine (media B) was added to chase the cells for various time points. Cells were treated as below depending on the protein of interest. After proteins were eluted, and run on 4-15% gradient SDS-PAGE gels (BioRad), the gels were dried

87

and phosphoimager screens detected radioactivity in each sample, which was quantified using scanning densitometry (BioRad).

5.15   HA TRYPSINIZATION

Pulse chase was performed as described above with a 15 minute pulse. Then HA was staged at the TGN by incubated the cells in a 19 degree water bath for 2 h. After chase, cells were warmed in a 37 degree water bath. At each time point the transwells were removed from the water bath and put on ice and media was replaced with 100 µg/ml TPCK trypsin (Sigma) diluted in ice cold media B. After 30 min, trypsin was removed and replaced with 200 µg/ml Soybean Trypsin Inhibitor diluted in cold media B for 10 min, followed by another 10 min incubation with the inhibitor solution. The filters were then cut out and placed into detergent solution (50 mM Tris-HCl, 2% NP-40, 0.4% deoxycholate, 62.5 mM EDTA, pH 8.0) and incubated at room temperature for 15 minutes, then vortexed and spun down at max speed for 2 min. The supernant was removed and placed into a new tube. Monoclonal Fc125 antibody and 5 µl 10% SDS was then added to each tube. The tubes were mixed end over end overnight. The following day, 25 µl of washed bugs were added to each tube and mixed end over end for 20 min. The tubes were then centrifuged for 1 min at high speed and the supernatant was discarded. The pellets were washed 3X in 1 mL RIPA buffer (1% Triton X-100, 1% sodium deoxycholate, and 0.1% SDS in 50 mM TrisHCl, pH 7.5). The protein was then eluted from the pellet with 30 µl SDS-PAGE sample buffer with 5% βME and heating for 3 min at 100°C and quantified as above.

5.16   ENSOL SECRETION

After incubation with ^{35}S–cysteine, 500 µL of MEM/BSA was added to the apical side and basolateral sides. The cells were then incubated for various time points at 37 degrees. At each time point the media was collected from the apical and basolateral sides. The supernatant was clarified at high speed (13200 rpm in Eppendorf Microcentrifuge 5415D) for 1 min. The supernatant was then transferred to a new tube and 5X detergent solution with aprotinin (120 µL to each fraction) was added. After time points were collected, filters were cut out and added to tubes containing 500 µL of 1X detergent solution with aprotinin for 15 minutes at room temperature. After vortexing, the tubes were centrifuged at high speed for 1 min to pellet debris. The supernatant was then transferred to new tube. Anti-endolyn (mAb 502) was added at a concentration of 25 µg/mL. The tubes were mixed end over end overnight. The following day, 25 µl of washed bugs were added to each tube and mixed end over end for 20 min. The tubes were then centrifuged for 1 min at high speed and the supernatant was discarded. The pellets were washed 3x in 1 mL RIPA buffer. The protein was then eluted from the pellet with 30 µl SDS-PAGE sample buffer with 5% βME and heated for 3 min at 100°C and quantified as above.

5.17   ENDOLYN DELIVERY

At each time point of chase, cells were put on ice in ice cold media B. After all time points were complete, cells were washed 4x 5 min with ice-cold DPBS^{++} on ice. Then endolyn was biotinylated as described previously (219). To immunoprecipitate the protein, anti-endolyn antibody (mAb 502) was used at a concentration of 25 µg/mL and 30 µL of a 50% slurry of

protein-G (Invitrogen) was also added to the lysate. Cell extracts with antibodies and protein G-beads were incubated at 4°C overnight with end-over-end mixing. The next day, tubes were centrifuged in a microcentrifuge for 1 min at 10,000 rpm. The supernatant was removed and the pellet is washed sequentially with (i) 1 mL 1% (v/v) Triton X-100 in HBS (10 mM HEPES-NaOH, pH 7.4, 150 mM NaCl) (ii) 1 mL 0.01% (w/v) SDS in HBS and (iii) 1 mL HBS. After the last wash, all the liquid was removed from the pellet. The immunoprecipitated protein was recovered by heating the pellet with 60 µL 1% SDS in HBS for 2 min at 90-100°C. The supernatant was moved to a clean tube. A 15-uL aliquot of supernatant was removed and saved at 4ºC (25% of the total immunoprecipitate). 800 mL of 0.5% (v/v) Trition X-100 in HBS (400 µL HBS + 400 µL 1% TX-100 in HBS) was added to the remaining 45 µL to dilute out the SDS. To isolate the biotinylated proteins, streptavidin-conjugated to agarose (30 µl) was added to the SDS-Triton sample and incubated at 4°C overnight with end-over-end mixing. The proteins bound to the avidin-conjugated beads were washed with (i) 1 mL 1% Triton X-100 in HBS and then (ii) 1 mL HBS. The biotinylated proteins were eluted from the avidin-conjugated beads by adding 30 µl SDS-PAGE sample buffer with 5% βME and heating for 3 min at 100°C. The avidin-conjugated beads were pelleted by centrifugation for 1 min in a microcentrifuge at top speed and the supernatant was loaded onto the SDS-PAGE gel. Aliquots representing the total immunoprecipitated protein were also loaded onto the SDS-PAGE gel to calculate the fraction biotinylated. Densitometric data was used to calculate the percent of the total protein found on the surface (percent biotinylated) at each time point.

5.18   MEASUREMENT OF CILIA LENGTH

siRNA transfected MDCK cells grown on Transwells and PC-12 cells cultured on coverslips were fixed and processed for indirect immunofluorescence as described above. Anti-acetylated tubulin monoclonal antibody (Sigma) was used at a dilution of 1:400 to visualize cilia, with secondary antibody and mounting media as described above. Multiple fields of cells were acquired using a Leica DM6000B epifluorescence microscope with a 100x/1.4 NA objective. Images were opened in image J and individual cilia were traced using the freehand drawing tool to measure length, standardized by tracing the scale bar. Nuclei in each field were counted to calculate the percent of ciliated cells.

5.19   MEASUREMENT OF CYST FORMATION

MDCK cells transfected with siRNA were plated on plastic for 1 day then trypsinized and 15,000 cells were resuspended in 80 µl basement membrane Matrigel (BD Biosiences). The Matrigel was allowed to solidify at 37°C in a 5% CO_2 incubator for 30 minutes before addition of growth medium. The media was changed every other day for 6 days. Indirect immunofluorescence of cysts was performed as described in (177). Knockdown was confirmed by RT-PCR in duplicate siRNA- treated samples grown on plastic.

BIBLIOGRAPHY

1.   Bonifacino JS, Glick BS. The mechanisms of vesicle budding and fusion. Cell. 2004;116(2):153-66.

2.   Shimkets RA, Lifton RP, Canessa CM. The activity of the epithelial sodium channel is regulated by clathrin-mediated endocytosis. Journal of Biological Chemistry. 1997;272(41):25537-41.

3.   Lifton RP. Molecular genetics of human blood pressure variation. Science. 1996;272(5262):676-80.

4.   Loffing J, Zecevic M, Feraille E, Kaissling B, Asher C, Rossier BC, et al. Aldosterone induces rapid apical translocation of ENaC in early portion of renal collecting system: possible role of SGK. American Journal of Physiology - Renal Physiology. 2001;280(4):F675-82.

5.   Butterworth MB, Edinger RS, Frizzell RA, Johnson JP. Regulation of the epithelial sodium channel by membrane trafficking. American Journal of Physiology - Renal Physiology. 2009;296(1):F10-24.

6.   Butterworth MB, Helman SI, Els WJ. cAMP-sensitive endocytic trafficking in A6 epithelia. American Journal of Physiology - Cell Physiology. 2001;280(4):C752-62.

7.   Potter BA, Weixel KM, Bruns JR, Ihrke G, Weisz OA. N-glycans mediate apical recycling of the sialomucin endolyn in polarized MDCK cells. Traffic. 2006;7(2):146-54.

8.   Weixel KM, Edinger RS, Kester L, Guerriero CJ, Wang H, Fang L, et al. Phosphatidylinositol 4-phosphate 5-kinase reduces cell surface expression of the epithelial sodium channel (ENaC) in cultured collecting duct cells. Journal of Biological Chemistry. 2007;282(50):36534-42.

9.   Naim HY, Dodds DT, Brewer CB, Roth MG. Apical and basolateral coated pits of MDCK cells differ in their rates of maturation into coated vesicles, but not in the ability to distinguish between mutant hemagglutinin proteins with different internalization signals. Journal of Cell Biology. 1995;129(5):1241-50.

10.   Rojas R, Ruiz WG, Leung SM, Jou TS, Apodaca G. Cdc42-dependent modulation of tight junctions and membrane protein traffic in polarized Madin-Darby canine kidney cells. Mol Biol Cell. 2001;12(8):2257-74. PMCID: 58593.

11.   Le Bivic A, Sambuy Y, Patzak A, Patil N, Chao M, Rodriguez-Boulan E. An internal deletion in the cytoplasmic tail reverses the apical localization of human NGF receptor in transfected MDCK cells. J Cell Biol. 1991;115(3):607-18. PMCID: 2289181.

12.   Mukherjee S, Ghosh RN, Maxfield FR. Endocytosis. Physiol Rev. 1997;77(3):759-803.

13.   Strickland DK, Gonias SL, Argraves WS. Diverse roles for the LDL receptor family. Trends Endocrinol Metab. 2002;13(2):66-74.

14.   Traub LM. Tickets to ride: selecting cargo for clathrin-regulated internalization. Nat Rev Mol Cell Biol. 2009;10(9):583-96.

15.   Benmerah A, Lamaze C. Clathrin-coated pits: vive la difference? Traffic. 2007;8(8):970-82.

16.   Haucke V. Phosphoinositide regulation of clathrin-mediated endocytosis. Biochemical Society Transactions. 2005;33(Pt 6):1285-9.

17.   Martin-Belmonte F, Gassama A, Datta A, Yu W, Rescher U, Gerke V, et al. PTEN-mediated apical segregation of phosphoinositides controls epithelial morphogenesis through Cdc42. Cell. 2007;128(2):383-97. PMCID: 1865103.

18.   Martin-Belmonte F, Mostov K. Phosphoinositides control epithelial development. Cell Cycle. 2007;6(16):1957-61.

19.   Gassama-Diagne A, Yu W, ter Beest M, Martin-Belmonte F, Kierbel A, Engel J, et al. Phosphatidylinositol-3,4,5-trisphosphate regulates the formation of the basolateral plasma membrane in epithelial cells.[erratum appears in Nat Cell Biol. 2006 Oct;8(10):1178]. Nature Cell Biology. 2006;8(9):963-70.

20.   Spudich G, Chibalina MV, Au JS, Arden SD, Buss F, Kendrick-Jones J. Myosin VI targeting to clathrin-coated structures and dimerization is mediated by binding to Disabled-2 and PtdIns(4,5)P2. Nat Cell Biol. 2007;9(2):176-83.

21.   Zheng J, Cahill SM, Lemmon MA, Fushman D, Schlessinger J, Cowburn D. Identification of the binding site for acidic phospholipids on the pH domain of dynamin: implications for stimulation of GTPase activity. Journal of Molecular Biology. 1996;255(1):14-21.

22.   Rohde G, Wenzel D, Haucke V. A phosphatidylinositol (4,5)-bisphosphate binding site within mu2-adaptin regulates clathrin-mediated endocytosis. Journal of Cell Biology. 2002;158(2):209-14.

23.   Di Paolo G, De Camilli P. Phosphoinositides in cell regulation and membrane dynamics. Nature. 2006;443(7112):651-7.

24.   Jean S, Kiger AA. Coordination between RAB GTPase and phosphoinositide regulation and functions. Nat Rev Mol Cell Biol. 2012;13(7):463-70.

25.   Lemmon MA. Phosphoinositide recognition domains. Traffic. 2003;4(4):201-13.

26.   Ford MG, Mills IG, Peter BJ, Vallis Y, Praefcke GJ, Evans PR, et al. Curvature of clathrin-coated pits driven by epsin. Nature. 2002;419(6905):361-6.

27.   Hyman J, Chen H, Di Fiore PP, De Camilli P, Brunger AT. Epsin 1 undergoes nucleocytosolic shuttling and its eps15 interactor NH(2)-terminal homology (ENTH) domain, structurally similar to Armadillo and HEAT repeats, interacts with the transcription factor promyelocytic leukemia Zn(2)+ finger protein (PLZF). J Cell Biol. 2000;149(3):537-46. PMCID: 2174850.

28.   Stolt PC, Jeon H, Song HK, Herz J, Eck MJ, Blacklow SC. Origins of peptide selectivity and phosphoinositide binding revealed by structures of disabled-1 PTB domain complexes. Structure. 2003;11(5):569-79.

29.   Spudich G, Chibalina MV, Au JS, Arden SD, Buss F, Kendrick-Jones J. Myosin VI targeting to clathrin-coated structures and dimerization is mediated by binding to Disabled-2 and PtdIns(4,5)P2. Nat Cell Biol. 2007;9(2):176-83. PMCID: 2670391.

30.   Cremona O, Di Paolo G, Wenk MR, Luthi A, Kim WT, Takei K, et al. Essential role of phosphoinositide metabolism in synaptic vesicle recycling. Cell. 1999;99(2):179-88.

31.   Traub LM, Lukacs GL. Decoding ubiquitin sorting signals for clathrin-dependent endocytosis by CLASPs. Journal of Cell Science. 2007;120(Pt 4):543-53.

32.   Mundell SJ, Luo J, Benovic JL, Conley PB, Poole AW. Distinct clathrin-coated pits sort different G protein-coupled receptor cargo. Traffic. 2006;7(10):1420-31.

33.   Puthenveedu MA, von Zastrow M. Cargo regulates clathrin-coated pit dynamics.[see comment]. Cell. 2006;127(1):113-24.

34.   Carvou N, Norden AG, Unwin RJ, Cockcroft S. Signalling through phospholipase C interferes with clathrin-mediated endocytosis. Cellular Signalling. 2007;19(1):42-51.

35.   Loijens JC, Anderson RA. Type I phosphatidylinositol-4-phosphate 5-kinases are distinct members of this novel lipid kinase family. J Biol Chem. 1996;271(51):32937-43.

36.   Ishihara H, Shibasaki Y, Kizuki N, Katagiri H, Yazaki Y, Asano T, et al. Cloning of cDNAs encoding two isoforms of 68-kDa type I phosphatidylinositol-4-phosphate 5-kinase. J Biol Chem. 1996;271(39):23611-4.

37.   Ishihara H, Shibasaki Y, Kizuki N, Wada T, Yazaki Y, Asano T, et al. Type I phosphatidylinositol-4-phosphate 5-kinases. Cloning of the third isoform and deletion/substitution analysis of members of this novel lipid kinase family. J Biol Chem. 1998;273(15):8741-8.

38.   Volpicelli-Daley LA, Lucast L, Gong LW, Liu L, Sasaki J, Sasaki T, et al. Phosphatidylinositol-4-phosphate 5-kinases and phosphatidylinositol 4,5-bisphosphate synthesis in the brain. J Biol Chem. 2010;285(37):28708-14. PMCID: 2937898.

39.   Padron D, Wang YJ, Yamamoto M, Yin H, Roth MG. Phosphatidylinositol phosphate 5-kinase Ibeta recruits AP-2 to the plasma membrane and regulates rates of constitutive endocytosis. Journal of Cell Biology. 2003;162(4):693-701.

40.   Barbieri MA, Heath CM, Peters EM, Wells A, Davis JN, Stahl PD. Phosphatidylinositol-4-phosphate 5-kinase-1beta is essential for epidermal growth factor receptor-mediated endocytosis. Journal of Biological Chemistry. 2001;276(50):47212-6.

41.   Wenk MR, Pellegrini L, Klenchin VA, Di Paolo G, Chang S, Daniell L, et al. PIP kinase Igamma is the major PI(4,5)P(2) synthesizing enzyme at the synapse. Neuron. 2001;32(1):79-88.

42.   Bairstow SF, Ling K, Su X, Firestone AJ, Carbonara C, Anderson RA. Type Igamma661 phosphatidylinositol phosphate kinase directly interacts with AP2 and regulates endocytosis. Journal of Biological Chemistry. 2006;281(29):20632-42.

43.   Collins BM, McCoy AJ, Kent HM, Evans PR, Owen DJ. Molecular architecture and functional model of the endocytic AP2 complex. Cell. 2002;109(4):523-35.

44.   Krauss M, Kukhtina V, Pechstein A, Haucke V. Stimulation of phosphatidylinositol kinase type I-mediated phosphatidylinositol (4,5)-bisphosphate synthesis by AP-2mu-cargo complexes. Proceedings of the National Academy of Sciences of the United States of America. 2006;103(32):11934-9.

45.   Szalinski CM, Guerriero CJ, Ruiz WG, Docter BE, Rbaibi Y, Pastor-Soler NM, et al. PIP5KIbeta Selectively Modulates Apical Endocytosis in Polarized Renal Epithelial Cells. PLoS One. 2013;8(1):e53790. PMCID: 3547069.

46.   Idevall-Hagren O, Dickson EJ, Hille B, Toomre DK, De Camilli P. Optogenetic control of phosphoinositide metabolism. Proc Natl Acad Sci U S A. 2012;109(35):E2316-23. PMCID: 3435206.

47.   Varnai P, Thyagarajan B, Rohacs T, Balla T. Rapidly inducible changes in phosphatidylinositol 4,5-bisphosphate levels influence multiple regulatory functions of the lipid in intact living cells. Journal of Cell Biology. 2006;175(3):377-82.

48.   Zoncu R, Perera RM, Sebastian R, Nakatsu F, Chen H, Balla T, et al. Loss of endocytic clathrin-coated pits upon acute depletion of phosphatidylinositol 4,5-bisphosphate. Proceedings of the National Academy of Sciences of the United States of America. 2007;104(10):3793-8.

49.   Boulant S, Kural C, Zeeh JC, Ubelmann F, Kirchhausen T. Actin dynamics counteract membrane tension during clathrin-mediated endocytosis. Nat Cell Biol. 2011;13(9):1124-31. PMCID: 3167020.

50.   Gottlieb TA, Ivanov IE, Adesnik M, Sabatini DD. Actin microfilaments play a critical role in endocytosis at the apical but not the basolateral surface of polarized epithelial cells. J Cell Biol. 1993;120(3):695-710. PMCID: 2119548.

51.   Hyman T, Shmuel M, Altschuler Y. Actin is required for endocytosis at the apical surface of Madin-Darby canine kidney cells where ARF6 and clathrin regulate the actin cytoskeleton. Mol Biol Cell. 2006;17(1):427-37. PMCID: 1345679.

52.   Merrifield CJ, Feldman ME, Wan L, Almers W. Imaging actin and dynamin recruitment during invagination of single clathrin-coated pits. Nat Cell Biol. 2002;4(9):691-8.

53.   Merrifield CJ, Qualmann B, Kessels MM, Almers W. Neural Wiskott Aldrich Syndrome Protein (N-WASP) and the Arp2/3 complex are recruited to sites of clathrin-mediated endocytosis in cultured fibroblasts. Eur J Cell Biol. 2004;83(1):13-8.

54.   Rohatgi R, Ma L, Miki H, Lopez M, Kirchhausen T, Takenawa T, et al. The interaction between N-WASP and the Arp2/3 complex links Cdc42-dependent signals to actin assembly. Cell. 1999;97(2):221-31.

55.   Rohatgi R, Ho HY, Kirschner MW. Mechanism of N-WASP activation by CDC42 and phosphatidylinositol 4, 5-bisphosphate. J Cell Biol. 2000;150(6):1299-310. PMCID: 2150699.

56.   Rozelle AL, Machesky LM, Yamamoto M, Driessens MH, Insall RH, Roth MG, et al. Phosphatidylinositol 4,5-bisphosphate induces actin-based movement of raft-enriched vesicles through WASP-Arp2/3. Curr Biol. 2000;10(6):311-20.

57.   Jahn R, Scheller RH. SNAREs--engines for membrane fusion. Nat Rev Mol Cell Biol. 2006;7(9):631-43.

58.   Fasshauer D, Sutton RB, Brunger AT, Jahn R. Conserved structural features of the synaptic fusion complex: SNARE proteins reclassified as Q- and R-SNAREs. Proc Natl Acad Sci U S A. 1998;95(26):15781-6. PMCID: 28121.

59.   Holt M, Varoqueaux F, Wiederhold K, Takamori S, Urlaub H, Fasshauer D, et al. Identification of SNAP-47, a novel Qbc-SNARE with ubiquitous expression. J Biol Chem. 2006;281(25):17076-83.

60.   Lafont F, Verkade P, Galli T, Wimmer C, Louvard D, Simons K. Raft association of SNAP receptors acting in apical trafficking in Madin-Darby canine kidney cells. Proc Natl Acad Sci U S A. 1999;96(7):3734-8. PMCID: 22363.

61.   Low SH, Roche PA, Anderson HA, van Ijzendoorn SC, Zhang M, Mostov KE, et al. Targeting of SNAP-23 and SNAP-25 in polarized epithelial cells. J Biol Chem. 1998;273(6):3422-30.

62.   Leung SM, Chen D, DasGupta BR, Whiteheart SW, Apodaca G. SNAP-23 requirement for transferrin recycling in Streptolysin-O-permeabilized Madin-Darby canine kidney cells. J Biol Chem. 1998;273(28):17732-41.

63.   Pryor PR, Mullock BM, Bright NA, Lindsay MR, Gray SR, Richardson SC, et al. Combinatorial SNARE complexes with VAMP7 or VAMP8 define different late endocytic fusion events. EMBO Rep. 2004;5(6):590-5. PMCID: 1299070.

64.   Ikonen E, Tagaya M, Ullrich O, Montecucco C, Simons K. Different requirements for NSF, SNAP, and Rab proteins in apical and basolateral transport in MDCK cells. Cell. 1995;81(4):571-80.

65.   Apodaca G, Cardone MH, Whiteheart SW, DasGupta BR, Mostov KE. Reconstitution of transcytosis in SLO-permeabilized MDCK cells: existence of an NSF-dependent fusion mechanism with the apical surface of MDCK cells. EMBO J. 1996;15(7):1471-81. PMCID: 450054.

66.   Low SH, Chapin SJ, Wimmer C, Whiteheart SW, Komuves LG, Mostov KE, et al. The SNARE machinery is involved in apical plasma membrane trafficking in MDCK cells. J Cell Biol. 1998;141(7):1503-13. PMCID: 2133007.

67.   Galli T, Zahraoui A, Vaidyanathan VV, Raposo G, Tian JM, Karin M, et al. A novel tetanus neurotoxin-insensitive vesicle-associated membrane protein in SNARE complexes of the apical plasma membrane of epithelial cells. Mol Biol Cell. 1998;9(6):1437-48. PMCID: 25366.

68.   Pocard T, Le Bivic A, Galli T, Zurzolo C. Distinct v-SNAREs regulate direct and indirect apical delivery in polarized epithelial cells. J Cell Sci. 2007;120(Pt 18):3309-20.

69.   Danglot L, Chaineau M, Dahan M, Gendron MC, Boggetto N, Perez F, et al. Role of TI-VAMP and CD82 in EGFR cell-surface dynamics and signaling. J Cell Sci. 2010;123(Pt 5):723-35.

70.   Advani RJ, Bae HR, Bock JB, Chao DS, Doung YC, Prekeris R, et al. Seven novel mammalian SNARE proteins localize to distinct membrane compartments. J Biol Chem. 1998;273(17):10317-24.

71.   Advani RJ, Yang B, Prekeris R, Lee KC, Klumperman J, Scheller RH. VAMP-7 mediates vesicular transport from endosomes to lysosomes. J Cell Biol. 1999;146(4):765-76. PMCID: 2156136.

72.   Matarazzo MR, Cuccurese M, Strazzullo M, Vacca M, Curci A, Miano MG, et al. Human and mouse SYBL1 gene structure and expression. Gene. 1999;240(1):233-8.

73.   D'Esposito M, Ciccodicola A, Gianfrancesco F, Esposito T, Flagiello L, Mazzarella R, et al. A synaptobrevin-like gene in the Xq28 pseudoautosomal region undergoes X inactivation. Nat Genet. 1996;13(2):227-9.

74.   Saito T, Parsia S, Papolos DF, Lachman HM. Analysis of the pseudoautosomal X-linked gene SYBL1in bipolar affective disorder: description of a new candidate allele for psychiatric disorders. Am J Med Genet. 2000;96(3):317-23.

75.	Muller DJ, Schulze TG, Jahnes E, Cichon S, Krauss H, Kesper K, et al. Association between a polymorphism in the pseudoautosomal X-linked gene SYBL1 and bipolar affective disorder. Am J Med Genet. 2002;114(1):74-8.

76.	Nakatani N, Hattori E, Ohnishi T, Dean B, Iwayama Y, Matsumoto I, et al. Genome-wide expression analysis detects eight genes with robust alterations specific to bipolar I disorder: relevance to neuronal network perturbation. Hum Mol Genet. 2006;15(12):1949-62.

77.	Danglot L, Zylbersztejn K, Petkovic M, Gauberti M, Meziane H, Combe R, et al. Absence of TI-VAMP/Vamp7 leads to increased anxiety in mice. J Neurosci. 2012;32(6):1962-8.

78.	Filippini F, Rossi V, Galli T, Budillon A, D'Urso M, D'Esposito M. Longins: a new evolutionary conserved VAMP family sharing a novel SNARE domain. Trends Biochem Sci. 2001;26(7):407-9.

79.	Rossi V, Banfield DK, Vacca M, Dietrich LE, Ungermann C, D'Esposito M, et al. Longins and their longin domains: regulated SNAREs and multifunctional SNARE regulators. Trends Biochem Sci. 2004;29(12):682-8.

80.	Arantes RM, Andrews NW. A role for synaptotagmin VII-regulated exocytosis of lysosomes in neurite outgrowth from primary sympathetic neurons. J Neurosci. 2006;26(17):4630-7.

81.	Coco S, Raposo G, Martinez S, Fontaine JJ, Takamori S, Zahraoui A, et al. Subcellular localization of tetanus neurotoxin-insensitive vesicle-associated membrane protein (VAMP)/VAMP7 in neuronal cells: evidence for a novel membrane compartment. J Neurosci. 1999;19(22):9803-12.

82.	Martinez-Arca S, Rudge R, Vacca M, Raposo G, Camonis J, Proux-Gillardeaux V, et al. A dual mechanism controlling the localization and function of exocytic v-SNAREs. Proc Natl Acad Sci U S A. 2003;100(15):9011-6. PMCID: 166429.

83.	Pols MS, van Meel E, Oorschot V, ten Brink C, Fukuda M, Swetha MG, et al. hVps41 and VAMP7 function in direct TGN to late endosome transport of lysosomal membrane proteins. Nat Commun. 2013;4:1361.

84.	Pryor PR, Jackson L, Gray SR, Edeling MA, Thompson A, Sanderson CM, et al. Molecular basis for the sorting of the SNARE VAMP7 into endocytic clathrin-coated vesicles by the ArfGAP Hrb. Cell. 2008;134(5):817-27. PMCID: 2648964.

85.	Rao SK, Huynh C, Proux-Gillardeaux V, Galli T, Andrews NW. Identification of SNAREs involved in synaptotagmin VII-regulated lysosomal exocytosis. J Biol Chem. 2004;279(19):20471-9.

86.	Proux-Gillardeaux V, Raposo G, Irinopoulou T, Galli T. Expression of the Longin domain of TI-VAMP impairs lysosomal secretion and epithelial cell migration. Biol Cell. 2007;99(5):261-71.

87.   Alberts P, Rudge R, Hinners I, Muzerelle A, Martinez-Arca S, Irinopoulou T, et al. Cross talk between tetanus neurotoxin-insensitive vesicle-associated membrane protein-mediated transport and L1-mediated adhesion. Mol Biol Cell. 2003;14(10):4207-20. PMCID: 207012.

88.   Martinez-Arca S, Alberts P, Zahraoui A, Louvard D, Galli T. Role of tetanus neurotoxin insensitive vesicle-associated membrane protein (TI-VAMP) in vesicular transport mediating neurite outgrowth. J Cell Biol. 2000;149(4):889-900. PMCID: 2174569.

89.   Martinez-Arca S, Coco S, Mainguy G, Schenk U, Alberts P, Bouille P, et al. A common exocytotic mechanism mediates axonal and dendritic outgrowth. J Neurosci. 2001;21(11):3830-8.

90.   Hasan N, Corbin D, Hu C. Fusogenic pairings of vesicle-associated membrane proteins (VAMPs) and plasma membrane t-SNAREs--VAMP5 as the exception. PLoS One. 2010;5(12):e14238. PMCID: 2997805.

91.   Hibi T, Hirashima N, Nakanishi M. Rat basophilic leukemia cells express syntaxin-3 and VAMP-7 in granule membranes. Biochem Biophys Res Commun. 2000;271(1):36-41.

92.   Martinez-Arca S, Proux-Gillardeaux V, Alberts P, Louvard D, Galli T. Ectopic expression of syntaxin 1 in the ER redirects TI-VAMP- and cellubrevin-containing vesicles. J Cell Sci. 2003;116(Pt 13):2805-16.

93.   Novick P, Field C, Schekman R. Identification of 23 complementation groups required for post-translational events in the yeast secretory pathway. Cell. 1980;21(1):205-15.

94.   He B, Guo W. The exocyst complex in polarized exocytosis. Curr Opin Cell Biol. 2009;21(4):537-42. PMCID: 2725219.

95.   Boyd C, Hughes T, Pypaert M, Novick P. Vesicles carry most exocyst subunits to exocytic sites marked by the remaining two subunits, Sec3p and Exo70p. J Cell Biol. 2004;167(5):889-901. PMCID: 2172445.

96.   He B, Xi F, Zhang X, Zhang J, Guo W. Exo70 interacts with phospholipids and mediates the targeting of the exocyst to the plasma membrane. Embo J. 2007;26(18):4053-65. PMCID: 2230670.

97.   Zhang X, Orlando K, He B, Xi F, Zhang J, Zajac A, et al. Membrane association and functional regulation of Sec3 by phospholipids and Cdc42. J Cell Biol. 2008;180(1):145-58. PMCID: 2213614.

98.   Liu J, Zuo X, Yue P, Guo W. Phosphatidylinositol 4,5-bisphosphate mediates the targeting of the exocyst to the plasma membrane for exocytosis in mammalian cells. Mol Biol Cell. 2007;18(11):4483-92. PMCID: 2043555.

99.   Grindstaff KK, Yeaman C, Anandasabapathy N, Hsu SC, Rodriguez-Boulan E, Scheller RH, et al. Sec6/8 complex is recruited to cell-cell contacts and specifies transport vesicle delivery to the basal-lateral membrane in epithelial cells. Cell. 1998;93(5):731-40.

100.	Oztan A, Silvis M, Weisz OA, Bradbury NA, Hsu SC, Goldenring JR, et al. Exocyst requirement for endocytic traffic directed toward the apical and basolateral poles of polarized MDCK cells. Mol Biol Cell. 2007;18(10):3978-92. PMCID: 1995710.

101.	Rogers KK, Wilson PD, Snyder RW, Zhang X, Guo W, Burrow CR, et al. The exocyst localizes to the primary cilium in MDCK cells. Biochem Biophys Res Commun. 2004;319(1):138-43.

102.	Lipschutz JH, Guo W, O'Brien LE, Nguyen YH, Novick P, Mostov KE. Exocyst is involved in cystogenesis and tubulogenesis and acts by modulating synthesis and delivery of basolateral plasma membrane and secretory proteins. Mol Biol Cell. 2000;11(12):4259-75. PMCID: 15071.

103.	Babbey CM, Bacallao RL, Dunn KW. Rab10 associates with primary cilia and the exocyst complex in renal epithelial cells. Am J Physiol Renal Physiol. 2010;299(3):F495-506. PMCID: 2944301.

104.	Zuo X, Guo W, Lipschutz JH. The exocyst protein Sec10 is necessary for primary ciliogenesis and cystogenesis in vitro. Mol Biol Cell. 2009;20(10):2522-9. PMCID: 2682593.

105.	Fogelgren B, Lin SY, Zuo X, Jaffe KM, Park KM, Reichert RJ, et al. The exocyst protein Sec10 interacts with Polycystin-2 and knockdown causes PKD-phenotypes. PLoS Genet. 2011;7(4):e1001361. PMCID: 3072367.

106.	Hsu SC, Ting AE, Hazuka CD, Davanger S, Kenny JW, Kee Y, et al. The mammalian brain rsec6/8 complex. Neuron. 1996;17(6):1209-19.

107.	Wiederkehr A, De Craene JO, Ferro-Novick S, Novick P. Functional specialization within a vesicle tethering complex: bypass of a subset of exocyst deletion mutants by Sec1p or Sec4p. J Cell Biol. 2004;167(5):875-87. PMCID: 2172455.

108.	Grote E, Carr CM, Novick PJ. Ordering the final events in yeast exocytosis. J Cell Biol. 2000;151(2):439-52. PMCID: 2192655.

109.	Schmid SL, Mellman I. Isolation of functionally distinct endosome subpopulations by free-flow electrophoresis. Prog Clin Biol Res. 1988;270:35-49.

110.	Weisz OA, Rodriguez-Boulan E. Apical trafficking in epithelial cells: signals, clusters and motors. J Cell Sci. 2009;122(Pt 23):4253-66. PMCID: 2779128.

111.	Mattila PE, Youker RT, Mo D, Bruns JR, Cresawn KO, Hughey RP, et al. Multiple biosynthetic trafficking routes for apically secreted proteins in MDCK cells. Traffic. 2012;13(3):433-42. PMCID: 3276681.

112.	Potter BA, Ihrke G, Bruns JR, Weixel KM, Weisz OA. Specific N-glycans direct apical delivery of transmembrane, but not soluble or glycosylphosphatidylinositol-anchored forms of endolyn in Madin-Darby canine kidney cells. Mol Biol Cell. 2004;15(3):1407-16. PMCID: 363156.

113. Cresawn KO, Potter BA, Oztan A, Guerriero CJ, Ihrke G, Goldenring JR, et al. Differential involvement of endocytic compartments in the biosynthetic traffic of apical proteins. Embo J. 2007;26(16):3737-48. PMCID: 1952228.

114. Brown PS, Wang E, Aroeti B, Chapin SJ, Mostov KE, Dunn KW. Definition of distinct compartments in polarized Madin-Darby canine kidney (MDCK) cells for membrane-volume sorting, polarized sorting and apical recycling. Traffic. 2000;1(2):124-40.

115. Cao X, Surma MA, Simons K. Polarized sorting and trafficking in epithelial cells. Cell Res. 2012;22(5):793-805. PMCID: 3343658.

116. Lapierre LA, Kumar R, Hales CM, Navarre J, Bhartur SG, Burnette JO, et al. Myosin vb is associated with plasma membrane recycling systems. Mol Biol Cell. 2001;12(6):1843-57. PMCID: 37346.

117. Roland JT, Kenworthy AK, Peranen J, Caplan S, Goldenring JR. Myosin Vb interacts with Rab8a on a tubular network containing EHD1 and EHD3. Mol Biol Cell. 2007;18(8):2828-37. PMCID: 1949367.

118. Schuck S, Gerl MJ, Ang A, Manninen A, Keller P, Mellman I, et al. Rab10 is involved in basolateral transport in polarized Madin-Darby canine kidney cells. Traffic. 2007;8(1):47-60.

119. Sato T, Mushiake S, Kato Y, Sato K, Sato M, Takeda N, et al. The Rab8 GTPase regulates apical protein localization in intestinal cells. Nature. 2007;448(7151):366-9.

120. Mandon B, Chou CL, Nielsen S, Knepper MA. Syntaxin-4 is localized to the apical plasma membrane of rat renal collecting duct cells: possible role in aquaporin-2 trafficking. J Clin Invest. 1996;98(4):906-13. PMCID: 507504.

121. Breton S, Inoue T, Knepper MA, Brown D. Antigen retrieval reveals widespread basolateral expression of syntaxin 3 in renal epithelia. Am J Physiol Renal Physiol. 2002;282(3):F523-9.

122. Kreitzer G, Schmoranzer J, Low SH, Li X, Gan Y, Weimbs T, et al. Three-dimensional analysis of post-Golgi carrier exocytosis in epithelial cells. Nat Cell Biol. 2003;5(2):126-36.

123. Li X, Low SH, Miura M, Weimbs T. SNARE expression and localization in renal epithelial cells suggest mechanism for variability of trafficking phenotypes. Am J Physiol Renal Physiol. 2002;283(5):F1111-22.

124. Fields IC, Shteyn E, Pypaert M, Proux-Gillardeaux V, Kang RS, Galli T, et al. v-SNARE cellubrevin is required for basolateral sorting of AP-1B-dependent cargo in polarized epithelial cells. J Cell Biol. 2007;177(3):477-88. PMCID: 2034334.

125. Le Bivic A, Quaroni A, Nichols B, Rodriguez-Boulan E. Biogenetic pathways of plasma membrane proteins in Caco-2, a human intestinal epithelial cell line. J Cell Biol. 1990;111(4):1351-61. PMCID: 2116246.

126.	Matter K, Stieger B, Klumperman J, Ginsel L, Hauri HP. Endocytosis, recycling, and lysosomal delivery of brush border hydrolases in cultured human intestinal epithelial cells (Caco-2). J Biol Chem. 1990;265(6):3503-12.

127.	Knodler A, Feng S, Zhang J, Zhang X, Das A, Peranen J, et al. Coordination of Rab8 and Rab11 in primary ciliogenesis. Proc Natl Acad Sci U S A. 2010;107(14):6346-51. PMCID: 2851980.

128.	Hehnly H, Chen CT, Powers CM, Liu HL, Doxsey S. The centrosome regulates the Rab11- dependent recycling endosome pathway at appendages of the mother centriole. Curr Biol. 2012;22(20):1944-50.

129.	Yoshimura S, Egerer J, Fuchs E, Haas AK, Barr FA. Functional dissection of Rab GTPases involved in primary cilium formation. J Cell Biol. 2007;178(3):363-9. PMCID: 2064854.

130.	Zilber Y, Babayeva S, Seo JH, Liu JJ, Mootin S, Torban E. The PCP effector Fuzzy controls cilial assembly and signaling by recruiting Rab8 and Dishevelled to the primary cilium. Mol Biol Cell. 2013;24(5):555-65. PMCID: 3583660.

131.	Mazelova J, Ransom N, Astuto-Gribble L, Wilson MC, Deretic D. Syntaxin 3 and SNAP-25 pairing, regulated by omega-3 docosahexaenoic acid, controls the delivery of rhodopsin for the biogenesis of cilia-derived sensory organelles, the rod outer segments. J Cell Sci. 2009;122(Pt 12):2003-13. PMCID: 2723154.

132.	Torkko JM, Manninen A, Schuck S, Simons K. Depletion of apical transport proteins perturbs epithelial cyst formation and ciliogenesis. J Cell Sci. 2008;121(Pt 8):1193-203.

133.	Goetz SC, Anderson KV. The primary cilium: a signalling centre during vertebrate development. Nat Rev Genet. 2010;11(5):331-44. PMCID: 3121168.

134.	Nauli SM, Alenghat FJ, Luo Y, Williams E, Vassilev P, Li X, et al. Polycystins 1 and 2 mediate mechanosensation in the primary cilium of kidney cells. Nat Genet. 2003;33(2):129-37.

135.	Pazour GJ, Dickert BL, Vucica Y, Seeley ES, Rosenbaum JL, Witman GB, et al. Chlamydomonas IFT88 and its mouse homologue, polycystic kidney disease gene tg737, are required for assembly of cilia and flagella. J Cell Biol. 2000;151(3):709-18. PMCID: 2185580.

136.	Tucker RW, Pardee AB, Fujiwara K. Centriole ciliation is related to quiescence and DNA synthesis in 3T3 cells. Cell. 1979;17(3):527-35.

137.	Sorokin S. Centrioles and the formation of rudimentary cilia by fibroblasts and smooth muscle cells. J Cell Biol. 1962;15:363-77. PMCID: 2106144.

138.	Garcia-Gonzalo FR, Reiter JF. Scoring a backstage pass: mechanisms of ciliogenesis and ciliary access. J Cell Biol. 2012;197(6):697-709. PMCID: 3373398.

139.	Gilula NB, Satir P. The ciliary necklace. A ciliary membrane specialization. J Cell Biol. 1972;53(2):494-509. PMCID: 2108734.

140.	Dishinger JF, Kee HL, Jenkins PM, Fan S, Hurd TW, Hammond JW, et al. Ciliary entry of the kinesin-2 motor KIF17 is regulated by importin-beta2 and RanGTP. Nat Cell Biol. 2010;12(7):703-10. PMCID: 2896429.

141.	Kee HL, Dishinger JF, Blasius TL, Liu CJ, Margolis B, Verhey KJ. A size-exclusion permeability barrier and nucleoporins characterize a ciliary pore complex that regulates transport into cilia. Nat Cell Biol. 2012;14(4):431-7. PMCID: 3319646.

142.	Milenkovic L, Scott MP, Rohatgi R. Lateral transport of Smoothened from the plasma membrane to the membrane of the cilium. J Cell Biol. 2009;187(3):365-74. PMCID: 2779247.

143.	Ishikawa H, Marshall WF. Ciliogenesis: building the cell's antenna. Nat Rev Mol Cell Biol. 2011;12(4):222-34.

144.	Follit JA, Tuft RA, Fogarty KE, Pazour GJ. The intraflagellar transport protein IFT20 is associated with the Golgi complex and is required for cilia assembly. Mol Biol Cell. 2006;17(9):3781-92. PMCID: 1593158.

145.	Guerriero CJ, Weixel KM, Bruns JR, Weisz OA. Phosphatidylinositol 5-kinase stimulates apical biosynthetic delivery via an Arp2/3-dependent mechanism. Journal of Biological Chemistry. 2006;281(22):15376-84.

146.	Rojas R, Apodaca G. Immunoglobulin transport across polarized epithelial cells. Nat Rev Mol Cell Biol. 2002;3(12):944-55.

147.	Apodaca G, Bomsel M, Arden J, Breitfeld PP, Tang K, Mostov KE. The polymeric immunoglobulin receptor. A model protein to study transcytosis. J Clin Invest. 1991;87(6):1877-82. PMCID: 296937.

148.	Apodaca G, Katz LA, Mostov KE. Receptor-mediated transcytosis of IgA in MDCK cells is via apical recycling endosomes. J Cell Biol. 1994;125(1):67-86. PMCID: 2120019.

149.	Aikawa Y, Martin TF. ARF6 regulates a plasma membrane pool of phosphatidylinositol(4,5)bisphosphate required for regulated exocytosis. J Cell Biol. 2003;162(4):647-59. PMCID: 2173784.

150.	Di Paolo G, Moskowitz HS, Gipson K, Wenk MR, Voronov S, Obayashi M, et al. Impaired PtdIns(4,5)P2 synthesis in nerve terminals produces defects in synaptic vesicle trafficking. Nature. 2004;431(7007):415-22.

151.	Holz RW, Hlubek MD, Sorensen SD, Fisher SK, Balla T, Ozaki S, et al. A pleckstrin homology domain specific for phosphatidylinositol 4, 5-bisphosphate (PtdIns-4,5-P2) and fused to green fluorescent protein identifies plasma membrane PtdIns-4,5-P2 as being important in exocytosis. J Biol Chem. 2000;275(23):17878-85.

152.   Wen P, Osborne S, Zanin M, Low P, Wang H, Schoenwaelder S, et al. Phosphatidylinositol(4,5)bisphosphate coordinates actin-mediated mobilization and translocation of secretory vesicles to the plasma membrane of chromaffin cells. Nature Communications. 2011(2).

153.   James DJ, Khodthong C, Kowalchyk JA, Martin TF. Phosphatidylinositol 4,5-bisphosphate regulates SNARE-dependent membrane fusion. J Cell Biol. 2008;182(2):355-66. PMCID: 2483516.

154.   Fang L, Garuti R, Kim BY, Wade JB, Welling PA. The ARH adaptor protein regulates endocytosis of the ROMK potassium secretory channel in mouse kidney. Journal of Clinical Investigation. 2009;119(11):3278-89.

155.   Cui S GC, Szalinski CM, Kinlough CL, Hughey RP, Weisz OA. OCRL1 function in renal epithelial membrane traffic. American Journal of Physiology - Renal Physiology 2010;298:F335-F45.

156.   Nagai M, Meerloo T, Takeda T, Farquhar MG. The adaptor protein ARH escorts megalin to and through endosomes. Mol Biol Cell. 2003;14(12):4984-96. PMCID: 284800.

157.   Oleinikov AV, Zhao J, Makker SP. Cytosolic adaptor protein Dab2 is an intracellular ligand of endocytic receptor gp600/megalin. Biochem J. 2000;347 Pt 3:613-21. PMCID: 1220996.

158.   Stahelin RV, Long F, Peter BJ, Murray D, De Camilli P, McMahon HT, et al. Contrasting membrane interaction mechanisms of AP180 N-terminal homology (ANTH) and epsin N-terminal homology (ENTH) domains. J Biol Chem. 2003;278(31):28993-9.

159.   Rappoport JZ, Kemal S, Benmerah A, Simon SM. Dynamics of clathrin and adaptor proteins during endocytosis. Am J Physiol Cell Physiol. 2006;291(5):C1072-81.

160.   Vasudevan KM, Garraway LA. AKT signaling in physiology and disease. Curr Top Microbiol Immunol. 2010;347:105-33.

161.   Volpicelli-Daley LA, Lucast L, Gong LW, Liu L, Sasaki J, Sasaki T, et al. Phosphatidylinositol-4-phosphate 5-kinases and phosphatidylinositol 4,5-bisphosphate synthesis in the brain. J Biol Chem. 2010;285(37):28708-14. PMCID: 2937898.

162.   Mao YS, Yamaga M, Zhu X, Wei Y, Sun HQ, Wang J, et al. Essential and unique roles of PIP5K-gamma and -alpha in Fcgamma receptor-mediated phagocytosis. J Cell Biol. 2009;184(2):281-96. PMCID: 2654300.

163.   Wang Y, Chen X, Lian L, Tang T, Stalker TJ, Sasaki T, et al. Loss of PIP5KIbeta demonstrates that PIP5KI isoform-specific PIP2 synthesis is required for IP3 formation. Proc Natl Acad Sci U S A. 2008;105(37):14064-9. PMCID: 2544579.

164.   Lokuta MA, Senetar MA, Bennin DA, Nuzzi PA, Chan KT, Ott VL, et al. Type Igamma PIP kinase is a novel uropod component that regulates rear retraction during neutrophil chemotaxis. Mol Biol Cell. 2007;18(12):5069-80. PMCID: 2096574.

165.   Jost M, Simpson F, Kavran JM, Lemmon MA, Schmid SL. Phosphatidylinositol-4,5-bisphosphate is required for endocytic coated vesicle formation. Curr Biol. 1998;8(25):1399-402.

166.   Antonescu CN, Aguet F, Danuser G, Schmid SL. Phosphatidylinositol-(4,5)-bisphosphate regulates clathrin-coated pit initiation, stabilization, and size. Mol Biol Cell. 2011;22(14):2588-600. PMCID: 3135483.

167.   Benesch S, Lommel S, Steffen A, Stradal TE, Scaplehorn N, Way M, et al. Phosphatidylinositol 4,5-biphosphate (PIP2)-induced vesicle movement depends on N-WASP and involves Nck, WIP, and Grb2. J Biol Chem. 2002;277(40):37771-6.

168.   McMahon HT, Ushkaryov YA, Edelmann L, Link E, Binz T, Niemann H, et al. Cellubrevin is a ubiquitous tetanus-toxin substrate homologous to a putative synaptic vesicle fusion protein. Nature. 1993;364(6435):346-9.

169.   Hager HA, Roberts RJ, Cross EE, Proux-Gillardeaux V, Bader DM. Identification of a novel Bves function: regulation of vesicular transport. EMBO J. 2010;29(3):532-45. PMCID: 2830705.

170.   Steegmaier M, Lee KC, Prekeris R, Scheller RH. SNARE protein trafficking in polarized MDCK cells. Traffic. 2000;1(7):553-60.

171.   Zeng Q, Subramaniam VN, Wong SH, Tang BL, Parton RG, Rea S, et al. A novel synaptobrevin/VAMP homologous protein (VAMP5) is increased during in vitro myogenesis and present in the plasma membrane. Mol Biol Cell. 1998;9(9):2423-37. PMCID: 25509.

172.   Ortiz PA. cAMP increases surface expression of NKCC2 in rat thick ascending limbs: role of VAMP. Am J Physiol Renal Physiol. 2006;290(3):F608-16.

173.   Takeda T, Yamazaki H, Farquhar MG. Identification of an apical sorting determinant in the cytoplasmic tail of megalin. Am J Physiol Cell Physiol. 2003;284(5):C1105-13.

174.   Singla V, Reiter JF. The primary cilium as the cell's antenna: signaling at a sensory organelle. Science. 2006;313(5787):629-33.

175.   Hsiao YC, Tuz K, Ferland RJ. Trafficking in and to the primary cilium. Cilia. 2012;1(1):4. PMCID: 3541539.

176.   Nachury MV, Seeley ES, Jin H. Trafficking to the ciliary membrane: how to get across the periciliary diffusion barrier? Annu Rev Cell Dev Biol. 2010;26:59-87. PMCID: 2952038.

177.   Rbaibi Y, Cui S, Mo D, Carattino M, Rohatgi R, Satlin LM, et al. OCRL1 modulates cilia length in renal epithelial cells. Traffic. 2012;13(9):1295-305.

178.   Boucrot E, Kirchhausen T. Endosomal recycling controls plasma membrane area during mitosis. Proc Natl Acad Sci U S A. 2007;104(19):7939-44. PMCID: 1876551.

179.   Kim J, Lee JE, Heynen-Genel S, Suyama E, Ono K, Lee K, et al. Functional genomic screen for modulators of ciliogenesis and cilium length. Nature. 2010;464(7291):1048-51. PMCID: 2929961.

180.   Doyotte A, Mironov A, McKenzie E, Woodman P. The Bro1-related protein HD-PTP/PTPN23 is required for endosomal cargo sorting and multivesicular body morphogenesis. Proc Natl Acad Sci U S A. 2008;105(17):6308-13. PMCID: 2359801.

181.   Germain DP. Fabry disease. Orphanet J Rare Dis. 2010;5:30. PMCID: 3009617.

182.   Vieira OV, Gaus K, Verkade P, Fullekrug J, Vaz WL, Simons K. FAPP2, cilium formation, and compartmentalization of the apical membrane in polarized Madin-Darby canine kidney (MDCK) cells. Proc Natl Acad Sci U S A. 2006;103(49):18556-61. PMCID: 1693701.

183.   Kotsis F, Boehlke C, Kuehn EW. The ciliary flow sensor and polycystic kidney disease. Nephrol Dial Transplant. 2013;28(3):518-26. PMCID: 3588856.

184.   Galvez-Santisteban M, Rodriguez-Fraticelli AE, Bryant DM, Vergarajauregui S, Yasuda T, Banon-Rodriguez I, et al. Synaptotagmin-like proteins control the formation of a single apical membrane domain in epithelial cells. Nat Cell Biol. 2012;14(8):838-49. PMCID: 3433678.

185.   Sharma N, Low SH, Misra S, Pallavi B, Weimbs T. Apical targeting of syntaxin 3 is essential for epithelial cell polarity. J Cell Biol. 2006;173(6):937-48. PMCID: 2063918.

186.   Calvo M, Pol A, Lu A, Ortega D, Pons M, Blasi J, et al. Cellubrevin is present in the basolateral endocytic compartment of hepatocytes and follows the transcytotic pathway after IgA internalization. J Biol Chem. 2000;275(11):7910-7.

187.   Franki N, Macaluso F, Schubert W, Gunther L, Hays RM. Water channel-carrying vesicles in the rat IMCD contain cellubrevin. Am J Physiol. 1995;269(3 Pt 1):C797-801.

188.   Ko DC, Gordon MD, Jin JY, Scott MP. Dynamic movements of organelles containing Niemann-Pick C1 protein: NPC1 involvement in late endocytic events. Mol Biol Cell. 2001;12(3):601-14. PMCID: 30967.

189.   Kent HM, Evans PR, Schafer IB, Gray SR, Sanderson CM, Luzio JP, et al. Structural basis of the intracellular sorting of the SNARE VAMP7 by the AP3 adaptor complex. Dev Cell. 2012;22(5):979-88. PMCID: 3549491.

190.   Nishimura N, Plutner H, Hahn K, Balch WE. The delta subunit of AP-3 is required for efficient transport of VSV-G from the trans-Golgi network to the cell surface. Proc Natl Acad Sci U S A. 2002;99(10):6755-60. PMCID: 124475.

191.   Le Borgne R, Alconada A, Bauer U, Hoflack B. The mammalian AP-3 adaptor-like complex mediates the intracellular transport of lysosomal membrane glycoproteins. J Biol Chem. 1998;273(45):29451-61.

192.   Rous BA, Reaves BJ, Ihrke G, Briggs JA, Gray SR, Stephens DJ, et al. Role of adaptor complex AP-3 in targeting wild-type and mutated CD63 to lysosomes. Mol Biol Cell. 2002;13(3):1071-82. PMCID: 99620.

193.   Gordon DE, Bond LM, Sahlender DA, Peden AA. A targeted siRNA screen to identify SNAREs required for constitutive secretion in mammalian cells. Traffic. 2010;11(9):1191-204.

194.   Jones LC, Moussa L, Fulcher ML, Zhu Y, Hudson EJ, O'Neal WK, et al. VAMP8 is a vesicle SNARE that regulates mucin secretion in airway goblet cells. J Physiol. 2012;590(Pt 3):545-62. PMCID: 3379700.

195.   Baust T, Anitei M, Czupalla C, Parshyna I, Bourel L, Thiele C, et al. Protein networks supporting AP-3 function in targeting lysosomal membrane proteins. Mol Biol Cell. 2008;19(5):1942-51. PMCID: 2366865.

196.   Hu Q, Milenkovic L, Jin H, Scott MP, Nachury MV, Spiliotis ET, et al. A septin diffusion barrier at the base of the primary cilium maintains ciliary membrane protein distribution. Science. 2010;329(5990):436-9. PMCID: 3092790.

197.   Chih B, Liu P, Chinn Y, Chalouni C, Komuves LG, Hass PE, et al. A ciliopathy complex at the transition zone protects the cilia as a privileged membrane domain. Nat Cell Biol. 2012;14(1):61-72.

198.   Kim SK, Shindo A, Park TJ, Oh EC, Ghosh S, Gray RS, et al. Planar cell polarity acts through septins to control collective cell movement and ciliogenesis. Science. 2010;329(5997):1337-40. PMCID: 3509789.

199.   Cui S. Role of Phosphatidylinositol Metabolism in Renal Epithelial Membrane Traffic. Pittsburgh: University of Pittsburgh; 2010.

200.   Kaksonen M, Toret CP, Drubin DG. A modular design for the clathrin- and actin-mediated endocytosis machinery. Cell. 2005;123(2):305-20.

201.   Doyon JB, Zeitler B, Cheng J, Cheng AT, Cherone JM, Santiago Y, et al. Rapid and efficient clathrin-mediated endocytosis revealed in genome-edited mammalian cells. Nat Cell Biol. 2011;13(3):331-7.

202.   Mettlen M, Loerke D, Yarar D, Danuser G, Schmid SL. Cargo- and adaptor-specific mechanisms regulate clathrin-mediated endocytosis. J Cell Biol. 2010;188(6):919-33. PMCID: 2845073.

203.   Pan W, Choi SC, Wang H, Qin Y, Volpicelli-Daley L, Swan L, et al. Wnt3a-mediated formation of phosphatidylinositol 4,5-bisphosphate regulates LRP6 phosphorylation. Science. 2008;321(5894):1350-3. PMCID: 2532521.

204. Park SJ, Itoh T, Takenawa T. Phosphatidylinositol 4-phosphate 5-kinase type I is regulated through phosphorylation response by extracellular stimuli. J Biol Chem. 2001;276(7):4781-7.

205. Pochynyuk O, Bugaj V, Vandewalle A, Stockand JD. Purinergic control of apical plasma membrane PI(4,5)P2 levels sets ENaC activity in principal cells. American Journal of Physiology - Renal Physiology. 2008;294(1):F38-46.

206. Marley A, von Zastrow M. DISC1 regulates primary cilia that display specific dopamine receptors. PLoS One. 2010;5(5):e10902. PMCID: 2878344.

207. Brailov I, Bancila M, Brisorgueil MJ, Miquel MC, Hamon M, Verge D. Localization of 5-HT(6) receptors at the plasma membrane of neuronal cilia in the rat brain. Brain Res. 2000;872(1-2):271-5.

208. Vogt IR, Shimron-Abarbanell D, Neidt H, Erdmann J, Cichon S, Schulze TG, et al. Investigation of the human serotonin 6 [5-HT6] receptor gene in bipolar affective disorder and schizophrenia. American journal of medical genetics. 2000;96(2):217-21.

209. Goetz SC, Liem KF, Jr., Anderson KV. The spinocerebellar ataxia-associated gene Tau tubulin kinase 2 controls the initiation of ciliogenesis. Cell. 2012;151(4):847-58. PMCID: 3496184.

210. Fatemi SH, Earle JA, Stary JM, Lee S, Sedgewick J. Altered levels of the synaptosomal associated protein SNAP-25 in hippocampus of subjects with mood disorders and schizophrenia. Neuroreport. 2001;12(15):3257-62.

211. Karson CN, Mrak RE, Schluterman KO, Sturner WQ, Sheng JG, Griffin WS. Alterations in synaptic proteins and their encoding mRNAs in prefrontal cortex in schizophrenia: a possible neurochemical basis for 'hypofrontality'. Mol Psychiatry. 1999;4(1):39-45.

212. Thompson PM, Sower AC, Perrone-Bizzozero NI. Altered levels of the synaptosomal associated protein SNAP-25 in schizophrenia. Biol Psychiatry. 1998;43(4):239-43.

213. Westlake CJ, Baye LM, Nachury MV, Wright KJ, Ervin KE, Phu L, et al. Primary cilia membrane assembly is initiated by Rab11 and transport protein particle II (TRAPPII) complex-dependent trafficking of Rabin8 to the centrosome. Proc Natl Acad Sci U S A. 2011;108(7):2759-64. PMCID: 3041065.

214. Mishra SK, Keyel PA, Hawryluk MJ, Agostinelli NR, Watkins SC, Traub LM. Disabled-2 exhibits the properties of a cargo-selective endocytic clathrin adaptor. EMBO Journal. 2002;21(18):4915-26.

215. Itoh T, Koshiba S, Kigawa T, Kikuchi A, Yokoyama S, Takenawa T. Role of the ENTH domain in phosphatidylinositol-4,5-bisphosphate binding and endocytosis.[see comment]. Science. 2001;291(5506):1047-51.

216. Hardy S, Kitamura M, Harris-Stansil T, Dai Y, Phipps ML. Construction of adenovirus vectors through Cre-lox recombination. J Virol. 1997;71(3):1842-9. PMCID: 191254.

217. Henkel JR, Weisz OA. Influenza virus M2 protein slows traffic along the secretory pathway. pH perturbation of acidified compartments affects early Golgi transport steps. J Biol Chem. 1998;273(11):6518-24.

218. Henkel JR, Apodaca G, Altschuler Y, Hardy S, Weisz OA. Selective perturbation of apical membrane traffic by expression of influenza M2, an acid-activated ion channel, in polarized madin-darby canine kidney cells. Mol Biol Cell. 1998;9(9):2477-90. PMCID: 25516.

219. Ihrke G, Bruns JR, Luzio JP, Weisz OA. Competing sorting signals guide endolyn along a novel route to lysosomes in MDCK cells. Embo J. 2001;20(22):6256-64. PMCID: 125743.

220. Bens M, Vallet V, Cluzeaud F, Pascual-Letallec L, Kahn A, Rafestin-Oblin ME, et al. Corticosteroid-dependent sodium transport in a novel immortalized mouse collecting duct principal cell line. Journal of the American Society of Nephrology. 1999;10(5):923-34.

221. Anderson JM, Stevenson BR, Jesaitis LA, Goodenough DA, Mooseker MS. Characterization of ZO-1, a protein component of the tight junction from mouse liver and Madin-Darby canine kidney cells. J Cell Biol. 1988;106(4):1141-9. PMCID: 2115004.

222. Costes SV, Daelemans D, Cho EH, Dobbin Z, Pavlakis G, Lockett S. Automatic and quantitative measurement of protein-protein colocalization in live cells. Biophys J. 2004;86(6):3993-4003. PMCID: 1304300.

223. Gong F, Alzamora R, Smolak C, Li H, Naveed S, Neumann D, et al. Vacuolar H+-ATPase apical accumulation in kidney intercalated cells is regulated by PKA and AMP-activated protein kinase. Am J Physiol Renal Physiol. 2010;298(5):F1162-9. PMCID: 2867405.

224. Breitfeld PP, Casanova JE, Harris JM, Simister NE, Mostov KE. Expression and analysis of the polymeric immunoglobulin receptor in Madin-Darby canine kidney cells using retroviral vectors. Methods in Cell Biology. 1989;32:329-37.

225. Oztan A, Rondanino C, Apodaca G. Transcytosis of polymeric immunoglobulin a in polarized Madin-Darby canine kidney cells. Methods Mol Biol. 2008;440:157-70. PMCID: 2603048.

226. Maples CJ, Ruiz WG, Apodaca G. Both microtubules and actin filaments are required for efficient postendocytotic traffic of the polymeric immunoglobulin receptor in polarized Madin-Darby canine kidney cells. J Biol Chem. 1997;272(10):6741-51.

227. Khandelwal P, Ruiz WG, Apodaca G. Compensatory endocytosis in bladder umbrella cells occurs through an integrin-regulated and RhoA- and dynamin-dependent pathway. EMBO J. 2010;29(12):1961-75. PMCID: 2892371.

228. Howard C, Reed M. Unbiased stereology. Three dimensional measurement in microscopy. . New York, NY: Springer-Verlag; 1998.

229.   Russ J, Dehoff R. Practical Stereology, 2nd edition. New York, NY: Kluwer Academic; 2000.